AMBIENT OZONE FORMATION POTENTIAL AND SOURCE APPORTIONMENT IN CHINA

A Thesis

by

YUAN CHEN

Submitted to the Office of Graduate and Professional Studies of
Texas A&M University
in partial fulfillment of the requirements for the degree of

MASTER OF SCIENCE

Chair of Committee,	Qi Ying
Committee Members,	Bill Batchelor
	Renyi Zhang
Head of Department,	Robin Autenrieth

May 2017

Major Subject: Civil Engineering

ABSTRACT

China has been suffering from increasingly higher ozone pollution in the past decade because of rapid economic growth and industrial development. Ozone formation is affected by the nitrogen oxides (NO_x) and various volatile organic compounds (VOCs) emitted from both natural and anthropogenic sources. In this study, incremental reactivity (IR) of 66 major VOCs in China was determined using a regional chemical transport model (CTM) and a photochemical box model. A source-oriented CTM was developed to determine the contributions of NO_x and VOC sources to ozone formation.

A modified regional Community Multi-scale Air Quality (CMAQ) model (v5.0.1) equipped with a detailed photochemical mechanism SAPRC-11 was used to simulate the ozone concentrations to determine IR under realistic ambient conditions in China during August 2013. The normalized incremental reactivity (NIR) of the VOC, defined as the ratio of the IR of the VOC to the IR of the VOC mixture, was also determined. C4+ aldehydes (NIR_{50}~30) and trimethyl benzenes (NIR_{50}~27) were found to be the most reactive species. The predicted chemical compositions of the VOC mixture from the regional model were used in a photochemical box model to determine the maximum incremental reactivity (MIR) of the VOCs at 34 provincial capital cities in China. The ozone-forming potential (OFP) values of VOCs in Nanjing were calculated using MIR and observed VOC concentrations. Isoprene (0.724), m-xylene (0.652) and toluene (0.555) are the top three species with large OFP values on a per carbon basis.

The source-oriented CTM applied reactive tracers for NO_x, VOC precursors and oxidation products for ozone source apportionment analysis. Chinese emissions account for approximately 50% of the hourly ozone concentrations on a monthly average basis, and can be as high as 70% on high ozone hours. Large urban areas such as the Yangtze River Delta and the Pearl River Delta are under VOC-limited conditions. Most of the ozone formation under VOC-limited conditions can be attributed to biogenic and industrial sources, and can be attributed to industrial, power plant and transportation sources under NO_x-limited conditions.

ACKNOWLEDGEMENTS

I would like to thank my committee chair, Dr. Qi Ying for the patience and inspiring guidance in the process of my research and studies. It is fortunate to have such a responsible and amiable advisor.

I would also like to express my gratitude to my committee members, Dr. Bill Batchelor and Dr. Renyi Zhang for their guidance and support throughout my research and studies. It is my honor to have them in my thesis committee.

Specially, I would like to thank Dr. William Carter for his technical guidance in the photochemical box model simulations and his patience in clearing problems we met during the process of this work.

Thanks also go to Mrs. Peng Wang and Mr. Jie Zhang in my research group. I am grateful to their generous sharing in their experience and their advices, which helped me to achieve much progress in my research.

Last but not least, I would like to thank my mother and father for their encouragement and support all the time in my life.

This work is far more than the achievement of me alone, but the accomplishment of everyone who has encouraged me during the process of this work. Thanks again to everyone who has enlightened me in this work and in my life.

CONTRIBUTORS AND FUNDING SOURCES

Contributors

This work was supervised by a thesis committee consisting of Professor Qi Ying and Professor Bill Batchelor of the Department of Civil Engineering and Professor Renyi Zhang of the Department of Atmospheric Sciences.

The data analyzed for Chapter 2 was provided by Dr. Jianjun Chen of California Air Resources Board.

The model applied in Chapter 3 was originally developed by Dr. William Carter of University of California, Riverside.

The computer simulations described in this thesis were conducted with the advanced computing resources provided by Texas A&M High Performance Research Computing.

All other work conducted for the thesis was completed by the student independently.

Funding Sources

There are no outside funding contributions to acknowledge related to the research and compilation of this document.

TABLE OF CONTENTS

Page

LIST OF FIGURES

Page

LIST OF TABLES

Page

1. INTRODUCTION

1.1 Statement of problems

Ground level ozone (O_3) is formed through reactions involving nitrogen oxides (NO_x) and volatile organic compounds (VOCs) in the presence of sunlight. Unlike stratospheric ozone, which could protect living organisms from harmful UV radiation, ground level ozone would do harm to human health, causing irritation of the respiratory system, reduce lung function and aggravate asthma. Exposure to higher concentrations of ozone is also known to have adverse effects on sensitive vegetation and ecosystems [1].

China has been suffered from severe ozone and particulate air pollution as a result of rapid economic growth and industrial developments [2]. While a significant amount of efforts has been made to understand the formation mechanisms, source contributions and mitigation strategies of particulate air pollution, significantly less amount of studies were reported for ozone. Surface ozone is usually not a primary pollutant directly emitted from sources, but formed secondarily in the atmosphere through the chemical reactions of its precursors. Both ozone itself and its precursors can be transported to downwind regions to cause regional ozone pollution in areas without significant emissions of precursors. Hence, both the chemical processes and the contributions from local, regional and super-regional ozone precursors influence significantly on local ozone concentrations [3].

A variety of VOC species with different molecular structures can participate in reactions leading to ozone formation. Liu et al. [4] found that olefins from anthropogenic emissions were the dominant VOCs in ozone formation, and isoprene from biogenic emissions contributed to ozone formation significantly during summer time in Beijing, China. Li et al. [3] indicated that both local and regional sources were responsible for the formation of high ozone episodes in the Pearl River Delta (PRD) in China. Similar conclusion was made in the study on the Yangtze River Delta (YRD) in China [5].

Since the ozone formation potential and transport distances of ozone precursors are very different, and different anthropogenic sources have a different emission mixture of precursors, it is necessary to quantify the ozone formation capability of different species and emission sources and determine the contributions of different precursor emission sources to observed ozone concentrations so that cost effective ozone mitigation strategies can be designed.

1.2 Background

1.2.1 Tropospheric ozone formation from photochemical reactions of NO_x and VOCs

In the presence of solar radiation (*hv*), photolysis of NO_2 will produce NO and excited atomic oxygen ($O\cdot$) as shown in reaction (R1-1):

$$NO_2 + hv = NO + O\cdot \quad \text{(R1-1)}$$

$O\cdot$ reacts with an oxygen molecule to form ozone in the presence of a buffer gas molecule (M) as shown in reaction (R1-2):

$$O_2 + O\cdot + M = O_3 + M \quad \text{(R1-2)}$$

The formed ozone can react with NO and be converted back to NO_2 as shown in reaction (R1-3), which completes the nitrogen cycle:

$$NO + O_3 = NO_2 + O_2 \quad \text{(R1-3)}$$

If there are no VOCs available, the net effect of reactions (R1-1)-(R1-3) leads to zero ozone formation. To have significant ozone formation, NO has to be converted back into NO_2 through reaction pathways other than (R1-3), in which VOCs play an important role. This role of VOCs in ozone formation can be illustrated using a generic reactive hydrocarbon (RH) as an example. First, it is oxidized by hydroxyl radical ($OH\cdot$) as shown in reaction (R1-4):

$$RH + OH\cdot + O_2 + M = RO_2\cdot + H_2O + M \quad \text{(R1-4)}$$

The produced peroxy radical ($RO_2\cdot$) then reacts with NO to regenerate NO_2 and $OH\cdot$ as shown in reaction set (R1-5):

$$RO_2\cdot + NO + O_2 = RCHO + NO_2 + HO_2\cdot$$

$$\mathrm{RCHO} + h\nu = \mathrm{RO_2}\cdot + \mathrm{HO_2}\cdot + \mathrm{CO}$$

$$\mathrm{HO_2}\cdot + \mathrm{NO} = \mathrm{NO_2} + \mathrm{OH}\cdot \qquad \text{(R1-5)}$$

In a typical polluted atmosphere, many different reactive VOCs can be involved in ozone formation. The VOCs are typically lumped into several groups based on their molecular structure and/or reactivity to simplify the representation of their reactions in atmospheric chemical transport models (CTMs).

NO_2 will be oxidized by $OH\cdot$ and form less-reactive HNO_3 as shown in reaction (R1-6). This reaction removes both $OH\cdot$ and NO_x from the photochemical reaction system, thus is called a termination reaction.

$$\mathrm{NO_2} + \mathrm{OH}\cdot = \mathrm{HNO_3} \qquad \text{(R1-6)}$$

1.2.2 O_3-NO_x-VOC sensitivity

Another important factor affecting the formation of ozone is the O_3-NO_x-VOC sensitivity, which means that different ratios of NO_x and VOC can lead to different trends in ozone formation [6]. Figure 1-1 shows the typical ozone isopleths generated using a photochemical box model to simulate ozone formation under different amount of NO_x and VOCs. The maximum ozone concentration obtained in each simulation was plotted as a function of the initial NO_x and VOC concentrations.

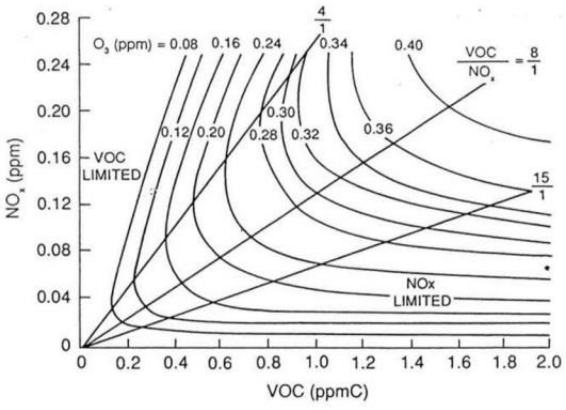

Figure 1- 1. Typical ozone isopleths [7]

Both VOCs and NO_2 compete for OH ; which is a key factor to ozone formation. Hence, the VOC/NO_x ratios affect ozone formation significantly. The regions with VOC/NO_x ratios lower than 4.0 are typically considered as VOC-limited. Under this VOC-limited condition, ozone concentration is sensitive to the changes of VOCs. Reducing VOC initial concentrations leads to lower reaction rate of (R1-4), which leads to slower formation of RO_2 and reproduction of $OH\cdot$ as shown in reactions (R1-5). Slower NO to NO_2 conversion by RO_2 radicals and lower $OH\cdot$ concentrations lead to lower ozone concentration. Reduction of NO_x will lead to less ozone titration by NO, as shown in reaction (R1-3) and lead to an increase in net ozone formation when the VOC/NO_x ratio is in the VOC-limited regime [8].

Regions with the VOC/NO_x ratio higher than 15.0 are determined as NO_x-limited. Under this NO_x-limited condition, the oxidation of NO to NO_2 and the subsequently photolysis of NO_2 as shown in reaction (R1-1) is the limiting factor for the ozone formation. The reduction of NO_x in this regime reduces the photolysis of NO_2 and the production of $O:$ The amount of ozone formed as in reaction (R1-2) would decrease as a result.

1.2.3 Incremental ozone reactivity of VOCs

Realizing that ozone formation potential in a polluted atmosphere is impacted significantly by different VOCs, various metrics have been applied to assess their relative importance on ozone formation. The most commonly used metric is the incremental reactivity (IR) of VOCs [9], which is defined as the incremental amount of ozone formed (ΔO_3) relative to the an incremental amount of VOC (ΔVOC) added to a base VOC mixture, as shown in equation (1-1):

$$\mathrm{IR} = \frac{\Delta O_3}{\Delta \mathrm{VOC}} \tag{1-1}$$

The IR of an organic compound depends on the relative availability of NO_x in the environment. In line with this, various IR metrics have been developed based on different VOC/NO_x ratios [9]. For instance, the maximum incremental reactivity (MIR)

metric corresponds to the conditions where NO_x concentrations are adjusted to a high level for the base VOC mixture to have the highest IR. It reflects relatively high NO_x scenarios where ozone formation is most sensitive to VOC emissions. The maximum ozone incremental reactivity (MOIR) represents lower NO_x scenarios that give the highest ozone concentrations. The equal benefit incremental reactivity (EBIR) corresponds to yet lower NO_x conditions where NO_x control and VOC control are equally effective in reducing ozone formation [10].

These metrics can be used to quantify contributions of different VOCs to ozone formation. By evaluating these, VOCs with higher incremental reactivity can be identified. Reactivity-based VOC control approaches are important in those areas where VOC control is the key factor in reducing ozone concentration [11].

While the incremental reactivity is useful to determine the importance of individual VOCs in ozone formation, its numerical value depends on the base VOC mixture. The variation of the reactivity scales to the changes of base VOC mixture has not been fully investigated. Since the VOC mixture in most polluted urban areas in China can be quite different from those in the United States due to differences in energy and industrial infrastructures, fuel composition and emission controls when the MIR scales were first calculated using representative VOC mixture from cities in the United States. Therefore, studies on the incremental reactivity of VOCs based on the situations in China are necessary, especially in those areas where VOCs control is expected to effective.

1.2.4 Ozone source apportionment

Sources with the same amount of total VOC emissions may contribute differently to overall ozone formation due to the difference in the chemical composition of VOCs. A region can also be under NO_x-limited condition so that ozone formation is more responsive to NO_x changes. Thus, a full source contribution analysis of ozone formation under realistic atmospheric conditions cannot be done with emission inventory analysis

alone. The sources of NO_x and VOC need to be tracked in the photochemical mechanism. Regional chemical transport models (CTMs) have been used to determine source contributions to ozone formation. The Ozone Source Apportionment Technology (OSAT) is a mass balance technique incorporated with the Comprehensive Air quality Model with extensions (CAMx). It can provide detailed surface ozone source apportionment for multiple source categories and source regions in one single simulation using non-reactive tracers [12]. The transport of surface ozone and its precursors can be quantified by different source categories and source regions [3]. Reactive tagged species method [13, 14] have also been used in previous source apportionment studies. In this method, the underlying photochemical mechanism in the CTMs was expended to directly track the concentrations of precursors from different source sectors and source regions with the help of additional source or source-region tagged species. The reactive tracer method not only considers the precursors but also keeps track of the sources of the reactive oxidation products from the precursors, thus could potentially provide more accurate source apportionment calculations. The resulted source-oriented photochemical mechanism typically contains a lot more reactions than the underlying base mechanism and is thus computationally more challenging. The reactive tracer method has been applied to study source apportionment of primary particulate matter, secondary inorganic and organic aerosols, and ozone formation under either NO_x- or VOC-limited conditions. However, a complete reactive tracer based model for ozone source apportionment has not been available.

1.3 Research objectives

The objective of this research is to (1) study ozone formation potentials of different VOC species using a regional photochemical transport model (CMAQ), (2) study ozone formation potentials of different VOC species using a photochemical box model with base VOC mixture from different Chinese cities, and (3) determine the

contributions of major emissions sectors (residential, power plants, industries, transportation, biogenic sources and wildfire) to summer ozone in China.

High ozone concentration over 60 ppb occurs in NCP, YRD, central China and in the Sichuan Basin near Chengdu and Chongqing. Most of these regions are under VOC-limited condition. Aldehydes butanal, hexanal and internal alkenes cis-2-butene and 1,3-butadiene are reactive VOC species. Considering emission rates, isoprene is the species with the highest ozone-forming potential. The source contributions from biogenic sources and industrial processes are the most significant to ozone formation.

2. THE CMAQ MODEL AND INCREMENTAL REACTIVITY CALCULATION

2.1 Introduction

As mentioned in the previous chapter, ozone formation is strongly dependent on the characterization of its precursors. Control of VOC can be effective in ozone reduction, especially in those areas where the ozone formation rate is limited by the amount of VOCs. Thus, an understanding on the reactivity of VOCs is necessary to determine which VOCs should be controlled primarily in designing emission control strategies.

China has been experiencing severe tropospheric ozone pollution with a rapid pace of development in industrialization and urbanization. A number of studies have been done on the characterization of different VOC species and their contributions to ozone formation. Tan et al. [15] measured non-methane hydrocarbons (NMHCs) and explored the ozone formation potentials (OFP) of each NMHCs in December 2008 in Foshan, China. Ethane, propane and n-butane were found to be the most abundant species but ethene, toluene and propene were the species that contributed to ozone formation most due to their relatively high MIR values and concentrations in the ambient air. An et al. [16] collected and analyzed VOC samples in Beijing from June through August 2008. Among the 50 VOC species analyzed, alkanes were found to be the most abundant by concentration, while aromatics were the most abundant when reactivity of the VOCs were considered. Propene, toluene, m,p-xylenes, 1-butene and 1,2,4-trimethylbenzene were the most reactive species. Ling et al. [17] applied the positive matrix factorization (PMF) model to identify major sources of VOCs and their contributions to ozone formation in Hong Kong. Among the identified sources, xylenes and ethyl-benzene in paint and sealant solvents, toluene in gasoline exhaust, butanes, ethane, propene and propane in liquefied petroleum gas (LPG) and n-butane and ethene in diesel exhaust are the most reactive species that made significant contributions to ozone formation. Lyu et al. [18] measured ambient VOCs from February 2013 to

October 2014 in Wuhan. Their modeling analysis with a photochemical box model revealed that the ozone formation in Wuhan is VOC-limited. Ethene and toluene were the primary species contributing to ozone formation. Jia et al. [19] studied the contributions of NMHCs in Lanzhou. In downtown Lanzhou, cis-2-butene and m,p-xylenes were the species contributing to ozone formation potentials most, while in suburb areas, ethene, propene and trans-2-butene played more important roles in summer ozone formation.

It can be expected that ozone formation potentials of VOCs species vary a lot in different areas in China, due to different industrial structures, vehicle fleet and fuel composition, residential emissions, meteorological conditions and other factors. Thus, a comprehensive study on roles of VOC species play in ozone formation is necessary to be made throughout China.

Regional chemical transport models (CTMs), such as the Community Multi-scale Air Quality (CMAQ) model [20-22] originally developed by the United States Environmental Protection Agency (US EPA), is able to analyze temporal and spatial variations of air pollutants under various meteorological conditions and can be applied to assess to ozone formation potential of VOCs under realistic conditions. For example, Wang et al. [23] applied the CMAQ modeling system to simulate the surface ozone episodes over the Pearl River Delta (PRD) region in October 2004, and suggested that ozone formation was sensitive to VOC. Li et al. [24] analyzed ozone sensitivity in urban and rural areas of Shanghai in July 2007 with CMAQ. It was found that ozone formation was more sensitive to VOCs in urban areas, but was more sensitive to NO_x in rural areas. Czader et al. [25] calculated the incremental reactivity of VOCs for the Houston-Galveston conditions using the CMAQ model with an extended version of SAPRC-99 mechanism. They found that ozone formation from trans-2-butene and cis-2-butene were most sensitive to the environment in which they were released, and ethene, propene and formaldehyde had the highest impact on ozone formation considering their individual incremental reactivity and concentrations in the atmosphere. However, the reactivity of specific VOC species and their contributions to ozone formation in China has not been

comprehensively discussed. It would be necessary to conduct similar study under China situation, which would enable us to have an overall view on ozone formation over various regions in China.

2.2 Methodology

In this study, the regional ozone reactivity of each of the 66 VOC species listed in Table A-1, which represent a significant fraction of anthropogenic and biogenic reactive hydrocarbons, was studied using the CMAQ model for a summer high ozone episode. Sensitivity simulations were conducted for each VOC by increasing its emission rate in the model domain by 10% uniformly while keeping the emission rates of other species unchanged. The change in the predicted ozone concentrations relative to the base case simulation during a specific time period (1-hour or 8-hour) was used to determine the reactivity of the species for ozone formation under realistic atmospheric conditions, as shown in equation (2-1):

$$\mathrm{IR}_{i,x,y} = \left(\frac{\Delta O_3}{\Delta \mathrm{VOC}_i}\right)_{x,y} \qquad (2\text{-}1)$$

where subscript x, y are grid cell indexes in the model domain; i is VOC species index; ΔO_3 and $\Delta \mathrm{VOC}$ are the changes of the ozone and VOC concentrations. For reference, an additional simulation was conducted to increase the emissions of the 65 anthropogenic VOCs among the 66 VOCs (except isoprene, which is mostly biogenic) by 10% as a measure to determine the reactivity of the anthropogenic VOC mixture. Isoprene was excluded because it is mainly emitted from biogenic sources. This simulation was referred to as the VOC mixture case and was applied to normalize the other individual sensitivity cases to evaluate the relative importance of individual VOC species from anthropogenic sources, as shown in equation (2-2):

$$\mathrm{NIR}_{i,x,y} = \left(\frac{\mathrm{IR}_i}{\mathrm{IR}_{mix}}\right)_{x,y} = \left(\frac{\Delta O_{3,i}}{\Delta O_{3,mix}}\right)_{x,y} \times \left(\frac{\Delta \mathrm{VOC}_{mix}}{\Delta \mathrm{VOC}_i}\right)_{x,y} \qquad (2\text{-}2)$$

where NIR_i represents the normalized incremental reactivity of the i^{th} individual VOC species relative to the VOC mixture. IR_i, IR_{mix}, $\Delta O_{3,mix}$ and $\Delta \mathrm{VOC}_{mix}$ represent the

incremental reactivity, change of ozone and change of VOC concentrations in the VOC mixture case, respectively. An NIR value of greater than one means that the species is more effective in generating ozone than the anthropogenic VOC precursor mixture.

The CMAQ model applied in this study is based on CMAQ v5.0.1 (https://www.cmascenter.org/cmaq/) modified to use an expanded SAPRC-11 (S11D) photochemical mechanism to represent the reactions of major primary VOCs explicitly, including the 66 VOC species listed in Table A-1. The reaction rate coefficients of these VOC species with OH radical at 300 K (k_{OH}) [26] are also included in Table A-1. Basically, species with higher k_{OH} tend to be more reactive. The S11D mechanism was a slightly simplified version of the very detailed SAPRC-11 mechanism that explicitly representing the atmospheric reactions of ~300 types of VOCs.

2.3 Model application

The CMAQ model with S11D mechanism was applied to simulate O_3 in August 2013 using a 36 km × 36 km horizontal resolution domain. The model domain covers China and surrounding countries in East Asia, as shown in Figure 2-1. August was chosen for this analysis because of high ozone conditions and availability of data for model evaluations. The anthropogenic and biogenic emissions were based on the Multi-resolution Emission Inventory of China (MEIC) and the MEGAN biogenic emission model [27], respectively. Meteorological inputs were generated using the Weather Research and Forecasting (WRF) model. More details of the model setup, input data preparation and evaluation of meteorological inputs have been described in detail by Hu et al [28] and the references therein.

The MEIC emission inventory provides speciated emissions for the lumped version of the SAPRC-99 (S99) photochemical mechanism. To generate the detailed emissions for S11D, lumped VOC emissions need to be split. The splitting factors of each lumped VOCs and the corresponding detailed VOC species were developed based on the detailed VOC measurements from local time 6 to 8 am in an urban site in Nanjing

during August 2013. The measured individual VOC compounds were assigned to both SAPRC99 and SAPRC11D species. Since SAPRC11D has more detailed representation of VOC compounds, the fraction of SAPRC11D species within the same SAPRC99 lumped species was determined based on the relative abundance of individual SAPRC11D species (i.e., relative mixing ratios of SAPRC11D species during 6-8am) (Table G-1, from Dr. Jianjun Chen, California Air Resources Board, personal communication). The same splitting factors were used to provide detailed emissions for the S11D mechanism from the lumped S99 emissions in all grid cells in the model domain.

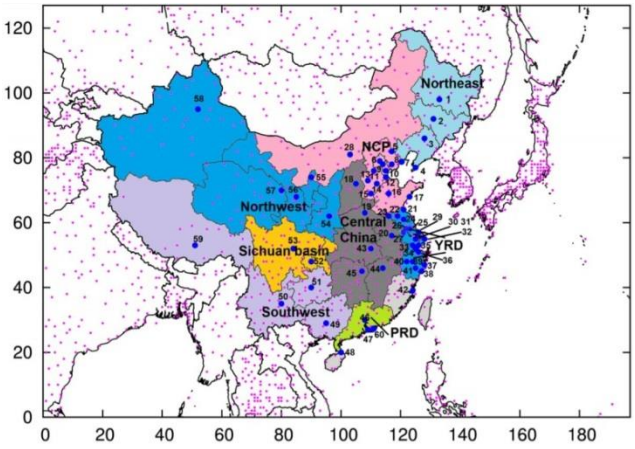

Figure 2- 1. Model domain. The axes are the number of grid cells. Blue circles show the locations of major cities in China (see Table 2-1) [28].

2.4 Results and discussion

2.4.1 Model performance evaluation

To validate that our model prediction was able to reproduce the concentrations of key species in polluted urban atmospheres, the predicted concentrations of O_3, NO_2, HCHO and several VOCs in August 2013 were compared with those from surface and satellite observations. The hourly observations of O_3 and NO_2 of August 2013 from a

total of 422 stations in 60 cities were obtained from the publishing website of China National Environmental Monitoring Center (http://113.108.142.147:20035/emcpublish/), as shown in Figure 2-1. The concentrations of pollutants have large spatial and temporal variation due to diverse meteorological conditions and emission sources in different regions throughout China. These 60 cities were grouped into 8 different geographical regions as listed in Table 2-1. Observations of VOCs were made on the roof top of the science building in Nanjing University of Science and Technology. In addition to the surface measurements, column density of NO_2 and HCHO from the Ozone Monitoring Instrument (OMI) on National Aeronautics and Space Administration (NASA)'s Aura satellite was also used in the model validation. The processed NO_2 column over China was taken from POMINO (http://www.atmos.pku.edu.cn/acm/acmProduct.html). The observation data of HCHO were retrieved from the Tropospheric Emission Monitoring Internet Service (TEMIS) (http://h2co.aeronomy.be/)

Table 2- 1. List of major cities in different regions in China

Region	**Cities**
Northeast	1. Harbin, 2. Changchun, 3. Shenyang, 4. Dalian
North China Plain (NCP)	5. Chengde, 6. Beijing, 7. Qinhuangdao, 8. Tangshan, 9. Langfang, 10. Tianjin, 11. Baoding, 12. Cangzhou, 13. Shijiazhuang, 14. Hengshui, 15. Handan. 16. Jinan, 17. Qingdao, 28. Hohhot
Yangtze River Delta (YRD)	21. Lianyungang, 22. Suqian, 23. Xuzhou, 24. Huai'an, 25. Taizhou, 26. Yangzhou, 27. Nanjing, 29. Nantong, 30. Suzhou, 31. Wuxi, 32. Shanghai, 33. Huzhou, 34. Hangzhou, 35. Jiaxing, 36. Shaoxing, 37. Zhoushan, 38. Wenzhou, 39. Jinhua, 40. Quzhou, 41. Lishui
Pearl River Delta (PRD)	46. Guangzhou, 47. Zhuhai, 60. Shenzhen
Central China	18. Taiyuan, 19. Zhengzhou, 20. Hefei, 43. Wuhan, 44. Nanchang, 45. Changsha
Northwest	54. Xi'an, 55. Yinchuan, 56. Lanzhou, 57. Xining, 58. Urumqi
Sichuan Basin (SCB)	52. Chongqing, 53. Chengdu
Southwest and other	42. Fuzhou, 48. Haikou, 49. Nanning, 50. Kunming, 51. Guiyang, 59. Lhasa

2.4.1.1 O_3 performance

The performance of the model in predicting surface ozone concentration at the 60 cities has been evaluated by Hu et al. [28]. In general, the model reproduces the monthly averaged diurnal variation of surface level ozone in most cities. The monthly averaged diurnal variation of ozone in August 2013 simulated by S11D in this study is shown in Figure 2-2. The average concentrations for each region were the mean concentrations of the cities within the region. The surface ozone concentrations are slightly over-predicted in all regions within the model domain but more significantly in the northern parts of the country. The agreement between predicted and observed concentrations in YRD, PRD and SCB are better than other regions. Predicted and observed ozone concentrations at each city are shown in Figure J-1. The poor predictions for NCP and other north regions are due to a few cities with significant errors in ozone predictions. Overall, the model can capture the ozone magnitude and diurnal variations in most cities reasonably well.

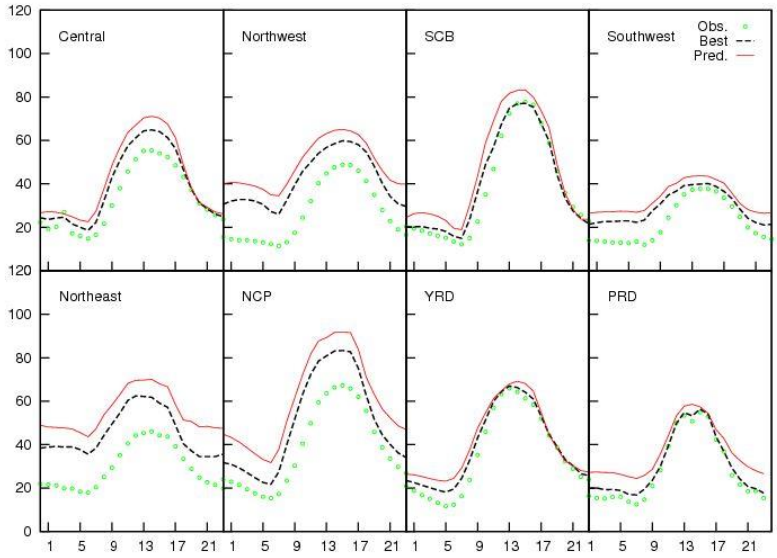

Figure 2- 2. Comparison of monthly averaged diurnal variations of hourly O_3 concentrations in August 2013 in different regions of China. Red lines are the values predicted at the grid cell where the monitors are located; Black dash lines are the values predicted within the 3×3 grid cell regions surrounding the monitoring site that are closest to the observations. Units are in ppbV.

2.4.1.2 NO_2 performance

The monthly averaged diurnal variation of NO_2 in August 2013 is shown in Figure 2-3. The surface NO_2 concentrations are under-predicted in all regions within the model domain, although the diurnal variations of NO_2 are generally well reproduced. The under-prediction of NO_2 is consistent with the results reported by Hu et al [18]. The under-prediction is more significant starting from midnight and continuing until late afternoon. The under-prediction in nighttime surface NO_2 concentrations is consistent with the over-prediction in surface O_3 concentrations, suggesting possible underestimation of NO_x emissions (mostly as NO) at night. If more NO were emitted, titration reaction of NO with O_3 can reduce O_3 and increase NO_2 concentrations, according to reaction (R1-3) in Chapter 1. During daytime, as ozone formation in most of the urban areas is VOC-limited, underestimation of NO emissions can lead to over-predictions of O_3, as illustrated by Figure 1-1. Similar analyses have been reported by Xie et al. [29] based on the observations of O_3 and NO_x in urban and suburban areas in Nanjing, China in 2008. Their results indicated that the lower NO_x concentrations in suburban areas consumed less ozone during night-time. Although less ozone was generated during day-time, the overall surface ozone concentrations were higher than that in urban areas. Predicted and observed NO_2 concentrations at each city are shown in Figure J-2.

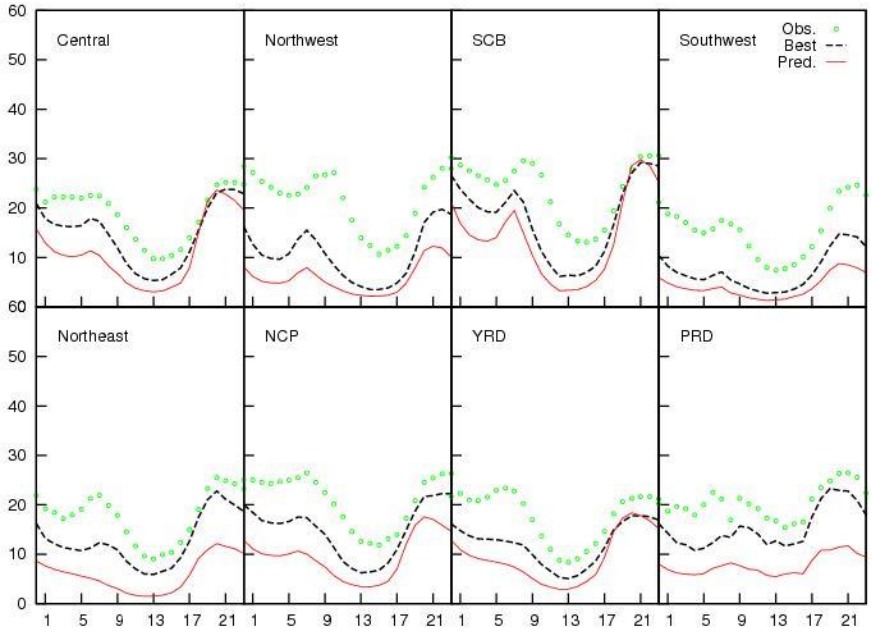

Figure 2- 3. Comparison of monthly averaged diurnal variations of hourly NO_2 concentrations in August 2013. Red lines are the values predicted at the grid cell where the monitors are located; Black dash lines are the values predicted within the 3×3 grid cell regions surrounding the monitoring site that are closest to the observations. Units are in ppbV.

2.4.1.3 VOC performance

The monthly averaged diurnal variation of 65 VOC species in August 2013 at the NUIST site in Nanjing is shown in Figure 2-4. HCHO was not included because there was no observation available. While the predicted monthly average concentrations of most species are in general agreement with observations, night time concentrations at the grid cell is significantly over-predicted. The observed VOCs concentrations typically show less diurnal variation than the predicted concentrations. Predicted VOC concentrations show significant spatial gradients at night, as indicated by the significant difference between the best matching predictions and the predictions at the corresponding grid cell. Uncertainties in meteorological fields such as wind speed and wind direction as well as emissions can contribute to the over-predictions. However, since the best matching predictions were much closer to the observations, uncertainties

in the wind fields might have a larger effect on model predictions. Isoprene (ISOP) concentrations were over-predicted in the morning and evening hours but concentrations of its major oxidation products, methacrolein (MACR) and methyl vinyl ketone (MVK) are well predicted throughout the day. Analysis of the time series of photolysis rates, OH concentrations, mixing height and isoprene emission rates shows that the increase of isoprene during early morning and later afternoon hours are due to a combination of lower mixing height and low OH concentrations. At later afternoon hours, solar radiation is still available for the plants to emit isoprene but the OH radical concentration and mixing height decrease very quickly. This leads to accumulation of isoprene in the surface layer. Since MVK and MACR are generated by isoprene oxidation, their concentrations do not increase with isoprene (see Figure K-1). Since the observation does not support an increase of isoprene in the morning and evening hours, it is likely that the model underestimate OH due to some missing OH pathways. Possible missing of OH and HO_2 in biogenic emission influenced areas in China have been reported in previous studies and should be explored in a future study to test if increasing OH will lead to better isoprene predictions.

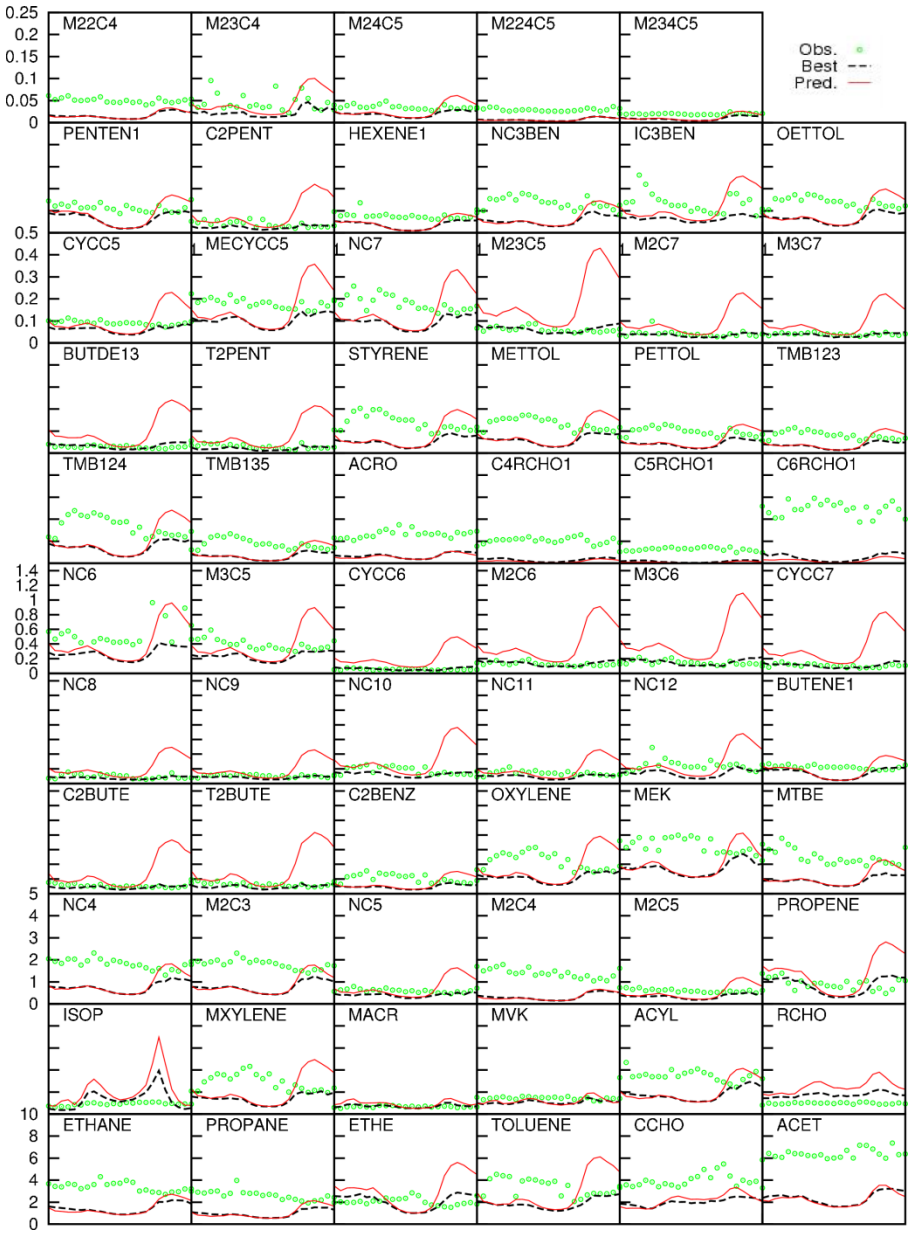

Figure 2- 4. Comparison of averaged diurnal variations of 65 VOC species in Nanjing in August 2013. Red lines are the predicted concentration at the grid cell where the NUIST site is located. The species are grouped based on their concentrations and in each group are arranged in the order of alkanes, alkenes, aromatics and oxygenated species. Unites are in ppbV. The complete names of each species are listed in Table A-1.

In addition to hourly VOC concentrations in Nanjing, predicted VOC composition expressed as mole fractions in Guangzhou were also compared with

observations as shown in Figure 2-5. The observed VOCs were reported by Zou et al. [30] as annual average concentrations from June 2011 to May 2012. The predicted VOCs were monthly average concentrations of August 2013. Only alkanes, alkenes and aromatic compounds are used in the comparison.

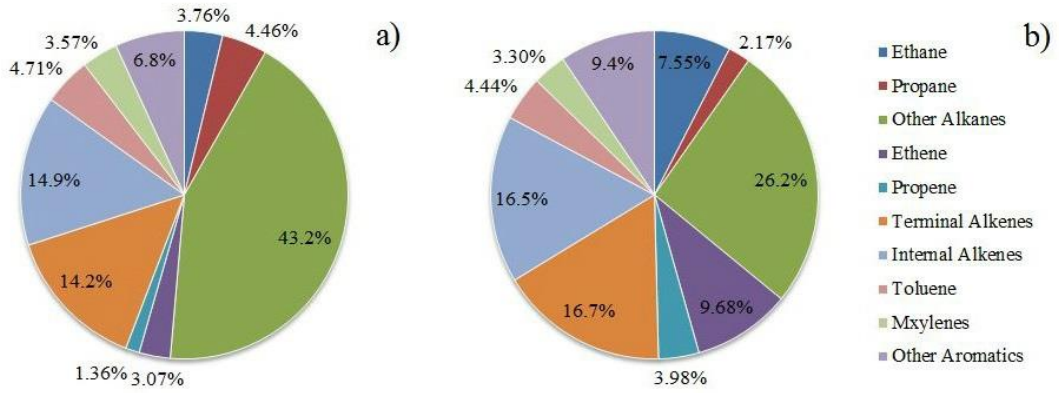

Figure 2- 5. Comparison of VOC compositions retrieved from a) observed data [30] and b) CMAQ model results

The fraction of alkanes in the observed VOC mixture (51%) is higher than that in the CMAQ predicted VOC mixture (36%), and the fraction of alkenes in the observed VOC (34%) is slightly lower than that in the predicted VOC composition (47%). The fractions of aromatic compounds are similar in these two situations.

2.4.1.4 NO_2 and HCHO performance compared with satellite observation

The ability of the model in predicting tropospheric NO_2 column and formaldehyde (HCHO) column density was also evaluated. HCHO is directly emitted as well as formed secondarily from the oxidation of other parent VOCs such as isoprene. The ability of the model in predicting HCHO will provide confidence in the VOC incremental reactivity and source apportionment calculations.

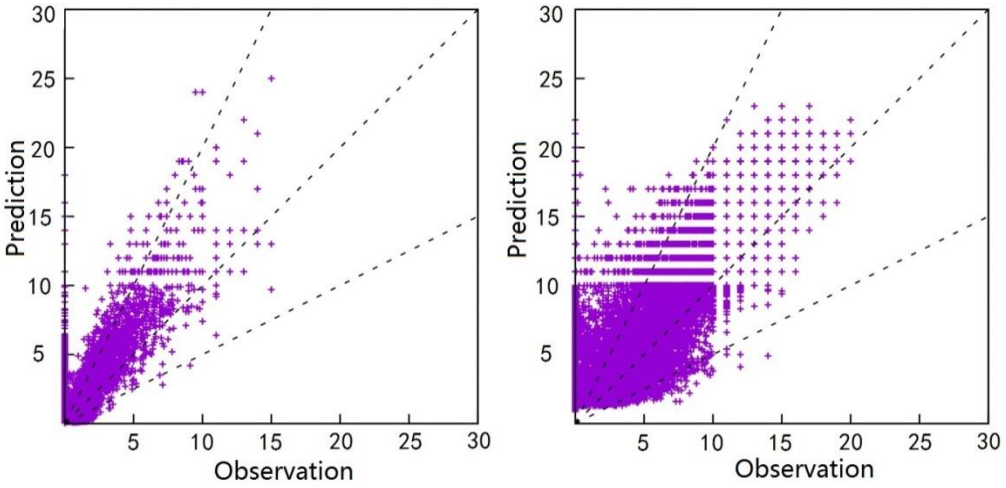

Figure 2- 6. Comparison of observed and predicted a) NO_2 and b) HCHO column densities; the units are in 10^{15} molecules cm^{-2}; the upper and lower dotted lines represent a prediction/observation ratio of 1:2 and 2:1, respectively.

Figure 2-6 compared the observation data and the predicted data from the CMAQ model of NO_2 and HCHO in August 2013. The model over-predicted NO_2 concentrations by approximately a factor of 1.5, compared with the observed NO_2 concentrations retrieved from the satellite. The result of over-prediction is opposite to that for the comparison of surface concentrations, which shows a general under-prediction of NO_2 concentrations. Under-prediction of surface layer NO_2 concentrations and the over-prediction of upper layer NO_2 concentrations can be attributed to over-prediction of power plant emissions and the incorrect vertical distribution of emitted NO concentrations. Total emissions from power plants were distributed into different model layers using a set of fixed layer distribution factors but the actual vertical distribution can be significantly affected the meteorological conditions and stack and exhaust parameters. Similar under-predictions of surface NO_2 and over-prediction of NO_2 column density has been reported. Kuhlmann et al. [31] compared the vertical column densities of NO_2 retrieved from the satellite data with their results of CMAQ modeling system from October 2006 to January 2007. The results of the model were found to overestimate the NO_2 VCD by approximately 15% in Hong Kong and Shenzhen, China.

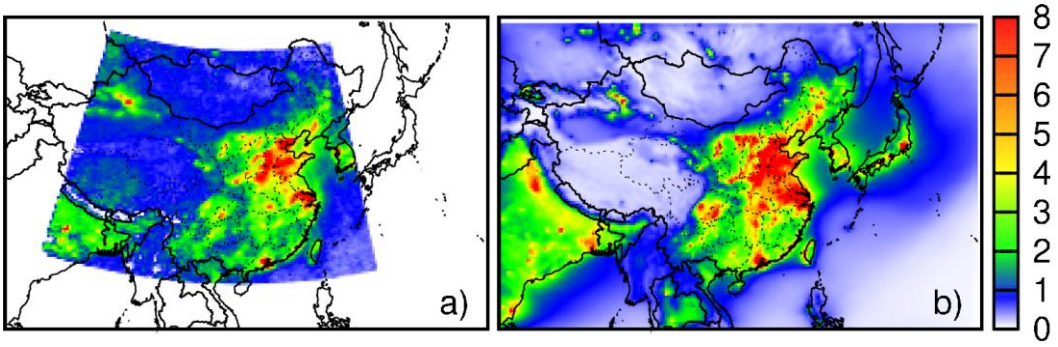

Figure 2- 7. a) Observed and b) predicted monthly averaged NO_2 concentration in August, 2013 over the model domain; the units are in 10^{15} molecules cm^{-2}.

Figure 2-7 shows the regional plots of predicted and observed monthly averaged NO_2 concentrations The distributions of NO_2 concentrations are generally similar. The regions where the highest NO_2 occurs are located surrounding the YRD, which are presented in both the results of satellite observation and CMAQ model simulation.

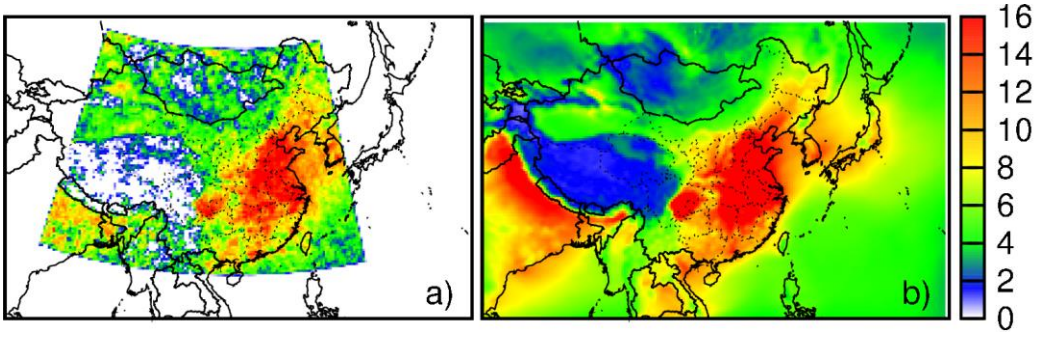

Figure 2- 8. a) Observed and b) predicted monthly averaged HCHO concentration in August, 2013 over the model domain; the units are in 10^{15} molecules cm^{-2}.

Figure 2-8 shows the regional plots of predicted and observed monthly averaged HCHO concentrations. The spatial distributions of HCHO column density are generally similar with wider distribution than that of NO_2. The regions where the highest HCHO

occurs are in eastern and central China and the Sichuan Basin, which are presented in both the results of satellite observation and CMAQ model simulation. The reasonable simulation performance of the CMAQ model on these two compounds provides confidence in the VOC incremental reactivity and source apportionment calculations.

The statistical model performance measures of mean normalized bias (MNB), mean normalized error (MNE), mean fractional bias (MFB) and mean fractional error (MFE) on NO_2 and HCHO column density using data at all grid cells are listed in Table 2-2. The statistical measures were calculated based on the observation and prediction data that are both higher than 7.5×10^{15} molecules cm^{-2}. The equations for the MNE, MNB, MFE and MFB calculations are shown in equations (2-3)-(2-6):

$$\mathrm{MNB} = \frac{1}{N}\sum_{i=1}^{N}\left(\frac{M_i - O_i}{O_i}\right) \times 100\% \quad (2\text{-}3)$$

$$\mathrm{MNE} = \frac{1}{N}\sum_{i=1}^{N}\left(\frac{|M_i - O_i|}{O_i}\right) \times 100\% \quad (2\text{-}4)$$

$$\mathrm{MFB} = \frac{1}{N}\sum_{i=1}^{N}\frac{(M_i - O_i)}{\frac{(M_i + O_i)}{2}} \quad (2\text{-}5)$$

$$\mathrm{MFE} = \frac{1}{N}\sum_{i=1}^{N}\frac{|M_i - O_i|}{\frac{(M_i + O_i)}{2}} \quad (2\text{-}6)$$

where N is the number of grid cells in the model domain; M_i and O_i are modeled and observed concentrations at the i^{th} grid cell, respectively. Based on these statistical values, NO_2 column density is over-predicted by approximately 28% with a normalized error of 36%. The HCHO predicted vertical column density has an over-prediction of 18% with a normalized error of 26%. Since a significant fraction of HCHO is produced by oxidation of isoprene, the isoprene emissions in the model might have been slightly over-predicted as well.

Table 2- 2. Model performance on NO_2 and HCHO in August, 2013

	NO_2	HCHO
MNB	0.279	0.177
MNE	0.357	0.260
MFB	0.193	0.132
MFE	0.282	0.231

2.4.2 Regional distribution of O_3

The CMAQ model predicted regional distribution of 8-hour maximum ozone for the base case simulation is shown in Figure 2-9(a). The right panel in Figure 2-9 shows the increase of the 8-hour maximum ozone concentrations between base case and VOC mixture case.

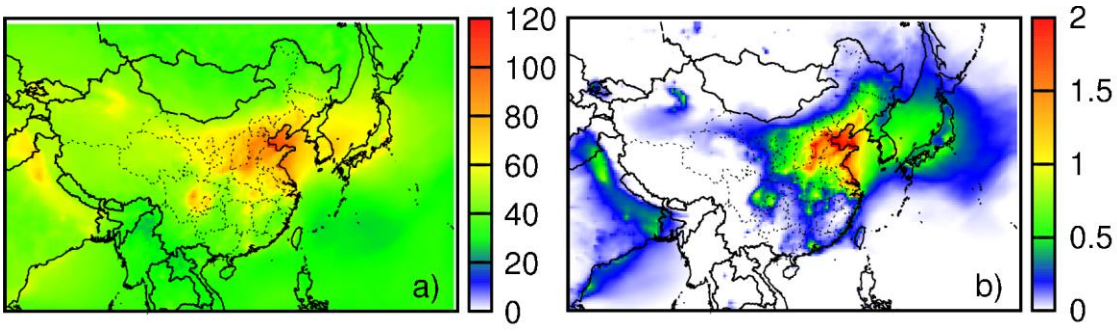

Figure 2- 9. a) 8-hr maximum ozone concentration of base case over the modeling domain; b) difference in ozone concentration of VOC mixture case and base case over the modeling domain. The units are in ppbV.

High ozone concentrations (over 60 ppb) occur in NCP, YRD, central China and in the Sichuan Basin near Chengdu and Chongqing, two major metropolitan areas in the region. The increase in VOC mixture concentrations leads to an increase in ozone formation in the areas where ozone formation is limited by the availability of VOC

species. The regions with higher base ozone concentrations tend to have higher incremental ozone concentrations.

2.4.3 Reactive VOC species with high NIR values

The change of daily 8-hour maximum ozone concentrations was used in equation (2-2) for NIR calculations. The VOC concentrations used in the calculation were the concentrations of the matching 8-hour with that of the maximum ozone concentrations. For each day, only the grid cells with ozone concentrations greater than 160 mg m^{-3} (approximately ~80 ppb), which is the Grade II standard for 8-hour maximum ozone set in the Chinese Ambient Air Quality Standards (GB3915-2012), were included in the analysis. By doing these, the results can be more focused on those regions with severe surface ozone pollution. The daily NIR values at each grid cell were then averaged to calculate the monthly NIR values for each species.

The regional distributions of monthly averaged NIR of the fifteen reactive species are shown in Figure 2-10. The ranking of species with concern was based on NIR_{50}, which is the median value of the monthly mean NIR for a given species at all grid cells. The numerical values of NIR_5, NIR_{25}, NIR_{50}, NIR_{75} and NIR_{95}, which represent the 5^{th}, 25^{th}, 50^{th}, 75^{th} and 95^{th} percentiles, are listed in Table B-1.

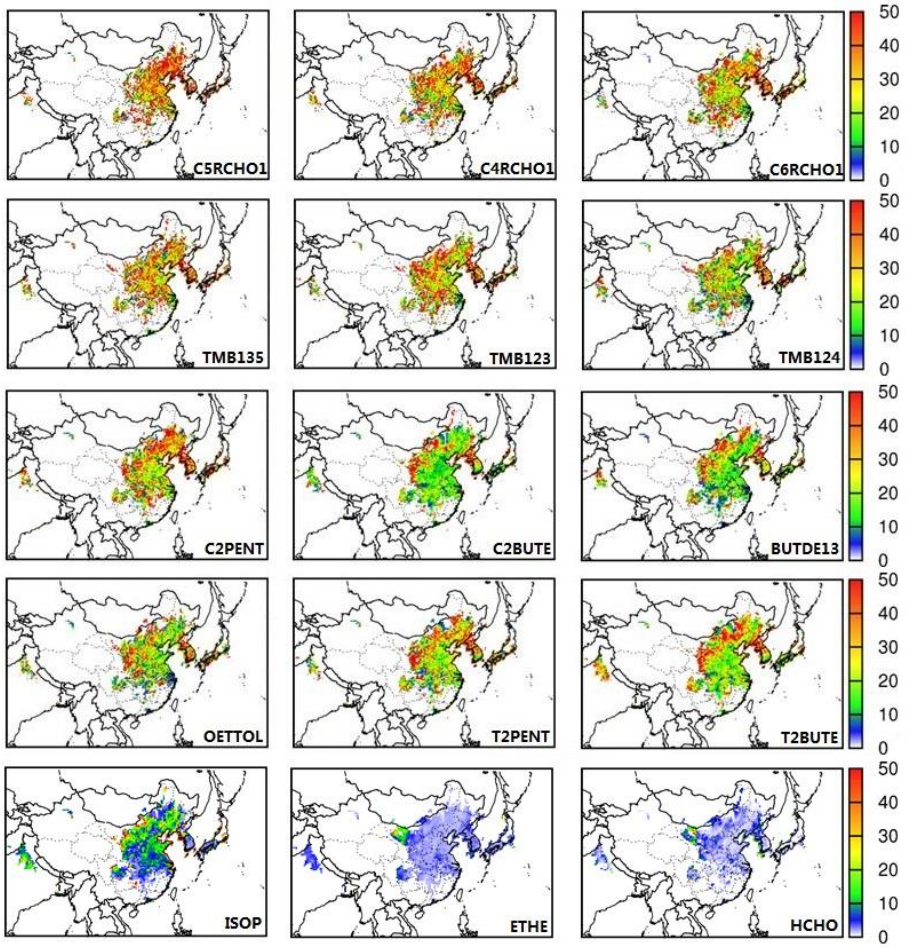

Figure 2- 10. NIRs of fifteen reactive anthropogenic VOC species. Figures are unit-less.

As shown in Figure 2-10, the three C4+ aldehyde species (butanal (NIR_{50}=30.5, NIR_{25}-NIR_{75}=18-44), pentanal (NIR_{50}=35.0, NIR_{25}-NIR_{75}=21-50) and hexanal (NIR_{50}=28.0, NIR_{25}-NIR_{75}=18-42)) rank high according to the value of NIR_{50}. 1,3,5-trimethyl benzene (NIR_{50}=30.5, NIR_{25}-NIR_{75}=18-44), cis-2-pentene (NIR_{50}=29.0, NIR_{25}-NIR_{75}=18-42), cis-2-butene (NIR_{50}=18.0, NIR_{25}-NIR_{75}=12-30) and 1,3-butadiene (NIR_{50}=19.0, NIR_{25}-NIR_{75}=12-32) have high values of NIR as well. These species are also top rank species based on the MIR values as reported by Carter [32]. Isoprene (NIR_{50}=9.0, NIR_{25}-NIR_{75}=4.0-16), ethene (NIR_{50}=2.0, NIR_{25}-NIR_{75}=1.8-3.0) and formaldehyde (NIR_{50}=1.8, NIR_{25}-NIR_{75}=1.0-3.2) are not among the species with high

values of NIR_{50}, while they are commonly considered as species have large contribution to ozone formation. Thus, the VOC emission rates need to be taken into consideration to determine the ozone-forming potential of individual VOC species. The listed species tend to be more reactive than others. When VOC control strategies need to be made, these species should be considered primarily.

2.5 Conclusions

In this Chapter, it was found that NCP, YRD, central China and the Sichuan Basin are experiencing severe ozone problems in August, with 8-hour maximum concentration exceeding the CNAAQS Grade II standard. Ozone formation in these regions appears to be VOC-limited, based on a sensitivity simulation that increases the VOC emissions by 10%, suggesting that VOC control is the key strategy in reduction of ozone formation. The CMAQ model was applied to study the incremental reactivity of 66 VOC species through a series of sensitivity simulations. Based on the NIR results of concerned VOC species in major cities in China, we found that the three C4+ aldehydes species (butanal, pentanal and hexanal) are highly reactive. Cis-2-pentene, cis-2-butene, 1,3-butadiene and trimethyl benzenes are also reactive. The possible strategies on control of these species are worthy of consideration in ozone mitigation strategies. The NIR values reported in this analysis is for one month period only and didn't consider the difference in the VOC emission rate, which is needed when calculating the actual ozone-forming potential (OFP). As different sources have different compositions of primary VOCs, contributions of different emission sources to observed ozone concentrations needs to be quantified. It is also necessary to compare the predicted NIR values with the MIR values (and relative MIR values) derived from photochemical box model simulations. These problems will be further explored in Chapters 3 and 4.

3. THE PHOTOCHEMICAL BOX MODEL AND MIR CALCULATION

3.1 Introduction

Among the various IR metrics, the maximum incremental reactivity (MIR) corresponds to the conditions where NO_x concentrations are adjusted to a high level for the base VOC mixture to have the highest IR. It reflects relatively high NO_x conditions where ozone formation is most sensitive to VOC emissions, which might be found in many urban areas.

The MIR metric for 118 VOCs was originally reported by Carter [33] based on an earlier version of the SAPRC photochemical mechanism. Updates to the MIR metric using newer versions the SAPRC mechanism were subsequently published [32, 34, 35]. The MIR metric has been widely applied to evaluate ozone formation potentials in China [15, 36, 37]. However, as discussed in Carter [33], the MIR values depend on the composition of the base VOC mixture. It is unknown whether the MIR values reported by Carter, which were based on a base mixture that represent VOC composition in US cities in the early 1990s, are applicable to Chinese conditions, due to different compositions of VOC mixture and other factors. Thus, in this study, the MIR values of 66 VOC species (see Table A-1) are updated using calculated based VOC mixture concentrations in China.

3.2 Box model for MIR calculations

A photochemical box model with a detailed chemical mechanism (SAPRC-07, or S07) was developed by Carter [26] to quantify the reactivity of various VOC species. The box model simulates how ozone formation would be affected by changes of the inputs of reactive organic gases (ROG) in one day episodes. The inputs to the model include initial fractions and emitted rate of ROGs and NO_x, time-varying changes in

humidity and temperature, inversion heights and entrainment of pollutants from aloft as the mixing height rises throughout the day.

3.2.1 Input files preparation

The files and programs necessary to run box model simulations with the S07 chemical mechanism (http://www.engr.ucr.edu/~carter/SAPRC/SAPRCfiles.pdf) prepared by Carter were modified to simulate reactivity of various VOC species for different cities in China. The file descriptions and the steps for the simulations are listed in Table 3-1.

Table 3- 1. Files used to run reactivity scale calculations with the SAPRC-07 mechanism [38]

File(s) name	Description
ARBMIX1.CMP	Composition of base ROG mixture of model species.
SCENARIO.PRM	Defines the total emission rate of HC and NO_x and aloft ozone concentrations for the base case for the city-specific scenarios.
*.INP	Input files for a particular base case reactivity scenario. Include the parameters of initial fractions and emission rate of ROG and NO_x, time-varying changes of humidity and temperature, inversion height and entrainment of pollutants from aloft as the height raises throughout the day.
LUMPALL.BAT	Prepares lumped VOC and mixture mechanism files needed for reactivity simulations. Need to be called once ARBMIX1.CMP, SCENARIO.PRM or *.INP is modified.
BASECALC.BAT	Used to run base case calculations for a type of NO_x condition, then find MIR NO_x level and run base case with the MIR NO_x condition.
RCTALL.BAT	Runs reactivity calculations and prepares a reactivity list of all VOCs for a given scenario*.
*.CLC	Contains reactivity calculation results for a given scenario.

* "scenarios" in this study refers to different cities.

The detailed description of parameters included in the input files is listed in Table C-1, Table C-2 and Table C-3. The values retrieved from the city of Nanjing are used as an example to show how the emission files were prepared.

In this study, monthly-averaged VOC concentrations at each hour predicted by the CMAQ model, as described in Chapter 2 were used to prepare the city-specific base ROG mixture. Emission rates of NO_x and VOCs were taken from the CMAQ emission input files and mixing height, temperature and relative humidity were taken from the meteorological input files used in the CMAQ simulations. These input data were also averaged to determine monthly average values for each hour. The city names and the city center longitude and latitude used to extract data from the CMAQ files are listed in Table D-1. The description of parameters determined in the input files and the files in the CMAQ model that contain the corresponding information are listed in Table 3-2.

Table 3- 2. Description of parameters in the input files and the corresponding CMAQ model input files used

Parameter name in the box model	**Description**	**File(s) for determination**
INI.HC	Fraction of the total ROG that is present initially.	ACONC[a]; METCRO2D[b]
INI.NOX	Fraction of the total NOx that is present initially.	ACONC; METCRO2D
TEMPR	Time-varying temperature in K from hour 08 to 18, local time.	METCRO3D[c]
H_2O	Time-varying humidity in ppm.	METCRO3D
HEIGHT	Time-varying mixing height in m.	METCRO2D
EMR.HC	Fraction of the total ROG emitted per hour in min^{-1}.	MEGAN[d]
EMR.NOX	Fraction of the total NOx emitted per hour in min^{-1}.	EMIS[e]

Table 3-2. Continued

CO	Time-varying carbon monoxide concentrations in 10^{-3} moles m^{-2} throughout the day.	EMIS[e]
ISOP	Time-varying isoprene concentrations in 10^{-3} moles m^{-2} throughout the day.	MEGAN
APIN	Time-varying terpene concentrations in 10^{-3} moles m^{-2} throughout the day.	MEGAN
UNKN	Time-varying concentrations of other biogenic ROG in 10^{-3} moles m^{-2} throughout the day.	MEGAN
E.HC	Emitted HC concentration in 10^{-3} moles m^{-2}.	Calculated
E.NOX	Emitted NOx concentration in 10^{-3} moles m^{-2}.	Calculated
ALO.O3	Aloft ozone concentration in ppm.	METCRO3D; ACONC
Fractions of NMHC species	Mole fractions of carbon numbers of individual VOC in the base ROG mixture.	ACONC; METCRO2D
Fractions of oxygenate species	Mole fractions of carbon numbers of oxygenate VOC in the base ROG mixture.	ACONC; METCRO2D

a. ACONC files: the 3-D CMAQ Chemistry-Transport Model (CCTM) hourly average concentration files that contain average model species concentrations for each model hour.
b. METCRO2D files: the time-dependent files that contain surface and other 2-D meteorological fields at cross points.
c. METCRO3D files: the time-dependent files that contain 3-D meteorological descriptions at cross points.
d. MEGAN files: the typed emission files that split the species in the original emission files into two sources: biogenic sources (typed one) and other sources (non-typed one).
e. EMIS files: the emission files that sort the emitted gas-phase species by grid cell and time.

3.2.2 Uncertainty analysis

Once the input files for the cities in China were prepared, the reactivity calculations for the 66 VOC species listed in Table A-1 could be done for each city. The input ROG and NO_x concentrations and meteorological conditions are taken from model simulations instead of field observations, thus all have uncertainties associated with

them. Among the parameters defined in the input files, mixing height was expected to have a significant influence on predicted ozone concentrations as the growth of the mixing height leads to entrainment of the aloft air, which often has different chemical composition from the air in the surface layer [39]. Among the aloft air species, ozone is typically in higher concentrations and has more influence on the chemical processes in the box model than other aloft species included. Thus, the uncertainty in aloft ozone concentrations and mixing heights is taken into consideration in this study. Additionally, total emission rate of anthropogenic VOCs and NO_x is known to have significant uncertainties and is also considered in the uncertainty analysis.

In this study, these input values are considered as random variables that follow a normal distribution. Derwent and Hov [39] applied relative uncertainties of ±50%, ±20% and ±30% in aloft ozone, concentrations, boundary layer depth and anthropogenic hydrocarbons (HC) and NO_x emissions for their photochemical ozone model. These values were applied in uncertainty analysis in this study. A Monte-Carlo simulation technique [40] was used to determine the uncertainty in the predicted MIR values by running the box model MIR calculations for each city multiple times. In each Monte-Carlo simulation, the values of one or more of the input parameters with uncertainties were randomly scaled based on the prescribed uncertainty values. The mean and standard deviation of the resulted multiple MIR values were then determined. The number of simulations was adjusted so that additional simulations did not lead to significant changes in the mean and standard deviation. Test runs in this study shows that 100 Monte-Carlo simulations are sufficient to get a stable mean and standard deviation.

3.3 Results and discussion

3.3.1 Variation of MIR among different cities

The MIR calculations were performed for 34 provincial capital cities in China. The averaged MIR and its standard deviation for each species were calculated and

compared with those reported for 39 cities in the United State by Carter [32], as shown in Figure 3-1. The mean MIR of the ROG mixture for each city can be found in Table E-1.

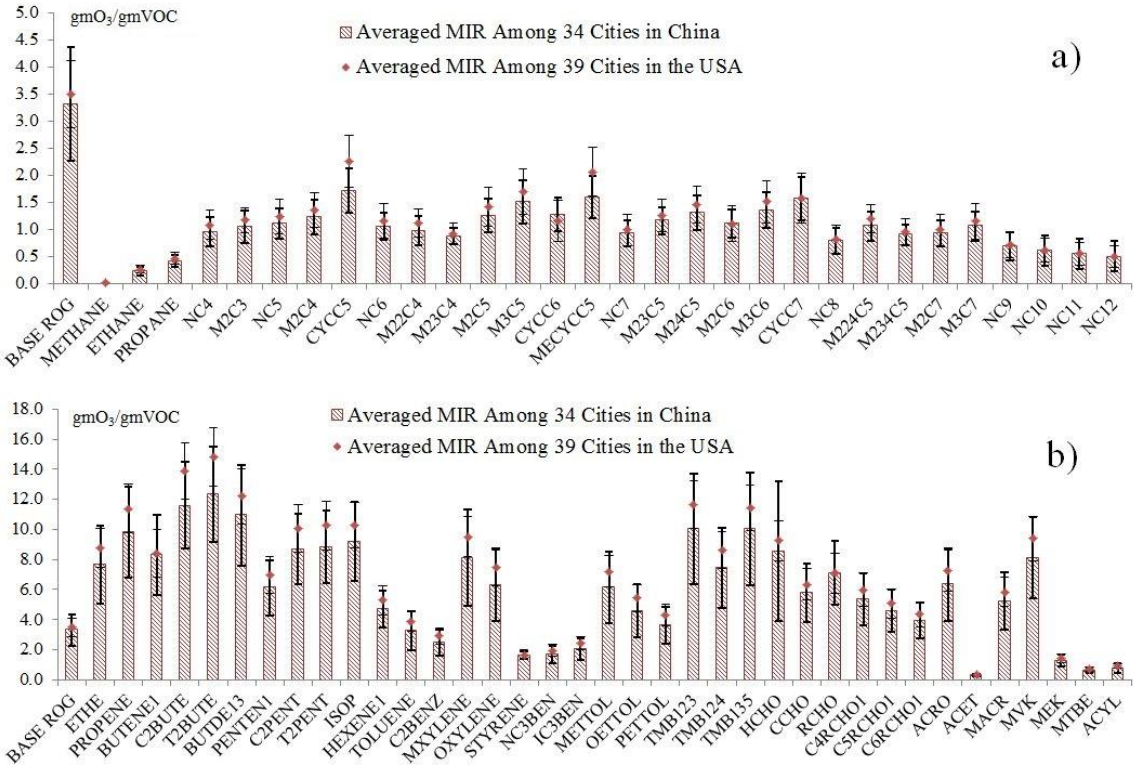

Figure 3- 1. Mean MIRs of a) alkanes and b) alkenes and aromatic VOCs based on the MIR values for 34 provincial capital cities in China and 39 major cities in US. The error bars represent one standard deviation around the mean.

Trans-2-butene (T2BUTE) is the most reactive species among the studied VOCs, with an averaged MIR of 12.337±3.177 gram O_3/gram VOC. Relative uncertainty based on one standard deviation is 25.8%. The relative uncertainty of MIRs of different species vary between 15.9% and 56.7%, which can be attributed to the large variation in the composition of the base ROG mixtures of different cities and hourly VOC emission profiles. The general rankings of MIRs and their absolute values between the US cities

and Chinese cities are similar, with most of them within the range of error bounds of each other, except for the value of cyclopentane (CYCC5) and methyl-cyclopentane (MECYCC5).

3.3.2 Uncertainty in the calculated MIRs

The relative uncertainty of MIR values (ratio of standard deviation to mean value) for each VOCs in Nanjing, China are listed in Table 3-3 to illustrate how these four uncertain parameters affect the MIR of VOC species. An additional set of calculations were conducted by allowing the four parameters to change simultaneously in Monto-Carlo calculation so that the overall uncertainty due to all four parameters can be explored. For the simulation that changes the hourly emission fractions of hydrocarbon (E.HC) and NOx (E.NO_x), only the total amount of emissions were changed. This would also change the fraction of HC and NO_x from the initial conditions. However, the diurnal variation of the emissions remains unchanged.

Table 3- 3. Relative uncertainty of MIR in Nanjing ($\sigma MIR/\overline{\mathbf{MIR}}$) due to each uncertain parameter

Species	**Aloft O_3**	**E.HC**	**E.NOx**	**Mixing Height**	**Combined**
ETHANE	2.94%	5.88%	0.94%	8.82%	8.82%
PROPANE	3.79%	5.73%	0.00%	10.96%	10.95%
NC4	3.60%	5.40%	1.31%	9.50%	9.47%
M2C3	3.58%	5.47%	1.27%	10.21%	10.17%
NC5	3.40%	5.04%	1.09%	8.46%	8.52%
M2C4	3.84%	5.54%	0.85%	10.10%	10.10%
CYCC5	3.41%	5.24%	1.12%	9.63%	9.61%
NC6	3.25%	4.92%	0.93%	9.33%	9.38%
M22C4	4.57%	5.73%	0.70%	10.06%	10.28%
M23C4	3.42%	5.24%	1.21%	9.48%	9.42%
M2C5	3.80%	4.84%	0.90%	7.51%	7.88%

Table 3-3. Continued

Species	Aloft O_3	E.HC	E.NOx	Mixing Height	Combined
M3C5	3.37%	5.09%	0.91%	9.91%	9.94%
CYCC6	3.41%	5.22%	0.79%	9.91%	9.89%
MECYCC5	4.18%	5.46%	0.83%	9.98%	10.16%
NC7	3.20%	4.77%	1.00%	9.39%	9.47%
M23C5	5.48%	5.75%	0.62%	9.92%	10.56%
M24C5	3.69%	5.01%	1.17%	8.81%	9.02%
M2C6	3.18%	4.98%	0.79%	9.26%	9.23%
M3C6	4.43%	5.42%	0.73%	9.78%	10.08%
CYCC7	3.55%	5.11%	0.97%	9.84%	9.94%
NC8	4.49%	4.44%	0.74%	8.63%	9.44%
M224C5	6.70%	5.91%	0.61%	9.89%	11.18%
M234C5	3.16%	4.93%	1.21%	8.73%	8.71%
M2C7	4.28%	5.07%	0.73%	8.75%	9.17%
M3C7	5.55%	5.57%	0.85%	9.82%	10.59%
NC9	5.04%	5.45%	1.01%	9.89%	10.44%
NC10	7.92%	5.92%	0.92%	9.93%	11.92%
NC11	8.96%	5.95%	1.19%	10.01%	12.67%
NC12	9.83%	5.99%	1.18%	10.08%	13.32%
ETHE	3.24%	4.07%	0.82%	6.80%	7.50%
PROPENE	4.07%	3.19%	1.20%	5.83%	6.49%
BUTENE1	2.26%	3.04%	1.19%	6.81%	7.79%
C2BUTE	2.76%	2.85%	1.45%	4.61%	5.06%
T2BUTE	3.52%	2.83%	1.48%	4.32%	4.97%
BUTDE13	3.52%	2.57%	1.41%	5.58%	6.47%
PENTEN1	3.20%	3.04%	1.17%	6.90%	7.62%
C2PENT	3.43%	2.73%	1.36%	5.79%	6.48%
T2PENT	2.95%	2.73%	1.37%	5.66%	6.43%
ISOP	3.57%	2.62%	1.41%	5.42%	6.07%
HEXENE1	2.39%	3.17%	1.06%	7.01%	7.31%

Table 3-3. Continued

Species	Aloft O_3	E.HC	E.NOx	Mixing Height	Combined
TOLUENE	4.77%	4.51%	0.81%	8.72%	9.54%
C2BENZ	4.12%	4.62%	0.72%	8.82%	9.31%
MXYLENE	6.00%	3.08%	1.51%	5.72%	8.05%
OXYLENE	5.32%	3.65%	1.20%	7.08%	8.59%
STYRENE	2.06%	2.45%	1.77%	4.92%	5.64%
NC3BEN	3.87%	4.87%	0.69%	9.25%	9.54%
IC3BEN	4.13%	4.69%	0.72%	8.95%	9.42%
METTOL	5.62%	3.32%	1.36%	6.27%	8.17%
OETTOL	5.01%	3.86%	1.07%	7.48%	8.72%
PETTOL	3.98%	4.04%	0.99%	7.69%	8.35%
TMB123	6.39%	2.78%	1.61%	5.20%	7.97%
TMB124	5.22%	2.87%	1.46%	5.59%	7.45%
TMB135	6.95%	2.55%	1.71%	4.31%	7.85%
HCHO	10.65%	2.68%	1.64%	1.93%	10.27%
CCHO	4.46%	2.60%	1.32%	5.75%	7.17%
RCHO	3.58%	0.93%	0.33%	5.73%	7.93%
C4RCHO1	3.38%	1.01%	0.33%	5.71%	7.73%
C5RCHO1	3.02%	1.08%	0.34%	5.66%	7.39%
C6RCHO1	2.79%	1.10%	0.34%	5.59%	7.17%
ACRO	5.24%	2.54%	1.44%	6.76%	8.47%
ACET	4.72%	3.44%	0.98%	6.89%	8.21%
MACR	4.84%	2.34%	1.47%	5.60%	7.29%
MVK	3.90%	3.01%	1.27%	6.31%	7.28%
MEK	4.34%	3.20%	0.84%	7.40%	8.39%
MTBE	3.37%	5.12%	1.01%	8.33%	8.34%
ACYL	5.47%	5.09%	0.99%	8.75%	9.83%

From Table 3-3, it can be seen that the mixing height is the most important factor that affects MIR, followed by the total amount of emitted HC and aloft ozone concentrations. The MIR values are not sensitive to the total emitted NO_x, since they were determined under high NO_x conditions. In general, the uncertainty in the predicted MIR due to assumed uncertainties in these four parameters are less than 10%.

The averaged MIRs for the city of Nanjing and their respective ranges based on the combined uncertainty of these four factors are shown in Figure 3-2. For comparison, mean values from 39 US cities shown in Figure 3-1 were reproduced in this figure. Generally, the MIR of each species in Nanjing is approximately 15% lower than that for average US cities.

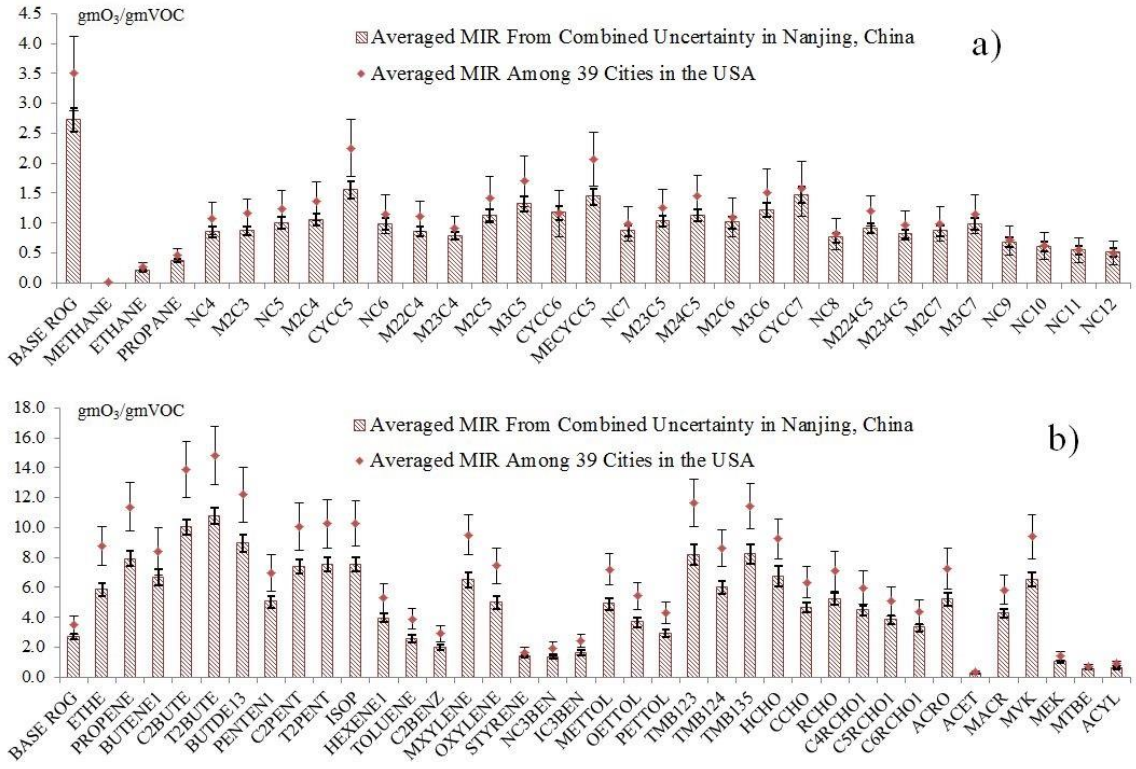

Figure 3- 2. Averaged MIR of a) alkanes and b) alkenes and aromatic VOCs based on combined uncertain parameters in Nanjing, China

3.3.3 Comparison of regional NIRs with box model MIRs

The NIRs of reactive species from CMAQ model was compared with the normalized MIRs of the same species from the box model, as shown in Figure 3-4. The MIRs of each species were normalized with the MIR of base VOC mixture.

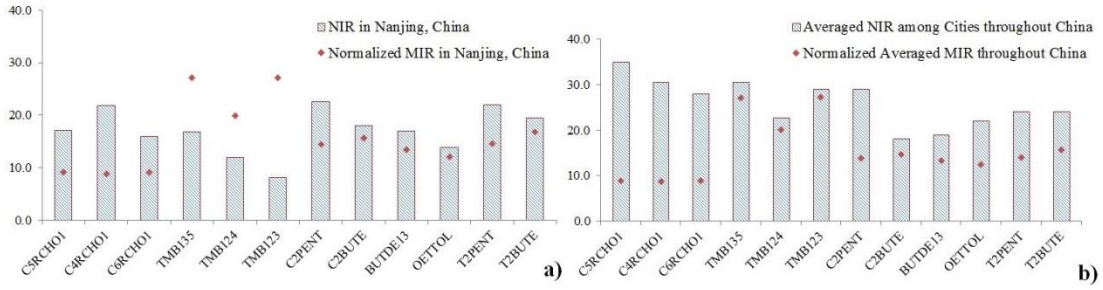

Figure 3- 3. Comparison of NIRs and normalized MIRs in a) Nanjing; b) averaged cities in China. Figures are unit-less.

It can be seen that except for 1,2,3-trimethyl benzene, 1,2,4-trimethyl benzene and 1,3,5-trimethyl benzene, the NIRs of remaining species are higher than that of the normalized MIR values. The exclusion of isoprene from the VOC mixture case can be the reason for high NIR values from the regional model results. Removal of isoprene in the VOC mixture would lead the mixture to be less reactive than that with isoprene included. Thus, the normalized incremental reactivity would be higher than the reactivity that is normalized by a VOC mixture with isoprene included.

3.4 Conclusions

Trans-2-butene, cis-2-butene, 1,3-butadiene, 1,2,3-trimethyl benzene and 1,3,5-trimethyl benzene are among the most reactive VOCs. However, to make an effective VOC control strategy, the total emission of VOCs should be considered as well. A

concept of ozone-forming potential (OFP) defined by Chang et al. [41] was referred in this study to calculate the per-carbon OFPs of VOC species using equation (3-1):

$$\mathrm{COFP_i} = \mathrm{MIR_i} \times \frac{\mathrm{CC_i}}{\mathrm{CC_e}} \quad (3\text{-}1)$$

where $COFP_i$ refers to the concentration-based ozone-forming potential per carbon of the i^{th} VOC species; MIR_i refers to the MIR of the i^{th} VOC species in $gO_3/gVOC$; CC_i refers to the molar concentration of carbon number of the i^{th} VOC species in ppbC; CC_e refers to the molar concentration of carbon number of the VOC mixture in ppbC.

The ambient VOC concentrations represent the concentrations after a series of reactions as shown in (R1-4) and (R1-5). Some reactive species with large amount of emissions, like isoprene, would be consumed more significantly than less reactive species with lower amount of emissions, and end up with similar ambient concentrations. Hence, the initial emission rates of species should be taken into consideration for OFP evaluation. A concept of emission-based OFP (EOFP) is calculated using equation (3-2):

$$\mathrm{EOFP_i} = \mathrm{MIR_i} \times \frac{\mathrm{EC_i}}{\mathrm{EC_e}} \quad (3\text{-}2)$$

where $EOFP_i$ refers to the emission-based ozone-forming potential per carbon of the i^{th} VOC species; MIR_i refers to the MIR of the i^{th} VOC species in $gO_3/gVOC$; EC_i refers to the emission rate of carbon number of the i^{th} VOC species in kmolC/day; EC_e refers to the molar concentration of carbon number of the VOC mixture in kmolC/day.

Table 3-4 lists the COFP and EOFP values of top 16 VOC species, from high to low based on EOFPs. The concentrations and emission rates of VOCs are in Nanjing. We can see that even though trans-2-butene and cis-2-butene are the most reactive VOCs, there emission amounts are relatively low compared with that of isoprene and m-xylene. Isoprene and m-xylene are not the most reactive species. However, considering the high amount of emissions of these species, the reduction on emission of these species should be given priority.

Table 3- 4. Ozone-forming potentials per carbon of top 16 VOC species

Species	MIR (gO_3/gVOC)	Carbon Number	Conc. (ppb)	COFP	Emission (kmol/day)	EOFP
ISOP	10.840	5	1.309	0.724	36049.8	3.801
MXYLENE	14.450	8	0.553	0.652	2872.4	0.646
TOLUENE	4.871	7	1.595	0.555	6607.8	0.438
PROPENE	6.994	3	1.372	0.294	7015.1	0.286
ETHE	3.418	2	3.215	0.224	13196.6	0.175
T2BUTE	12.850	4	0.113	0.059	1646.3	0.165
OXYLENE	11.120	8	0.183	0.166	879.1	0.152
C2BUTE	11.920	4	0.107	0.052	1334.4	0.124
TMB124	15.140	9	0.053	0.073	287.8	0.076
BUTENE1	7.875	4	0.186	0.060	964.2	0.059
CCHO	4.293	2	2.304	0.202	2879.2	0.048
TMB123	20.630	9	0.024	0.046	132.9	0.048
METTOL	12.310	9	0.044	0.050	221.8	0.048
TMB135	20.680	9	0.021	0.041	130.8	0.047
T2PENT	11.160	5	0.030	0.017	414.5	0.045
CYCC6	2.039	6	0.311	0.039	1320.0	0.031

4. OZONE SOURCE APPORTIONMENT IN CMAQ

4.1 Introduction

Photochemical formation of ozone depends on the availability of NO_x and VOCs. The major sources of NO_x and VOCs in a polluted urban atmosphere can be quite different. For example, while coal-fired power plants can be a significant source of NO_x in downwind regions, their emissions of VOCs are usually much smaller than other fuel combustion sources. While gasoline vehicles are important sources of VOCs, their NO_x emissions are typically lower than those of diesel vehicles. Some industrial sources such as oil refineries can be large emitters of VOCs. The reactivity of VOCs from different sources can also be quite different. For example, emissions from solvent utilizations are often small alkanes that have low ozone incremental reactivity. VOC emissions from vehicles and oil refineries are much more reactive due to higher fractions of aromatics and unsaturated hydrocarbons such as alkenes.

The formation rate of ozone in the ambient environment depends not only on the reactivity of VOCs, but also the relative abundances of NO_x and VOCs. In the VOC-limited regime, control of VOCs emissions is more effective in reducing ozone concentration by reducing the production of peroxy radicals, which are necessary for the conversion of NO to NO_2 and continuous production of ozone. A larger fraction of the $OH\cdot$ radical is lost through reaction with NO_2 to form HNO_3. In contrast, reduction of NO_x in the VOC-limited region will lead to less ozone titration by NO and lead to an increase in net ozone formation [8]. In the NO_x-limited regime, the NO to NO_2 conversion rate is largely controlled by availability of NO. The reduction of NO_x in this regime reduces the photolysis rate of NO_2 and thus the production of ozone. Analyses that aim to quantify the source contributions to ozone need to consider the reactivity of individual VOCs, sources of VOCs and NO_x as well as the ozone formation regime.

Field measurements and modeling studies have shown that ozone formation in urban areas in China is mostly VOC-limited while its formation in rural areas is mostly

NO_x-limited. For example, Liu et al. [42] characterized NO_x and detailed VOC concentrations in Tianjin, China from November 2014 to October 2015, and determined that Tianjin was a VOC-limited region based on the observed VOC/NO_x ratio. The major sources of VOCs were automobile exhaust and industrial emissions based on a receptor modeling analysis. Li et al. [43] applied the Ozone Source Apportionment Technique (OSAT) with tagged tracers coupled with a regional chemical transport model (CTM), the Comprehensive Air Quality Model with Extensions (CAMx), to study the source contribution to surface ozone in Yangtze River Delta (YRD), China in summer of 2013. The results showed that ozone formation was mainly VOC-limited in urban areas. Industry and vehicle exhaust were the most significant anthropogenic emission source sectors contributing to ozone pollution.

The studies reported in the literature are focused on a specific region in China and a complete source apportionment analysis of ozone in the entire country is still lacking. In our study, a new reactive tagged species method that tags ozone precursors and their intermediate oxidation products from each emission sector was developed to determine the contributions of NO_x and VOC to surface ozone formation in China from residential, power generation, industries, transportation, wildfire and biogenic sources.

4.2 Methodology

4.2.1 Source-oriented SAPRC-99 mechanism for ozone source apportionment

In previous ozone source apportionment studies using regional CTMs, source contributions to ozone under VOC-limited conditions were based on ratios of the maximum incremental reactivity (MIR) weighted concentrations of ozone precursors from different sources. However, intermediate products from VOC oxidation precursors such as formaldehyde and methacrolein can also contribute to ozone formation at a given model time step. Thus, to fully account for the source contributions, it is necessary to also track the sources of VOC oxidation products in the photochemical mechanisms.

A more detailed reactive tagged species method was developed by implementing tagged chemical reactions based on the SAPRC-99 (S99) photochemical mechanism [44]. The reactive tagged species approach has been applied previously to the NO_x related reactions [45] for source apportionment of nitrate aerosol [46] and ozone formation under NO_x-limited conditions [45], and to the VOC related reactions for source apportionment of VOCs and ozone formation in VOC-limited urban areas [47], respectively. In this study, reactive nitrogen species and VOC species related with ozone formation are all tagged in the source-oriented mechanism, thus allowing a complete ozone source apportionment analysis. The reactive tagged species approach used in this study is briefly summarized below. For simplicity, the expanded mechanism only includes one explicit source. The rest of the emissions from other sources are lumped together during emission processing and are represented by non-tagged species. However, the same approach can be expanded to include multiple sources.

Reactions involving NO_x without VOCs were expanded into two reactions by adding a similar reaction with NO_x and their reactive products tagged (e.g. R4-1 for the HONO formation reaction):

$$\mathrm{OH\cdot + NO = HONO}$$
$$\mathrm{OH\cdot + NO^{X1} = HONO^{X1}} \qquad \text{(R4-1)}$$

The superscript X1 denotes species from the explicit emission source X1. Similarly, reactions involving VOCs without organic nitrogen in them were expanded into two reactions by adding a similar reaction with precursor VOCs and their reactive products tagged (e.g. R4-2 for the NO oxidation by methyl peroxy radicals):

$$\mathrm{C\_O_2 + NO = NO_2 + HCHO + HO_2}$$
$$\mathrm{C\_O_2{}^{X1} + NO = NO_2 + HCHO^{X1} + HO_2{}^{X1}} \qquad \text{(R4-2)}$$

Reactions involving species with organic nitrogen were expanded into four reactions. For example, the formation reaction of peroxyacyl nitrate (PAN) can be expanded as R4-3:

$$\mathrm{CCO\_O_2 + NO_2 = PAN}$$
$$\mathrm{CCO\_O_2 + NO_2{}^{X1} = PAN^{X0\_1}}$$

$$CCO\_O_2^{X1} + NO2 = PAN^{X1\_0}$$

$$CCO\_O_2^{X1} + NO_2^{X1} = PAN^{X1\_1} \quad \text{(R4-3)}$$

The numbers 0 and 1 in the superscript denote the contributions of either nitrogen or organic components from the lumped and explicit sources, respectively.

As the source-oriented mechanism is prepared from the base mechanism by hand, quality assurance steps are needed. To test whether the source-oriented mechanism is correctly prepared to simulation ozone formation and to keep track of the tagged and non-tagged VOC and NO_x species properly, two simulations were conducted. First, ozone concentrations were simulated with source-oriented mechanism with regular emission files (i.e. all emissions go to the non-tagged species). In a second simulation, all emissions were treated as if they were from one explicit source and there were no emissions for the lumped source. The results from the two sets of simulations were compared with the base case simulation with the original S99 mechanism. Both simulations led to identical ozone concentrations as the base case model. Therefore, this exercise provides confidence that the source-oriented mechanism is appropriately for the subsequent ozone source apportionment analysis.

4.2.2 O_3 sensitivity regime determination

A number of different indicators have been proposed to determine whether ozone formation in a grid cell is NO_x-limited or VOC-limited at a given time step. Ozone formation under NO_x-limited or VOC-limited conditions will be attributed to NO_x or VOC sources solely. A summary of these indicators reported in the literature is given in Table 4-1. The second indicator is based on the formation rates of hydrogen peroxide (H_2O_2), peroxide (ROOH) and nitric acid (HNO_3). The remaining indicators are based on the concentrations of relating species.

Table 4- 1. Regime indicators and threshold values

Indicators	NOX-limited	VOC-limited	References
H_2O_2/HNO_3	≥0.2	<0.2	[48]; [49]; [50]; [51]; [52]; [53]
$(P_{H2O2} + P_{ROOH}) / P_{HNO3}$	≥0.5	<0.5	[54]
$H_2O_2/(O_3 + NO_2)$	≥0.02	<0.02	[55]
NO_y [a]	≤20 ppb	>20 ppb	[56]; [48]; [50]; [57]
O_3/NO_x	≥15	<15	[51]; [55]; [53]
O_3/NO_y	≥7	<7	[49]; [53]
O_3/NO_z [b]	≥7	<7	[48]; [50]; [53]
$HCHO/NO_y$	≥0.28	<0.28	[48]; [50]
$HCHO/NO_2$	≥1	<1	[55]; [58]

a. $NO_y = NO_x$ + nitrogen trioxide (NO_3) + dinitrogen pentoxide (N_2O_5) + nitrous acid (HONO) + nitric acid (HNO_3) + pernitric acid (HNO_4) + peroxyacyl nitrate (PAN) [59]
b. $NO_z = NO_y - NO_x$ [59]

In our research, two indicators were applied. The first indicator is based on the NO to NO_2 conversion rate as shown in equation (4-1). As pointed out by Krish0 and Ying [47], ozone formation rate in regional models show a clear linear dependence on how fast NO_2 is regenerated from NO by the HO_2 and RO_2 radicals.

$$I1 = \frac{P_{NO_2|HO_2}}{P_{NO_2|HO_2} + P_{NO_2|RO_2}} \quad (4\text{-}1)$$

In the above equation, $P_{NO_2|HO_2}$ is the formation rate of NO_2 due to $HO_2 \cdot$ reaction with NO; $P_{NO_2|RO_2}$ is the formation rate of NO_2 due to $RO_2 \cdot$ reaction with NO. Under NO_x-limited conditions, there are sufficient amounts of VOCs to react with OH radicals. The concentration of RO_2 radicals, which represent first generation peroxy radicals from the oxidation of parent VOCs, is expected to be higher than that of HO_2 radicals, which are generated in subsequent reactions of the RO_2 radicals. Hence, in this study, regions with I1 <0.5 are considered as NO_x-limited, and regions with I1 ≥0.5 are considered as VOC-limited. The second parameter is the ratio of peroxides to nitric acid formation rate as shown in equation (4-2).

$$I2 = \frac{P_{H_2O_2} + P_{ROOH}}{P_{HNO_3}} \quad (4\text{-}2)$$

In the above equation, $P_{H_2O_2}$ is the formation rate of hydrogen peroxide (H_2O_2); P_{ROOH} is the formation rate of peroxide (ROOH); P_{HNO_3} is the formation rate of nitric acid (HNO_3). This is the indicator used in OSAT in the CAMx model. It is based on the idea that under NO_x-limited conditions, the formation rate of HNO_3 from NO_2 and $OH\cdot$ is slower than the formation of peroxides, which is due to the reactions of organic peroxides with HO_2. If I2 $\leq$0.5, ozone formation is determined as VOC-limited; if I2 > 0.5, ozone formation is determined as NO_x-limited. The cut-off value of 0.5 used for I2 has been evaluated in a study in California [55]. However, the appropriateness of using the same cut off value in China needs to be carefully tested. The formation rates needed for equations (3) and (4) are determined using the Integrated Reaction Rate (IRR) analysis tool in CMAQ [60]. A full description of the reactions included in the IRR analysis is listed in Table H-1.

4.2.3 Attribution of ozone formation to NO_x or VOC sources

Once the O_3 sensitivity region is determined, net ozone formation in a model time step can be attributed to different NO_x or VOC source sectors. In our study, four ozone tracers were introduced to track ozone from two sources under NO_x or VOC-limited conditions: (1) ozone due to NO_x from an explicit source (O_3_NO_x_X1); (2) ozone due to NO_x from other lumped sources (O_3_NO_x); (3) ozone due to VOC from an explicit source (O_3_VOC_X1); and (4) ozone due to VOC from other lumped sources (O_3_VOC). These tracers are used for book-keeping and are chemically non-reactive. Their concentrations are adjusted at each time step based on the net ozone formation rate (either positive or negative) as described below. These non-reactive tracer species will go through the transport, and dry and wet deposition processes identical to the regular ozone species.

Under NO_x-limited conditions, if net ozone formation (ΔO_3) is positive, photolysis of NO_2 is the only significant source of $O\cdot$ in the troposphere, which is

directly responsible for ozone formation. The ozone formation is attributed to the lumped or explicit NO_x sources based on their relative contributions to the formation of $O\cdot$ from these two sources, as shown in equations (4-3) to (4-5).

$$f = \frac{P_{O\cdot|NO_2}}{P_{O\cdot|NO_2} + P_{O\cdot|NO_{2\_X1}}} \quad (4\text{-}3)$$

$$\Delta O_3\_NO_x = \Delta O_3 \times f \quad (4\text{-}4)$$

$$\Delta O_3\_NO_x\_X1 = \Delta O_3 \times (1\text{-}f) \quad (4\text{-}5)$$

In the above equations, $P_{O\cdot|NO_2}$ is the production rate of $O\cdot$ from NO_2 from other lumped sources; $P_{O\cdot|NO_{2\_X1}}$ is the production rate of $O\cdot$ from NO_2 from the explicit source.

Under VOC-limited conditions, if net ozone formation is positive, the VOC-related ozone tracers would be updated, as shown in equation (4-6) to equation (4-8), based on the NO to NO_2 conversion rate. The NO_x-related tracers would remain unchanged.

$$f = \frac{P_{NO_2|HO_2\cdot} + P_{NO_2|RO_2\cdot}}{P_{NO_2|HO_2\cdot} + P_{NO_2|RO_2\cdot} + P_{NO_2|HO_{2\cdot\_X1}} + P_{NO_2|RO_{2\cdot\_X1}}} \quad (4\text{-}6)$$

$$\Delta O_3\_VOC = \Delta O_3 \times f \quad (4\text{-}7)$$

$$\Delta O_3\_VOC\_X1 = \Delta O_3 \times (1\text{-}f) \quad (4\text{-}8)$$

$P_{NO_2|HO_{2\_X1}}$ is the formation rate of NO_2 due to $HO_2\cdot$ reaction with NO from the explicit source; $P_{NO_2|RO_{2\_X1}}$ is the formation rate of NO_2 due to $RO_2\cdot$ reaction with NO from the explicit source. This approach is different from the VOC source attribution method used in OSAT and other similar studies that calculated f with equation (4-9) under NO_x-limited conditions and equation (4-10) under VOC-limited conditions. In equations (4-9) and (4-10), $NO_{x,i}$ represents the concentration of NO_x of the i^{th} sector; $VOC_{i,j}$ represents the concentration of the j^{th} VOC species of the i^{th} sector; MIR_j represents the maximum incremental reactivity of the j^{th} VOC species.

$$f = \frac{NO_{x,i}}{\sum NO_{x,i}} \quad (4\text{-}9)$$

$$f = \frac{VOC_{i,j} \times MIR_j}{\sum VOC_{i,j} \times MIR_j} \quad (4\text{-}10)$$

If net ozone formation is negative (i.e. reduction of ozone) due to chemical reactions, the concentrations of the ozone tracers (ΔO_3_tracer) would be reduced according to their relative abundance in the mixture, as shown in equation (4-11) and (4-12):

$$f_i = \frac{O3\_tracer\_i}{O_3} \quad (4\text{-}11)$$

$$\Delta O_3\_tracer\_i = \Delta O_3 \times f_i \quad (4\text{-}12)$$

where O_3 is the concentration of ozone and O_3_tracer_i indicates the concentration of one of the four ozone tracers discussed above.

4.3 Model application

The CMAQ model with the expanded source-oriented S99 mechainsm was applied to simulate O_3 in August 2013 using a 36 km × 36 km horizontal resolution domain. The model domain covers China and surrounding countries in East Asia. The anthropogenic and biogenic emissions were based on the Multi-resolution Emission Inventory of China (MEIC) and the MEGAN biogenic emission model [27], respectively. Meteorological inputs were generated using the Weather Research and Forecasting (WRF) model. More details of the model setup, input data preparation and evaluation of meteorological inputs have been described in detail by Hu et al [28] and the references therein.

The MEIC emission inventory that provides speciated emissions for the lumped version of the S99 photochemical mechanism was applied for this study. The total emissions of each S99 species of each sector on a typical week day (Wednesday, August 21st, 2013) are listed in Table 4-2.

Table 4- 2. Total emissions of each S99 species of each sector on a typical week day in kmol/day.

S99 Species	Industries	Transportation	Wildfire	Residential	Biogenic	Other Countries	Power Plants
NO	1.69E+07	1.05E+07	6.39E+04	7.93E+05	1.99E+06	1.81E+07	1.30E+07
NO_2	8.91E+05	5.53E+05	9.95E+04	4.18E+04	0	8.63E+05	6.84E+05
Total VOC	1.71E+07	2.07E+06	6.90E+05	3.71E+06	6.08E+07	1.08E+08	7.87E+04
ACET	2.66E+05	5.67E+04	2.48E+04	1.08E+05	2.16E+06	3.01E+06	3.12E+01
ALK1	1.86E+06	4.28E+04	4.54E+04	2.99E+05	5.12E+04	6.95E+06	4.79E+03
ALK2	2.01E+06	9.54E+04	1.66E+04	4.99E+05	3.49E+03	1.91E+06	3.27E+03
ALK3	1.34E+06	4.18E+04	9.57E+02	1.60E+05	9.36E+05	2.82E+06	2.01E+03
ALK4	1.62E+06	2.24E+05	1.46E+03	1.59E+05	1.28E+05	2.41E+06	1.43E+04
ALK5	1.97E+06	1.89E+05	1.03E+03	2.84E+05	5.63E+04	1.50E+06	1.10E+03
ARO1	2.81E+06	1.04E+05	3.90E+04	1.66E+05	1.16E+05	1.26E+06	1.17E+04
ARO2	1.44E+06	1.46E+05	2.08E+03	1.42E+05	4.69E+04	1.03E+06	3.11E+04
CCHO	2.90E+01	1.29E+05	8.78E+04	6.75E+04	9.79E+05	1.42E+06	0
ETHENE	1.63E+06	3.28E+05	4.86E+04	6.17E+05	3.18E+06	5.08E+06	0
HCHO	1.32E+05	1.84E+05	6.91E+04	1.10E+05	5.31E+05	1.19E+06	1.50E+03
ISOPRENE	5.58E+03	1.05E+03	1.54E+04	6.07E+03	2.28E+07	3.66E+07	0
MACR	2.45E+03	1.25E+04	3.20E+02	1.63E+04	0	1.39E+04	0
MEK	7.96E+04	1.34E+04	2.91E+04	2.71E+04	2.13E+04	9.51E+04	0
MVK	0	0	0	0	0	9.51E+02	0
OLE1	9.04E+05	2.10E+05	2.25E+04	2.79E+05	2.42E+06	4.02E+06	5.69E+03
OLE2	8.27E+05	1.90E+05	6.36E+03	1.68E+05	6.53E+05	1.17E+06	3.19E+03
RCHO	3.93E+02	5.70E+04	6.36E+04	3.42E+04	4.51E+04	1.63E+05	0
BACL	1.07E+04	1.11E+03	0	1.42E+04	0	2.80E+03	0
BALD	0	3.30E+03	8.67E+02	1.69E+03	3.26E+03	5.34E+04	0
CCO_OH	0	0	7.46E+04	0	1.99E+05	3.14E+05	0
CRES	1.34E+03	1.01E+03	0	1.52E+04	0	4.98E+03	0
GLY	1.91E+02	4.01E+03	0	1.73E+05	0	7.51E+03	0
HCOOH	0	0	2.75E+04	0	2.60E+05	3.57E+05	0
IPROD	5.41E+01	2.33E+04	0	8.06E+03	0	3.76E+04	0
MEOH	8.06E+04	9.91E+01	7.76E+04	2.38E+05	2.24E+07	3.12E+07	0
MGLY	1.23E+02	2.49E+03	1.19E+04	6.65E+04	0	1.17E+04	0
PHEN	2.21E+03	0	1.77E+04	7.46E+03	0	1.43E+04	0
PROD2	9.31E+04	3.97E+03	5.22E+03	1.51E+04	0	5.59E+04	0
RCO_OH	0	0	0	0	2.62E+04	3.53E+04	0
RNO3	0	0	0	0	0	0	0
SESQ	0	0	0	0	1.92E+05	2.15E+05	0
TRP1	1.17E+04	2.66E+03	2.30E+02	3.23E+04	3.57E+06	5.52E+06	0

4.4 Results and discussion

4.4.1 Regional distribution of ozone regime indicators

The regional distributions of monthly averaged regime indicators for all daytime hours based on I1 and I2 are shown in Figure 4-1. Red regions are under VOC-limited conditions. White regions are under NO_x-limited conditions. Figure 4-1(a) shows the regional distribution of regime indicator based on indicator I1. YRD, NCP, SCB and central China have I1 higher than 0.5, which are under VOC-limited conditions. Figure 4-1(b) shows the regional distribution of regime indicator based on I2. Northern part of YRD, southern part of NCP and eastern parts of central China have I2 lower than 0.5, which are under VOC-limited conditions. Most of the regions are under NO_x-limited conditions.

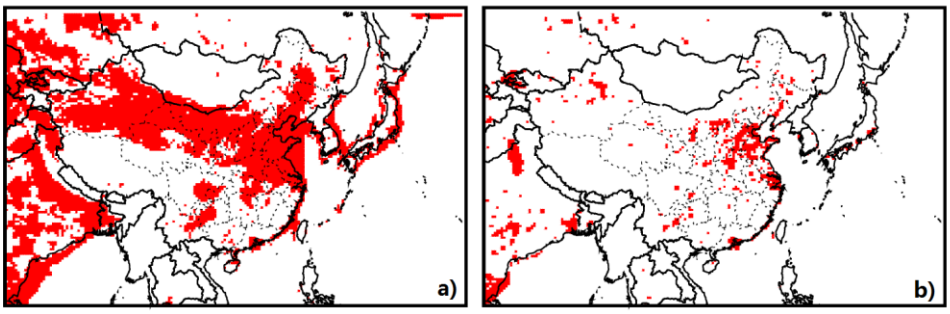

Figure 4- 1. Regional distributions of monthly averaged ozone regime indicators for all daytime hours based on a) indicator I1 and b) indicator I2.

4.4.2 Regional distribution of NO_x- and VOC-limited ozone formation

The regional distributions of monthly average ozone formed under NO_x- and VOC-limited conditions based on indicator I1 are shown in Figure 4-2. Figure 4-2(a) shows that ozone formed under NO_x-limited conditions has higher concentrations in SCB, PRD, southwest and the southern part of central China, with a maximum monthly

concentration of approximately 10 ppb. Figure 4-2(b) shows that ozone formed under VOC-limited conditions has higher concentrations in YRD, NCP and the eastern part of central China, with a maximum concentration of approximately 30 ppb. Concentrations up to 50 ppb are located over the Yellow Sea.

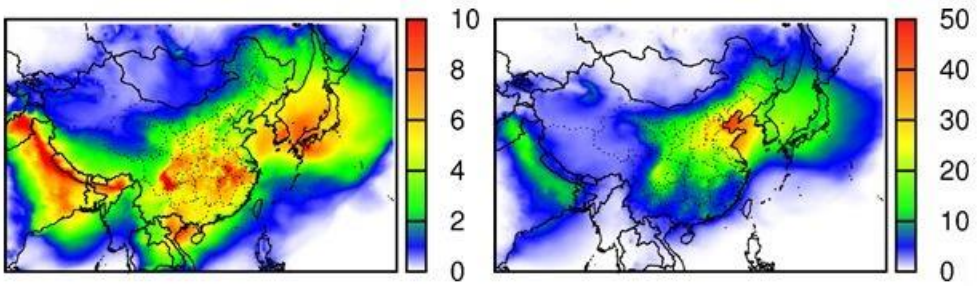

Figure 4- 2. Regional distribution of monthly average ozone formed under a) NO_x-limited and b) VOC-limited regime based on indicator I1; units are in ppbV.

The regional distributions of monthly average ozone formed under NO_x- and VOC-limited conditions based on indicator I2 are shown in Figure 4-3. Figure 4-3(a) shows that ozone formed under NO_x-limited condition has higher concentrations in SCB, Central China and locations over the Yellow Sea, with a maximum monthly concentration of approximately 30 ppb. Figure 4-3(b) shows that ozone formed under VOC-limited conditions has higher concentrations in YRD, NCP and eastern part of central China, with a maximum concentration of approximately 15 ppb. Concentrations up to 25 ppb are located over the Yellow Sea. These results are different from the ones based on indicator I1 with more ozone produced under NO_x-limited conditions and less ozone produced under VOC-limited conditions.

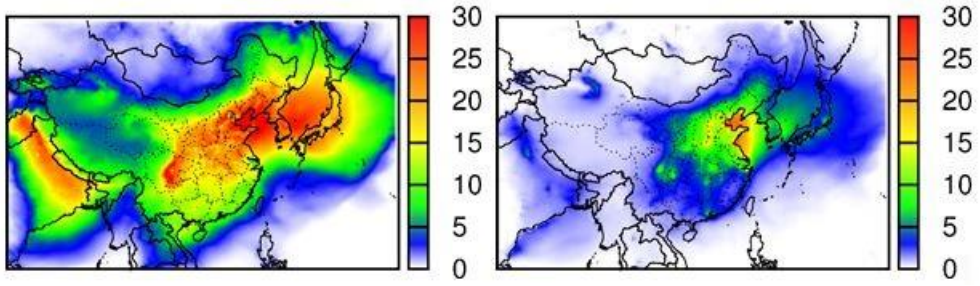

Figure 4- 3. Regional distribution of ozone formation under a) NO_x-limited and b) VOC-limited regime based on indicator I2; units are in ppbV.

In addition to ozone formed through chemical reactions, a considerable fraction of ozone is due to background concentrations, which is the ozone that centers the modeling area through boundary conditions. In this study the boundary concentrations of ozone were set using a constant vertical profile that represents clean continental conditions. The background ozone concentration can be calculated as the difference of the total ozone concentration and the sum of the ozone attributed to NO_x and VOC sources. As can be seen from Figure 4-4(c), the background ozone concentrations are approximately 40 ppb. On a monthly average basis, background ozone accounts for approximately 50% of total ozone concentrations in high ozone concentration areas while the rest is due to photochemical formation in the domain.

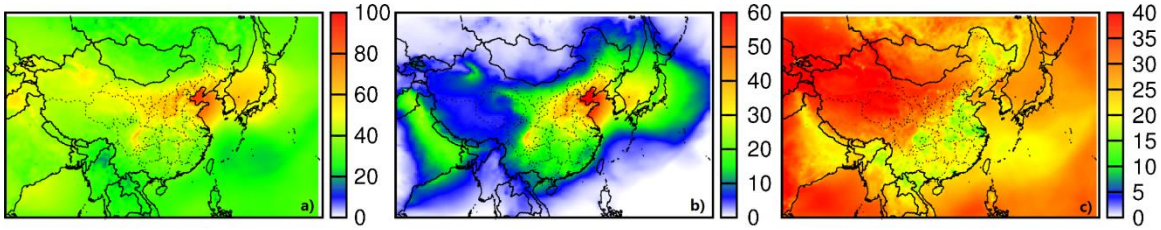

Figure 4- 4. Regional distribution of ozone a) with background concentrations; b) without background concentrations and c) background ozone concentrations; units are in ppbV.

4.4.3 Regional source apportionment of ozone concentrations

The regional distribution of monthly average ozone concentration formed under NO_x-limited conditions (based on indicator I1), which is attributed to NO_x emissions from explicit sources, is shown in Figure 4-5. The first panel shows the summation of ozone formed under NO_x-limited conditions from all explicit emission sources. Emissions from industrial processes contribute most significantly to ozone formation with a maximum concentration of approximately 3 ppb, followed by emissions from vehicle exhausts, power plants and biogenic sources. NO_x emissions from other countries do not have a significant contribution to ozone concentrations in China in most places, although some border provinces are slightly affected. The relative contributions of different NO_x sources generally agree with their emission rates in the modeling area. NO_x from biogenic sources is mainly due to microbial activities in soil and is in the form of NO. NO_x emissions from other combustion sources are mostly in the form of NO with a typical NO_2/NO_x ratio of 5-10%. This explains why the biogenic sources have similar contributions to sources that have much higher emissions of NO_x.

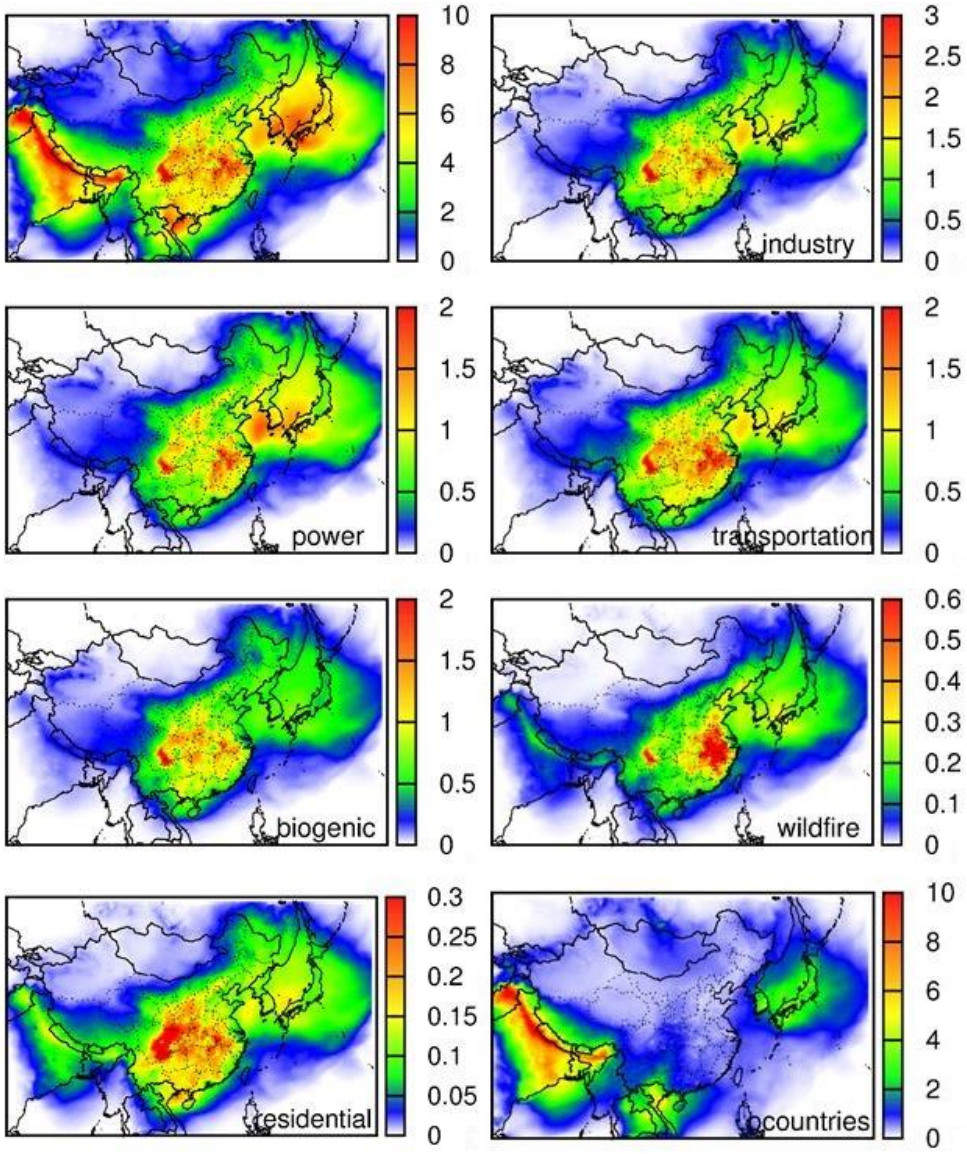

Figure 4- 5. Regional distribution of monthly average ozone formed under NO_x-limited condition from explicit emission sources based on indicator I1; units are in ppbV. "Industries" is the emission from industrial processes; "power" is the emission from power plants; "transportation" is the emission from vehicle exhausts; "biogenic" is the emission from biogenic sources; "wildfire" is the emission from wildfire burning; "residential" is the emission from residential usage; "Ocountries" is the emission from other countries.

The ozone formed under VOC-limited conditions from explicit emission sources is shown in Figure 4-6. Under VOC-limited conditions, VOC emissions from biogenic sources contribute most significantly to ozone formation with a maximum monthly

average concentration of approximately 15-20 ppb, followed by emissions from industrial sources (5-10 ppb). The contribution from biogenic source is high since the major VOC emitted from biogenic sources is isoprene, which is among one of the most reactive VOCs. The higher MIR value and large emissions lead to its large contributions.

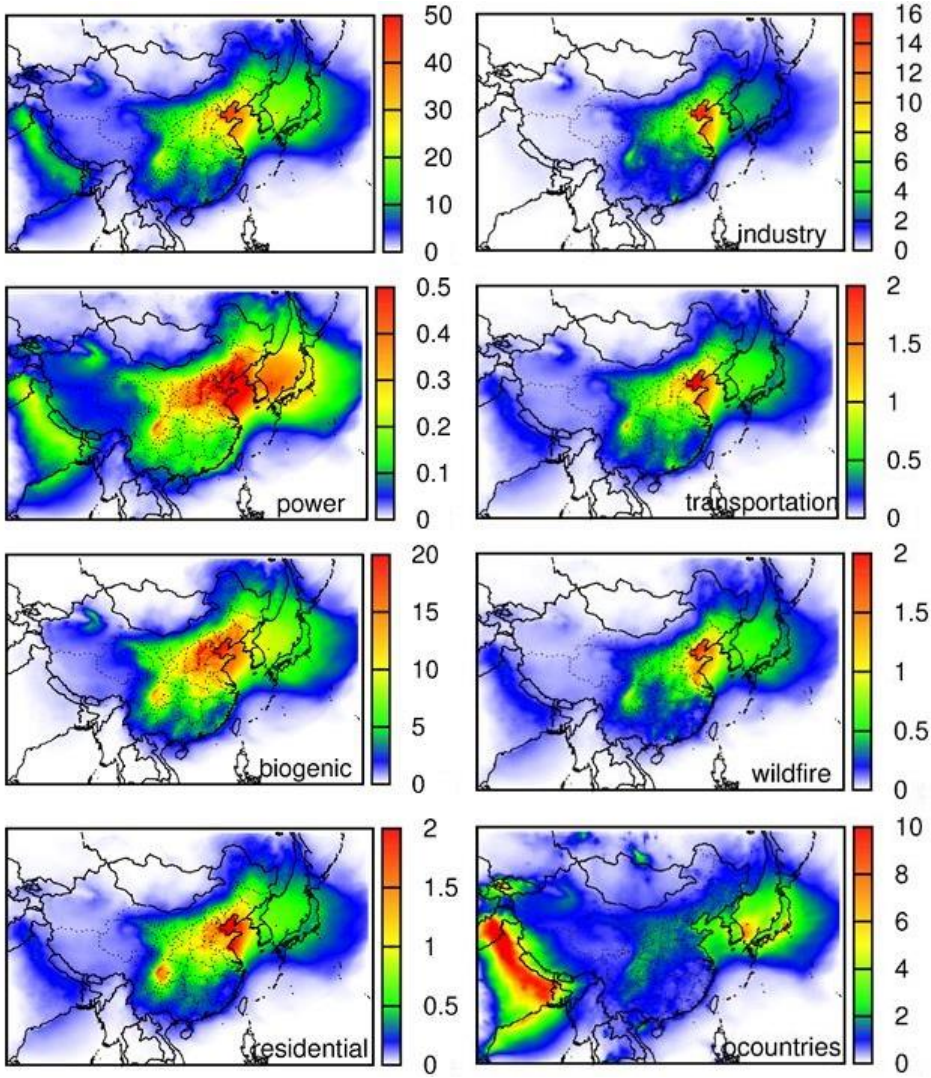

Figure 4- 6. Regional distribution of ozone formation under VOC-limited condition from explicit emission sources based on indicator I1; units are in ppbV.

The ozone formed under NO_x-limited condition from explicit emission sources based on indicator I2 is shown in Figure 4-7. Under NO_x-limited conditions, the emissions from industrial processes contribute most significantly to ozone formation (with a maximum concentration of approximately 10 ppb), followed by emissions from vehicle exhausts (6 ppb) and power plants (6 ppb). The contribution from other countries is high, but the impacts are mainly focused in coastal areas.

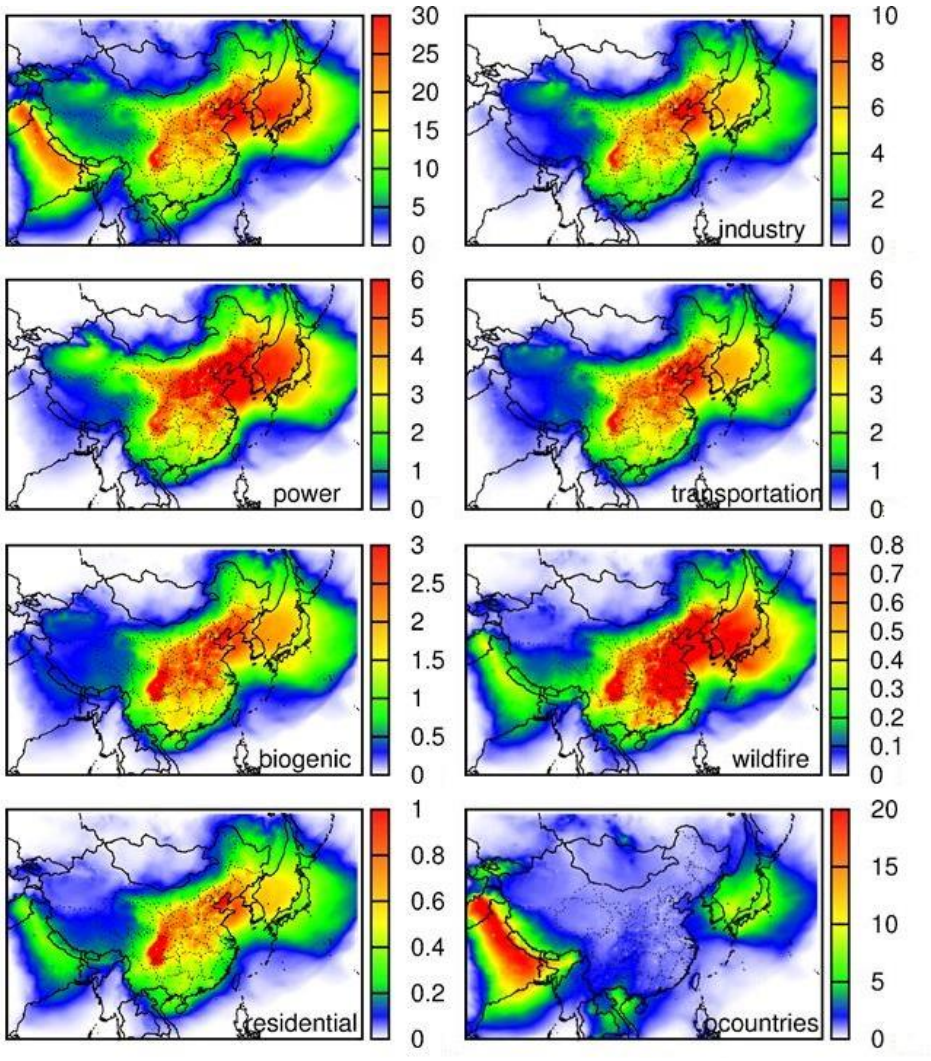

Figure 4- 7. Regional distribution of ozone formation under NO_x-limited condition from explicit emission sources based on indicator I2; units are in ppbV.

The ozone formed under VOC-limited condition from explicit emission sources based on indicator I2 is shown in Figure 4-8. Under VOC-limited conditions, the emissions from industrial processes contribute to almost half of the total ozone formed under VOC-limited condition, followed by emissions from biogenic sources.

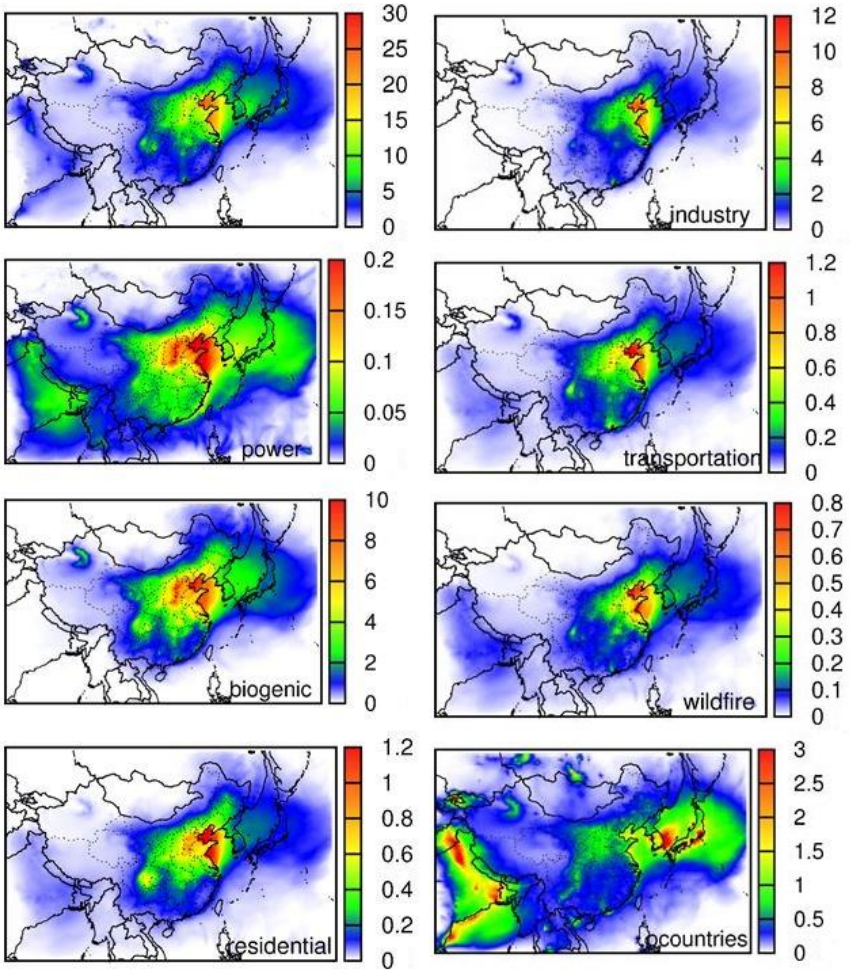

Figure 4- 8. Regional distribution of ozone formation under VOC-limited condition from explicit emission sources based on indicator I2; units are in ppbV.

4.4.4 Source contributions to ozone in selected metropolitan areas

The diurnal variations of hourly averaged ozone and the contributions of each explicit emission sector based on indicator I1 in four metropolitan cities in China (Beijing, Shanghai, Chongqing and Guangzhou) in August 2013 are shown in Figure 4-9. The results based on indicator I2 are shown in Figure I-1.

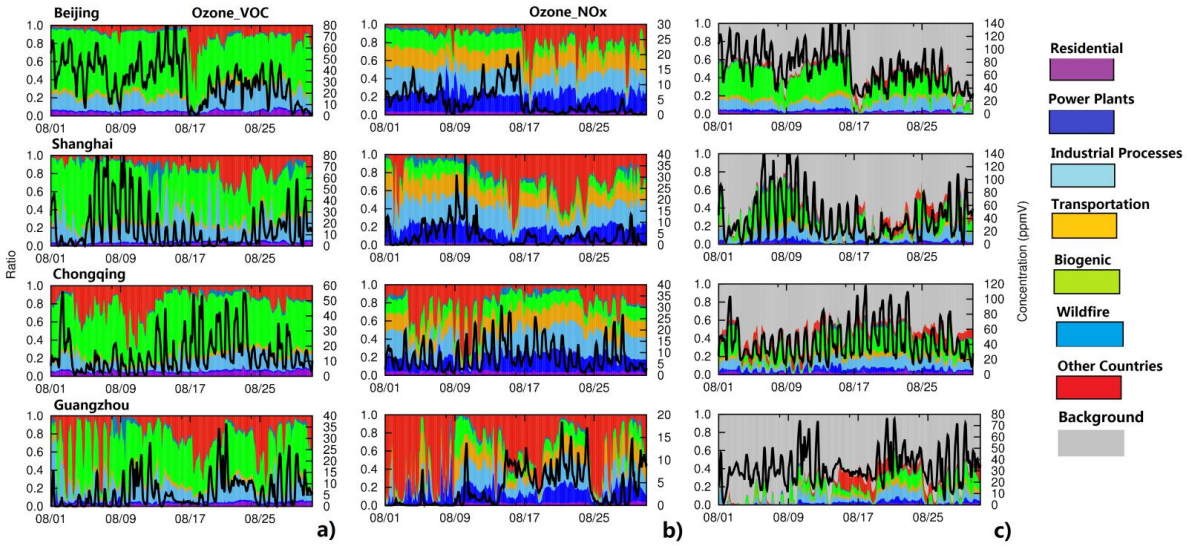

Figure 4- 9. Diurnal variations of hourly averaged ozone and the contributions of each sector to a) VOC-attributed ozone formation; b) NO_x-attributed ozone formation and c) total ozone concentrations in Beijing, Shanghai, Chongqing and Guangzhou, China in August 2013. Concentrations of ozone, and ozone attributed to NO_x and VOC sources are shown as black lines against the second y axis on the right of each panel. Note that the scales for ozone concentrations are different. Ozone concentrations are in units of ppbV.

In all cities, biogenic source is the major contributor to ozone formed under VOC-limited conditions, which is due to the fact of large amount of isoprene emitted from biogenic sources. Under NO_x-limited conditions, the contributions of industrial sources, transportation and power plants are high. Considering the ozone formed under both conditions, the major contributions are from biogenic sources and industrial processes.

Increase in ozone concentrations in all cities except in Guangzhou on a few days are always associated with increases in the contributions from the ozone formed from the explicit NO_x and VOC sources. Background ozone becomes much more important on low ozone days.

The overall source contributions to total ozone concentrations in Beijing, Shanghai, Chongqing and Guangzhou averaged over the entire month are shown in Figure 4-10, based on indicators I1 and I2. Compared with other cities, the contribution of background ozone to Guangzhou is higher. Guangzhou is a coastal city, which tends to be affected by the background ozone from the ocean, and the dominate wind direction in summer is usually from south to north. Furthermore, the concentration of ozone formed from anthropogenic activities in Guangzhou is lower compared with the three other cities, which makes the background ozone concentrations account for a higher percentage out of the total ozone concentrations. Contributions from biogenic sources are lower at all four cities based on indicator I2 because it predicts for ozone formation are under NO_x-limited conditions. Correspondingly, the contributions from power plants and transportation based on indicator I2 are higher.

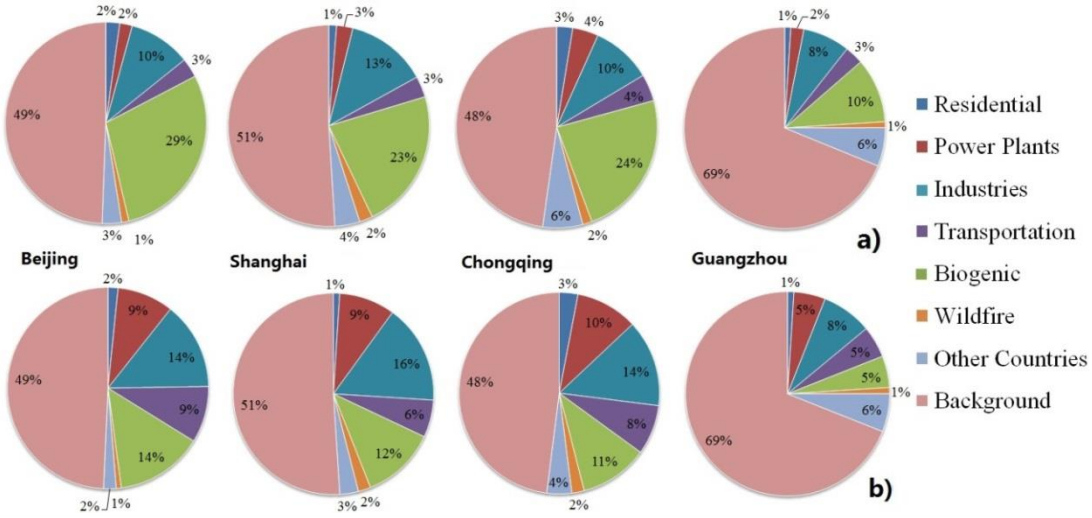

Figure 4- 10. Relative contributions of each emission sector to ozone formation estimated by a) regime indicator I1 and b) regime indicator I2 in Beijing, Shanghai, Chongqing and Guangzhou, China in August 2013.

4.4.5 Source-specific reactivity and ozone forming potential

Based on the analyses in the previous sections, VOCs could have significant contributions to ozone formation. As the two indicators used in this study leads to different estimations of the relative importance of different VOC sectors on ozone formation, they are compared with source-specific reactivity and ozone forming potential with the incremental reactivity measures developed in Chapter 2 and 3.

The source-specific normalized incremental reactivity (SSNIR) of each sector can be calculated using equation (4-13):

$$SSNIR = \sum_{i=1}^{N} f_i NIR_i \qquad (4\text{-}13)$$

where NIR_i represents the normalized incremental reactivity values of the i^{th} emission species from a specific source sector and f_i is the fraction of the i^{th} species in the total VOC emissions from that sector; In this case, the NIR values of the species were taken from the NIR_{50} values as listed in Table B-1. The splitting factors listed in Table G-1 were used to calculate the emissions rate of detailed VOCs from lumped S99 species for each sector, as listed in Table G-2.

The calculated SSNIR values are listed in Table 4-3. The SSNIR can be considered as a metric that represents the capability ozone formation per unit emission of VOCs from a specific source under atmospheric conditions experienced during a study period. Based on the current emission estimation, power plant emissions, biogenic emissions and transportation emissions have relatively large SSNIR values. Power plant emissions have a large SSNIR value because it has higher fractions of highly reactive aromatic compounds with large NIR values.

The source-specific ozone-forming potential based on NIR (SOP_{NIR}) can be operationally defined as the product of the total emission (E_{tot}) of reactive VOCs (only the ones included in the SSNIR calculations) in the entire study area and the SSNIR of that source, as shown in equation (4-14).

$$SOP_{NIR} = E_{tot} SSNIR \qquad (4\text{-}14)$$

Similarly, source-specific normalized ozone-forming potential based on NIR ($SNOP_{NIR}$) of a specific source i can be defined by equation (4-15):

$$SNOP_{NIR,i} = \frac{SOP_{NIR,i}}{\sum_{i=1}^{N} SOP_{NIR,i}} \qquad (4\text{-}15)$$

where N is the number of total source sectors with VOC emissions.

In addition to applying NIR values for ozone-forming potential assessment, MIR values retrieved from the box model results was applied to evaluate the MIR-based ozone-forming potential of each emission sector. The source-specific maximum incremental reactivity (SSMIR) of each sector can be calculated using equation (4-16):

$$SSMIR = \sum_{i=1}^{N} f_i MIR_i \qquad (4\text{-}16)$$

where MIR_i represents the normalized incremental reactivity values of the i^{th} emission species from a specific source sector and f_i is the fraction of the i^{th} species in the total VOC emissions from that sector; In this case, the MIR values of the species were taken from the averaged values of 34 provincial capital cities in China as shown in Figure 3-3. The splitting factors are the same as those used for SSNIR calculation.

The calculated SSMIR values are listed in Table 4-3 as well. The sectors that have relatively large SSMIR values are power plant emissions, biogenic emissions and transportation emissions.

The source-specific ozone-forming potential based on MIR (SOP_{MIR}) can be operationally defined as the product of the total emission (E_{tot}) of reactive VOCs in the entire study area and the SSMIR of that source, as shown in equation (4-17).

$$SOP_{MIR} = E_{tot} SSMIR \qquad (4\text{-}17)$$

Similarly, source-specific normalized ozone-forming potential based on MIR ($SNOP_{MIR}$) of a specific source i can be defined by equation (4-18):

$$SNOP_{MIR,i} = \frac{SOP_{MIR,i}}{\sum_{i=1}^{N} SOP_{MIR,i}} \qquad (4\text{-}18)$$

where N is the number of total source sectors with VOC emissions.

Based on the both the $SNOP_{NIR}$ and $SNOP_{MIR}$ values, biogenic emissions and industrial emissions are the two most important sources, accounting for 46% (53% based on $SNOP_{MIR}$) and 31% (24% based on $SNOP_{MIR}$) of total ozone formation due to VOCs, respectively. In general, the SNOP values agree better with the ozone source apportionments using indictor I1 than those using indicator I2. The contribution of transportation based on $SNOP_{NIR}$ values is higher than that based on $SNOP_{MIR}$ values because transportation emissions have high fraction of aldehydes species. The rankings of these aldehydes species are higher based on NIR values than the rankings based on MIR values.

Table 4- 3. SSNIR, $SNOP_{NIR}$, SSMIR and $SNOP_{MIR}$ values of explicit sectors

Emission sector	**SSNIR**	**$SNOP_{NIR}$**	**SSMIR**	**$SNOP_{MIR}$**
Industrial	4.1	31%	3.3	24%
Transportation	5.9	5.9%	5.6	5.2%
Wildfire	5.0	7.2%	4.1	8.0%
Residential	3.9	5.0%	4.3	5.9%
Biogenic	7.3	46%	4.6	53%
Other Countries	3.5	4.6%	3.1	4.0%
Power	8.2	0.3%	5.5	0.2%

4.5 Conclusions

In this section, a reactive tagged species approach based on a source-oriented SAPRC-99 photochemical mechanism was developed and applied to study ozone source apportionment in China. Two regime indicators were applied to determine whether ozone formation is under NO_x- or VOC-limited condition. The first indicator is based on the conversion rate of NO to NO_2 due to HO_2 and RO_2 radicals. The second regime

indicator is based on ratio of the formation rates of H_2O_2 and ROOH to that of HNO_3. The VOC-limited regions are located in the northern part of YRD, southern part of NCP and eastern part of central China based on both indicators.

Based on indicator I1, ozone formation in China is mostly under VOC-limited conditions. The major contributions of ozone formed under VOC-limited condition are from biogenic sources and industrial processes. For ozone formation under NO_x-limited conditions, transportation and power plants have large contributions due to the large amount of NO_x emissions. Based on the source-specific normalized incremental reactivity analysis, VOC mixture emitted from power plants is most reactive among all the emission sectors, followed by that of transportation, biogenic source and industrial processes. However, due to the low emission amounts of VOCs from power plants and transportation, the ozone-forming potentials of these two sources are not as significant as that of biogenic sources and industrial processes.

In cities where ozone concentrations are mainly attributed to ozone formation from VOCs or NO_x emissions, contributions of background ozone concentrations are not as large as those cities with less ozone formation from anthropogenic activities. For example, the background ozone concentrations averaged over the entire month account for approximately 50% in Beijing, while account for almost 70% in Guangzhou.

5. CONCLUSIONS

China has been suffered from severe ozone pollution problem as a result of rapid economic growth and industrial developments. Ozone formation is affected by its precursors, nitrogen oxides (NO_x) and volatile organic compounds (VOCs) emitted from both biogenic and anthropogenic sources. In this study, the incremental reactivity (IR) and ozone forming potential (OFP) of the VOCs, and the contributions of different NO_x and VOC emission sources to ozone concentrations in China during August 2013 were looked into to provide supports to effective ozone mitigation strategies.

In the first part of the study, a regional Community Multi-scale Air Quality (CMAQ) model (v5.0.1) equipped with a detailed photochemical mechanism SAPRC-11 and a photochemical box model equipped with a SAPRC-07 photochemical mechanism were used to determine IR of 66 major VOCs under realistic ambient conditions in China. High ozone episodes occur in YRD, NCP, central China and Chongqing and Chengdu in SCB, where the industrialization and economics are highly developed. The normalized incremental reactivity (NIR) of the VOC, defined as the ratio of the IR of the VOC to the IR of the VOC mixture, was determined to evaluate the reactivity of VOCs. According to the NIR values of VOCs, C4+ aldehydes (NIR_{50}~30), trimethyl benzenes (NIR_{50}~27), small alkenes and dienes (NIR_{50}~24) were found to be the most reactive species, which are more reactive than formaldehyde (NIR_{50}~1.8), ethene (NIR_{50}~2.0) and isoprene (NIR_{50}~9.0).

The chemical compositions of the VOC mixture retrieved from the CMAQ model results were applied in a photochemical box model to determine the maximum incremental reactivity (MIR) of the VOCs at 34 provincial capital cities in China. The MIR metric reflects relatively high NO_x conditions where ozone formation is most sensitive to VOC emissions. The average MIR value of the base VOC mixture in the Chinese cities is 3.32, which is close to the average MIR value of the base VOC mixture in 39 US cities (3.50). The average MIR values of individual VOCs based on 34 Chinese cities are also similar to those determined by Carter using representative VOC mixture

for US cities. Uncertainty analysis was done to determine the factors that affect the calculated MIR significantly. The uncertainty of mixing height and total emitted amount of hydrocarbons is on the order of 10% determined by 100 Monte-Carlo simulations. According to the MIR values, alkanes trans-2-butene (MIR~12.3), cis-2-butene (MIR~11.6) and 1,3-butadiene (MIR~11.0) are among the most reactive VOCs. Considering the amount of emission rate, isoprene (EOFP~3.801), m-xylene (EOFP~0.646) and toluene (EOFP~0.438) have the highest ozone-forming potentials, which need to be considered primarily when making VOC control strategies.

In the second part of the study, a reactive tagged species method was applied to study ozone source apportionment in China by implementing a source-oriented SAPRC-99 mechanism in the CMAQ model. Two regime indicators were applied to determine whether a region is under NO_x- or VOC-limited condition. The first regime indicator is based on the fraction of NO to NO_2 conversion due to RO_2 to the overall conversion rate. The second regime indicator is based on the ratio of the production rate of peroxides to the production rate of nitric acid. The VOC-limited regions are located in large urban areas such as the Yangtze River Delta, the Pearl River Delta and Chongqing and Chengdu in Sichuan Basin based on both indicators. However, more regions are determined to be NO_x-limited based on the second indicator. Further studies are needed to determine the appropriate cut-off values of these two indicators to determine whether a region is under VOC- or NO_x-limited conditions.

The major contributions of ozone formed under VOC-limited condition are from biogenic sources (~20%) and industrial processes (~10%). Transportation and power plants contribute a lot to ozone formed under NO_x-limited condition. The VOC mixture of power plants is most reactive among all the emission sectors, followed by that of transportation, biogenic source and industrial processes. However, due to the fact that the emission amounts of VOCs from power plants and transportation are much lower compared with those from biogenic sources and industrial processes, the major contributors to ozone formation are from biogenic sources and industrial processes.

REFERENCES

[1] EPA, *Ozone Pollution.* 2016.

[2] Chan, C.K. and X. Yao, *Air pollution in mega cities in China.* Atmospheric environment, 2008. **42**(1): p. 1-42.

[3] Li, Y., et al., *Ozone source apportionment (OSAT) to differentiate local regional and super‐regional source contributions in the Pearl River Delta region, China.* Journal of Geophysical Research: Atmospheres, 2012. **117**(D15).

[4] Liu, Y., et al., *Distributions and source apportionment of ambient volatile organic compounds in Beijing city, China.* Journal of Environmental Science and Health, 2005. **40**(10): p. 1843-1860.

[5] Gao, J., et al., *A case study of surface ozone source apportionment during a high concentration episode, under frequent shifting wind conditions over the Yangtze River Delta, China.* Science of The Total Environment, 2016. **544**: p. 853-863.

[6] Stockwell, W.R., et al., *A review of tropospheric atmospheric chemistry and gas-phase chemical mechanisms for air quality modeling.* Atmosphere, 2011. **3**(1): p. 1-32.

[7] Dodge, M.C., *Combined use of modeling techniques and smog chamber data to derive ozone-precursor relations.* 1977(International Conference on Photochemical Oxidant Pollution and its Control, Proceedings, Volume II, U.S. EPA, Research Triangle Park, N.C): p. 881–889 EPA-600/3-77-001b.

[8] Finlayson-Pitts, B.J. and J.N. Pitts, *Tropospheric air pollution: ozone, airborne toxics, polycyclic aromatic hydrocarbons, and particles.* Science, 1997. **276**(5315): p. 1045-1051.

[9] Carter, W.P., *Development of ozone reactivity scales for volatile organic compounds.* Journal Of The Air & Waste Management Association, 1994. **44**(7): p. 881-899.

[10] Carter, W.P., *Estimation of ozone reactivities for volatile organic compound speciation profiles in the Speciate 4.2 Database.* Center for Environmental Research and Technology, University of California, USA, 2013.

[11] EPA, *Interim Guidance on Control of Volatile Organic Compounds in Ozone State Implementation Plans, Code of Federal Register 40 Part 51*. 2003.

[12] Yarwood, G., et al., *Development of a methodology to assess geographic and temporal ozone control strategies for the South Coast Air Basin.* Prepared for South Coast Air Quality Management District, Diamond Bar, CA, 1996.

[13] Ying, Q. and M.J. Kleeman, *Source contributions to the regional distribution of secondary particulate matter in California.* Atmospheric Environment, 2006. **40**(4): p. 736-752.

[14] Ying, Q. and A. Krishnan, *Source contributions of volatile organic compounds to ozone formation in southeast Texas.* Journal of Geophysical Research: Atmospheres, 2010. **115**(D17).

[15] Tan, J.-H., et al., *Non-methane hydrocarbons and their ozone formation potentials in Foshan, China.* Aerosol Air Qual Res, 2012. **12**(3): p. 387-398.

[16] Jun-lin, A., et al., *Characterizations of volatile organic compounds during high ozone episodes in Beijing, China.* Environmental monitoring and assessment, 2012. **184**(4): p. 1879-1889.

[17] Ling, Z. and H. Guo, *Contribution of VOC sources to photochemical ozone formation and its control policy implication in Hong Kong.* Environmental science & policy, 2014. **38**: p. 180-191.

[18] Lyu, X., et al., *Ambient volatile organic compounds and their effect on ozone production in Wuhan, central China.* Science of the Total Environment, 2016. **541**: p. 200-209.

[19] Jia, C., et al., *Non-methane hydrocarbons (NMHCs) and their contribution to ozone formation potential in a petrochemical industrialized city, Northwest China.* Atmospheric Research, 2016. **169**: p. 225-236.

[20] Byun, D. and K.L. Schere, *Review of the Governing Equations, Computational Algorithms, and Other Components of the Models-3 Community Multiscale Air Quality (CMAQ) Modeling System.* Applied Mechanics Reviews, 2006. **59**(2): p. 51-77.

[21] Carlton, A.G., et al., *Model Representation of Secondary Organic Aerosol in CMAQv4.7.* Environmental Science & Technology, 2010. **44**(22): p. 8553-8560.

[22] Appel, K.W., et al., *Evaluation of dust and trace metal estimates from the Community Multiscale Air Quality (CMAQ) model version 5.0.* Geosci. Model Dev. Discuss., 2013. **6**(1): p. 1859-1899.

[23] Wang, X., et al., *Process analysis and sensitivity study of regional ozone formation over the Pearl River Delta, China, during the PRIDE-PRD2004 campaign using the Community Multiscale Air Quality modeling system.* Atmospheric Chemistry and Physics, 2010. **10**(9): p. 4423-4437.

[24] Li, L., et al., *Ozone sensitivity analysis with the MM5-CMAQ modeling system for Shanghai.* Journal of Environmental Sciences, 2011. **23**(7): p. 1150-1157.

[25] Czader, B.H., et al., *A study of VOC reactivity in the Houston-Galveston air mixture utilizing an extended version of SAPRC-99 chemical mechanism.* Atmospheric Environment, 2008. **42**(23): p. 5733-5742.

[26] Carter, W.P., *Development of the SAPRC-07 chemical mechanism.* Atmospheric Environment, 2010. **44**(40): p. 5324-5335.

[27] Guenther, A., et al., *Estimates of global terrestrial isoprene emissions using MEGAN (Model of Emissions of Gases and Aerosols from Nature).* Atmospheric Chemistry and Physics, 2006. **6**: p. 3181-3210.

[28] Hu, J., et al., *One-year simulation of ozone and particulate matter in China using WRF/CMAQ modeling system.* Atmos. Chem. Phys, 2016. **16**: p. 10333-10350.

[29] Xie, M., et al., *Temporal characterization and regional contribution to O 3 and NO x at an urban and a suburban site in Nanjing, China.* Science of The Total Environment, 2016. **551**: p. 533-545.

[30] Zou, Y., et al., *Characteristics of 1 year of observational data of VOCs, NO x and O 3 at a suburban site in Guangzhou, China.* Atmospheric Chemistry and Physics, 2015. **15**(12): p. 6625-6636.

[31] Kuhlmann, G., et al., *Development of a custom OMI NO 2 data product for evaluating biases in a regional chemistry transport model.* Atmospheric Chemistry and Physics, 2015. **15**(10): p. 5627-5644.

[32] Carter, W.P., *Updated maximum incremental reactivity scale and hydrocarbon bin reactivities for regulatory applications.* California Air Resources Board Contract, 2009: p. 07-339.

[33] Carter, W.P.L., *Development of ozone reactivity scales for volatile organic-compounds.* Journal of the Air & Waste Management Association, 1994. **44**(7): p. 881-899.

[34] Carter, W.P., *Development of the SAPRC-07 chemical mechanism and updated ozone reactivity scales*. 2007: Citeseer.

[35] Carter, W.P.L., *Documentation of the SAPRC-99 Chemical Mechanism for VOC Reactivity Assessment, Report to the California Air Resources Board. Available at http://cert.ucr.edu/~carter/absts.htm#saprc99 and http://www.cert.ucr.edu/~carter/reactdat.htm*. 2000.

[36] Wang, G., et al., *Characteristics and source apportionment of VOCs in the suburban area of Beijing, China.* Atmospheric Pollution Research, 2016. **7**(4): p. 711-724.

[37] Wang, N., et al., *Investigation of chemical reactivity and active components of ambient VOCs in Jinan, China.* Air Quality, Atmosphere & Health, 2016. **9**(7): p. 785-793.

[38] Carter, W.P., *SAPRC-07 chemical mechanisms, test simulations, and environmental chamber simulation files.* 2012.

[39] Derwent, R. and Ø. Hov, *Application of sensitivity and uncertainty analysis techniques to a photochemical ozone model.* Journal of Geophysical Research: Atmospheres, 1988. **93**(D5): p. 5185-5199.

[40] Metropolis, N. and S. Ulam, *The monte carlo method.* Journal of the American statistical association, 1949. **44**(247): p. 335-341.

[41] Chang, T.Y. and S. Rudy, *Ozone-forming potential of organic emissions from alternative-fueled vehicles.* Atmospheric Environment. Part A. General Topics, 1990. **24**(9): p. 2421-2430.

[42] Liu, B., et al., *Characterization and source apportionment of volatile organic compounds based on 1-year of observational data in Tianjin, China.* Environmental Pollution, 2016. **218**: p. 757-769.

[43] Li, L., et al., *Source apportionment of surface ozone in the Yangtze River Delta, China in the summer of 2013.* Atmospheric Environment, 2016. **144**: p. 194-207.

[44] Carter, W.P., *Documentation of the SAPRC-99 chemical mechanism for VOC reactivity assessment.* Contract, 2000. **92**(329): p. 95-308.

[45] Zhang, H. and Q. Ying, *Contributions of local and regional sources of NOx to ozone concentrations in Southeast Texas.* Atmospheric Environment, 2011. **45**(17): p. 2877-2887.

[46] Zhang, H., et al., *Source apportionment of PM2.5 nitrate and sulfate in China using a source-oriented chemical transport model.* Atmospheric Environment, 2012. **62**(0): p. 228-242.

[47] Ying, Q. and A. Krishnan, *Source contributions of volatile organic compounds to ozone formation in southeast Texas.* Journal of Geophysical Research-Atmospheres, 2010. **115**(D17): p. D17306.

[48] Sillman, S., *The use of NO y, H2O2, and HNO3 as indicators for ozone‐NO x‐hydrocarbon sensitivity in urban locations.* Journal of Geophysical Research: Atmospheres, 1995. **100**(D7): p. 14175-14188.

[49] Sillman, S., et al., *The use of photochemical indicators to evaluate ozone-NOx-hydrocarbon sensitivity: Case studies from Atlanta, New York, and Los Angeles.* Journal of the Air & Waste Management Association, 1997. **47**(10): p. 1030-1040.

[50] Lu, C. and J.S. Chang, *On the indicator-based approach to assess ozone sensitivities.* Journal of Geophysical Research, 1998. **103**(D3): p. 3453-3462.

[51] Tonnesen, G.S. and R.L. Dennis, *Analysis of radical propagation efficiency to assess ozone sensitivity to hydrocarbons and NO x: 1. Local indicators of instantaneous odd oxygen production sensitivity.* Journal of Geophysical Research: Atmospheres, 2000. **105**(D7): p. 9213-9225.

[52] Hammer, M.U., B. Vogel, and H. Vogel, *Findings on H2O2/HNO3 as an indicator of ozone sensitivity in Baden‐Württemberg, Berlin‐Brandenburg, and the Po valley based on numerical simulations.* Journal of Geophysical Research: Atmospheres, 2002. **107**(D22).

[53] Liang, J., B. Jackson, and A. Kaduwela, *Evaluation of the ability of indicator species ratios to determine the sensitivity of ozone to reductions in emissions of volatile organic compounds and oxides of nitrogen in northern California.* Atmospheric Environment, 2006. **40**(27): p. 5156-5166.

[54] Kwok, R., et al., *Photochemical grid model implementation and application of VOC, NO x, and O 3 source apportionment.* Geoscientific Model Development, 2015. **8**(1): p. 99-114.

[55] Tonnesen, G.S. and R.L. Dennis, *Analysis of radical propagation efficiency to assess ozone sensitivity to hydrocarbons and NO x: 2. Long‐lived species as indicators of ozone concentration sensitivity.* Journal of Geophysical Research: Atmospheres, 2000. **105**(D7): p. 9227-9241.

[56] Milford, J.B., et al., *Total reactive nitrogen (NO y) as an indicator of the sensitivity of ozone to reductions in hydrocarbon and NO x emissions.* Journal of Geophysical Research: Atmospheres, 1994. **99**(D2): p. 3533-3542.

[57] Vogel, B., et al., *Findings on NOy as an indicator for ozone sensitivity.* J. Geophys. Res, 1999. **104**: p. 3605-3620.

[58] Martin, R.V., A.M. Fiore, and A. Van Donkelaar, *Space‐based diagnosis of surface ozone sensitivity to anthropogenic emissions.* Geophysical Research Letters, 2004. **31**(6).

[59] Zhang, Y., et al., *Probing into regional O3 and particulate matter pollution in the United States: 2. An examination of formation mechanisms through a process analysis technique and sensitivity study.* Journal of Geophysical Research: Atmospheres, 2009. **114**(D22).

[60] Gipson, G.L. and J. Young, *Process analysis.* Science Algorithms of the EPA Models-3 Community Multiscale Air Quality (CMAQ) Modeling System, 1999.

APPENDIX A. MAJOR REACTIVE VOC SPECIES AND THEIR REACTION RATE COEFFICIENTS WITH OH RADICAL AT 300 K

Table A- 1. Description of major reactive VOC species and their reaction rate coefficients with OH radical at 300 K

Abbreviation	Description	k_{OH} (cm^3 $molec^{-1}$ s^{-1})
ACET	Acetone	1.91E-13
ACRO	Acrolein	1.99E-11
ACYL	Acetylene	7.56E-13
BUTDE13	1,3-butadiene	6.59E-11
BUTENE1	1-butene	3.11E-11
C2BENZ	ethyl benzene	7.00E-12
C2BUTE	cis-2-butene	5.58E-11
C2PENT	cis-2-pentene	6.50E-11
C4RCHO1	Butanal (butyraldehyde)	2.35E-11
C5RCHO1	Pentanal (valeraldehyde)	2.78E-11
C6RCHO1	Hexanal (hexanaldehyde)	3.00E-11
CCHO	Acetaldehyde	1.49E-11
CYCC5	Cyclopentane	5.02E-12
CYCC6	Cyclohexane	7.02E-12
CYCC7	C7 cycloalkanes	1.24E-11
ETHANE	Ethane	2.54E-13
ETHE	Ethene	8.15E-12
HCHO	Formaldehyde	8.47E-12
HEXENE1	1-hexene	3.70E-11
IC3BEN	isopropyl benzene (cumene)	6.30E-12
ISOP	Isoprene	9.96E-11
M224C5	2,2,4-trimethyl pentane	3.38E-12
M22C4	2,2-dimethyl butane	2.27E-12
M234C5	2,3,4-trimethyl pentane	6.60E-12
M23C4	2,3-dimethyl butane	5.79E-12

Table A-1. Continued

Abbreviation	Description	k_{OH} (cm^3 $molec^{-1}$ s^{-1})
M23C5	2,3-dimethyl pentane	7.15E-12
M24C5	2,4-dimethyl pentane	4.77E-12
M2C3	Isobutane	2.14E-12
M2C4	Isopentane	3.60E-12
M2C5	2-methyl pentane	5.20E-12
M2C6	2-methyl hexane	6.89E-12
M2C7	2-methyl heptane	8.31E-12
M3C5	3-methyl pentane	5.20E-12
M3C6	3-methyl hexane	7.17E-12
M3C7	3-methyl heptane	8.59E-12
MACR	Methacrolein	2.84E-11
MECYCC5	methyl cyclopentane	5.68E-12
MEK	methyl ethyl ketone	1.20E-12
METTOL	m-ethyl toluene	1.86E-11
MTBE	methyl t-butyl ether	2.95E-12
MVK	Methyl Vinyl Ketone	1.99E-11
MXYLENE	m-xylene	2.31E-11
NC10	n-decane	1.10E-11
NC11	n-undecane	1.23E-11
NC12	n-dodecane	1.32E-11
NC3BEN	n-propyl benzene	5.80E-12
NC4	n-butane	2.38E-12
NC5	n-pentane	3.84E-12
NC6	n-hexane	5.25E-12
NC7	n-heptane	6.81E-12
NC8	n-octane	8.16E-12
NC9	n-no0e	9.75E-12
OETTOL	o-ethyl toluene	1.19E-11
OXYLENE	o-xylene	1.36E-11

Table A-1. Continued

Abbreviation	Description	k_{OH} (cm^3 $molec^{-1}$ s^{-1})
PENTEN1	1-pentene	3.14E-11
PETTOL	p-ethyl toluene	1.18E-11
PROPANE	Propane	1.11E-12
PROPENE	Propene	2.60E-11
RCHO	Lumped C3+ Aldehydes (mechanism based on propionaldehyde)	1.97E-11
STYRENE	Styrene	5.80E-11
T2BUTE	trans-2-butene	6.32E-11
T2PENT	trans-2-pentene	6.70E-11
TMB123	1,2,3-trimethyl benzene	3.27E-11
TMB124	1,2,4-trimethyl benzene	3.25E-11
TMB135	1,3,5-trimethyl benzene	5.67E-11
TOLUENE	Toluene	5.58E-12

APPENDIX B. VALUES OF NORMALIZED INCREMENTAL REACTIVITIES OF 66 INDIVIDUAL VOC SPECIES

The numerical values of NIR_5, NIR_{25}, NIR_{50}, NIR_{75} and NIR_{95}, which represent the 5^{th}, 25^{th}, 50^{th}, 75^{th} and 95^{th} percentiles of NIR values in all grid cells with simulated 8-hour ozone greater than 80 ppb are listed in Table B-1 for the 66 individual VOC species. The unit of NIR is in mol O_3/mol VOC.

Table B- 1. NIRs of 66 individual VOC species

Species	**NIR_5**	**NIR_{25}**	**NIR_{50}**	**NIR_{75}**	**NIR_{95}**
ACET	0.001	0.06	0.09	0.14	0.25
ACRO	0.50	18.0	29.0	42.0	77.5
ACYL	0.002	0.12	0.21	0.37	0.75
BUTDE13	0.25	12.5	19.0	32.0	60.5
BUTENE1	0.05	6.0	8.0	12.5	22.5
C2BENZ	0.02	3.0	7.0	14.8	31.0
C2BUTE	0.05	12.5	18.0	29.5	55.0
C2PENT	0.25	18.0	29.0	42.0	76.0
C4RCHO1	0.01	18.0	30.5	43.5	81.5
C5RCHO1	0.02	21.0	35.0	50.0	92.4
C6RCHO1	0.01	18.0	28.0	41.5	76.0
CCHO	0.001	2.0	3.0	4.5	8.5
CYCC5	0.001	3.0	6.5	13.0	28.0
CYCC6	0.001	2.0	3.0	5.5	11.0
CYCC7	0.001	2.2	5.5	11.0	24.0
ETHANE	0.001	0.06	0.11	0.16	0.29
ETHE	0.2	1.8	2.0	3.0	4.8
HCHO	0.001	1.0	1.8	3.2	6.0
HEXENE1	0.05	13.5	21.5	33.5	62.5
IC3BEN	0.02	6.5	12.0	22.0	45.0
ISOP	1.0	4.2	9.0	16.0	33.0
M224C5	0.02	13.0	22.5	34.5	66.5
M22C4	0.01	6.0	11.5	19.5	40.5
M234C5	0.02	16.5	28.0	42.0	80.0
M23C4	0.01	6.6	12.4	22.5	47.5
M23C5	0.01	4.2	6.6	14.6	30.0
M24C5	0.01	9.0	17.0	28.0	57.5

Table B-1. Continued

Species	NIR_5	NIR_{25}	NIR_{50}	NIR_{75}	NIR_{95}
M2C3	0.0	0.5	0.6	1.1	2.0
M2C4	0.001	1.3	2.2	3.8	7.6
M2C5	0.001	1.6	2.2	4.2	8.4
M2C6	0.001	2.0	3.0	7.6	15.0
M2C7	0.001	6.0	12.0	22.5	48.0
M3C5	0.0	2.0	3.6	7.0	13.0
M3C6	0.001	2.5	4.5	8.0	16.0
M3C7	0.0	7.2	12.6	24.8	51.5
MACR	0.1	17.0	28.0	42.0	79.0
MECYCC5	0.02	2.5	4.5	8.5	17.6
MEK	0.0	0.7	1.2	1.9	3.8
METTOL	0.0	10.0	17.5	29.0	58.0
MTBE	0.001	0.8	1.3	2.3	4.5
MVK	0.1	24.8	41.5	58.0	100.0
MXYLENE	0.01	6.0	10.0	19.0	37.5
NC10	0.1	3.2	6.8	14.0	32.0
NC11	0.1	4.0	8.0	16.0	33.0
NC12	0.1	4.0	8.0	16.8	34.8
NC3BEN	0.1	9.6	17.5	30.0	61.0
NC4	0.05	0.5	0.7	0.9	1.6
NC5	0.01	1.0	1.6	2.8	5.4
NC6	0.05	1.5	2.7	5.0	10.6
NC7	0.05	3.0	5.8	11.0	24.0
NC8	0.05	3.6	7.0	13.6	29.0
NC9	0.05	3.5	7.6	14.0	30.0
OETTOL	0.1	12.0	22.0	33.0	65.0
OXYLENE	0.01	3.0	7.5	15.4	33.6
PENTEN1	0.01	8.0	15.0	25.0	50.0
PETTOL	0.01	8.0	17.5	29.0	61.0
PROPANE	0.001	0.2	0.3	0.5	0.9
PROPENE	0.05	4.5	5.6	8.0	14.0
RCHO	0.0	7.0	12.4	20.0	40.0
STYRENE	0.05	10.4	33.0	37.0	77.0
T2BUTE	1.0	16.5	24.0	36.5	66.0
T2PENT	1.0	15.8	24.0	36.5	69.0
TMB123	1.0	17.6	29.0	43.0	80.0
TMB124	1.0	13.0	22.6	36.0	69.5
TMB135	1.0	18.5	30.5	44.0	81.5

APPENDIX C. PARAMETERS INCLUDED IN THE INPUT FILES FOR MAXIMUM INCREMENTAL REACTIVITY (MIR) SIMULATIONS

ARBMIX1.CMP contains the fractions of Non-Methane Hydro-Carbon (NMHC) species (See Table C-1) and the fractions of oxygenated species (See Table C-2). The NMHC fraction is normalized to 1 ppm carbon. The oxygenated fraction is normalized to 0.0475 ppm carbon.

The fraction of each NMHC species is calculated using equation (C-1):

$$F_{NMHC,i} = \frac{C_{NMHC,i}}{\sum_1^{95} C_{NMHC,i} \times CN_{NMHC,i}} \quad \text{(C-1)}$$

$F_{NMHC,i}$ is the fraction of each NMHC species; $C_{NMHC,i}$ is the concentration of each NMHC species in ppm; $CN_{NMHC,i}$ is the carbon number of each NMHC species. A total of 95 species were included in the original mixture used to derive MIR by Carter [26].

Table C- 1. Fractions of NMHC species in Nanjing based on CMAQ predicted concentrations

Species	**Description**	**Fraction (ppm/ppm)**
ETHANE	Ethane	1.08E-02
PROPANE	Propane	5.63E-03
NC4	n-butane	4.10E-03
NC5	n-pentane	2.02E-03
NC6	n-hexane	1.13E-03
NC7	n-heptane	3.77E-04
NC8	n-octane	4.66E-04
NC9	n-no0e	4.19E-04
NC10	n-decane	6.85E-04
NC11	n-undecane	4.05E-04
NC12	n-dodecane	5.91E-04
NC13	n-tridecane	2.66E-05
M2C3	Isobutane	4.03E-03
M2C4	Isopentane	1.60E-03

Table C-1. Continued

Species	Description	Fraction(ppm/ppm)
M2C5	2-methyl pentane	1.41E-03
M3C5	3-methyl pentane	1.06E-03
M22C4	2,2-dimethyl butane	7.57E-05
M23C4	2,3-dimethyl butane	1.17E-04
M24C5	2,4-dimethyl pentane	7.35E-05
M3C6	3-methyl hexane	1.05E-03
M23C5	2,3-dimethyl pentane	4.15E-04
CYCC5	Cyclopentane	2.73E-04
MECYCC5	Methyl cyclopentane	4.17E-04
CYCC6	Cyclohexane	1.61E-03
MECYCC6	Methyl cyclopentane	1.60E-03
ETCYCC6	Ethyl cyclopentane	4.21E-04
BRC6	Branched C6 alkanes	5.61E-04
BRC7	Branched C7 alkanes	4.91E-03
BRC8	Branched C8 alkanes	9.48E-03
BRC9	Branched C9 alkanes	4.02E-03
BRC10	Branched C10 alkanes	3.66E-03
BRC11	Branched C11 alkanes	3.88E-04
BRC12	Branched C12 alkanes	7.67E-04
BRC13	Branched C13 alkanes	3.38E-05
CYCC7	C7 cycloalkanes	7.66E-04
ETHE	Ethene	1.64E-02
PROPENE	Propene	1.08E-02
BUTENE1	1-butene	5.63E-03
C4OLE1	C4 terminal alkenes	4.10E-03
M3BUT1	3-methyl-1-butene	2.02E-03
PENTEN1	1-pentene	1.13E-03
HEXENE1	1-hexene	3.77E-04
ISOBUTEN	Isobutene	4.66E-04

Table C-1. Continued

Species	Description	Fraction(ppm/ppm)
M2BUT1	2-methyl-1-butene	4.19E-04
T2BUTE	Trans-2-butene	6.85E-04
C2BUTE	Cis-2-butene	4.05E-04
M2BUT2	2-methyl-2-butene	5.91E-04
BUTDE13	1,3-butadiene	2.66E-05
ISOP	Isoprene	4.03E-03
CYCHEXE	Cyclohexene	1.60E-03
APINENE	Alpha-pinene	1.41E-03
CARENE3	3-carene	1.06E-03
C5OLE1	C5 terminal alkenes	7.57E-05
C6OLE1	C6 terminal alkenes	1.17E-04
C7OLE1	C7 terminal alkenes	7.35E-05
C8OLE1	C8 terminal alkenes	1.05E-03
C9OLE1	C9 terminal alkenes	4.15E-04
C10OLE1	C10 terminal alkenes	2.73E-04
C11OLE1	C11 terminal alkenes	4.17E-04
C4OLE2	C4 internal alkenes	1.61E-03
C5OLE2	C5 internal alkenes	1.60E-03
C6OLE2	C6 internal alkenes	4.21E-04
C7OLE2	C7 internal alkenes	5.61E-04
C8OLE2	C8 internal alkenes	4.91E-03
C9OLE2	C9 internal alkenes	1.30E-04
C10OLE2	C10 internal alkenes	5.08E-05
C7OL2D	C7 cyclic or di-olefins	1.01E-04
BENZENE	Benzene	2.29E-03
TOLUENE	Toluene	6.41E-03
C2BENZ	Ethyl benzene	2.91E-04
NC3BEN	n-propyl benzene	7.37E-05
IC3BEN	Isopropyl benzene	1.30E-04

Table C-1. Continued

Species	Description	Fraction(ppm/ppm)
C9BEN1	C9 monosub benzenes	1.09E-04
SC4BEN	s-butyl benzene	1.60E-04
C10BEN1	C10 monosub benzenes	1.28E-04
C11BEN1	C11 monosub benzenes	4.49E-04
C12BEN1	C12 monosub benzenes	1.92E-05
OXYLENE	o-xylene	5.77E-04
PXYLENE	p-xylene	1.53E-03
MXYLENE	m-xylene	1.53E-03
C9BEN2	C9 disub benzenes	1.72E-03
C10BEN2	C10 disub benzenes	1.06E-03
C11BEN2	C11 disub benzenes	6.41E-05
C12BEN2	C12 disub benzenes	5.77E-05
TMB135	1,3,5-trimethyl benzene	5.09E-05
TMB123	1,2,3-trimethyl benzene	6.22E-05
C9BEN3	C9 trisub benzenes	1.63E-03
C10BEN3	C10 trisub benzenes	1.12E-03
C11BEN3	C11 trisub benzenes	6.41E-05
C12BEN3	C12 trisub benzenes	5.77E-05
C10BEN4	C10 tetrasub benzenes	2.88E-04
C9STYR	C9 styrenes	3.27E-04
C10STYR	C10 styrenes	2.56E-04
ACYL	Acetylene	4.37E-03
C11OLE2	C11 internal alkenes	1.01E-04

For those species whose concentrations are not simulated by the S11D mechanism, their concentrations were estimated based on the concentrations of a species that has similar structures with the unknown species and the ratio of these two species in

the ARBMIX1.CMP file prepared by Carter [38]. For example, the fractions of NC12 and NC13 in the original ARBMIX1.CMP are 3.4174e-04 and 1.5388e-05, respectively. Although the concentration of NC13 is not included in the CMAQ output, it can be estimated from NC12, since these two species have similar molecular structures. The concentration of NC13 can be estimated as $\frac{1.5388e-05}{3.4174e-04} \times$ [NC12]. The same method was applied to estimate their concentrations and fractions for other missing species.

The fraction of each oxygenated species is calculated using equation (C-2):

$$F_{OXYGENATED,i} = 0.0475 \times \frac{C_{OXYGENATED,i}}{\sum_1^9 C_{OXYGENATED,i} \times CN_{OXYGENATED,i}} \quad \text{(C-2)}$$

$F_{OXGENATED,i}$ is the fraction of each oxygenated species; $C_{OXYGENATED,i}$ is the concentration of each oxygenated species in ppm; $CN_{OXYGENATED,i}$ is the carbon number of each oxygenated species.

Table C- 2. Fractions of NMHC species

Species	Fraction (ppm/ppm)
FORMALD	1.18E-02
ACETALD	4.71E-03
PROPALD	3.31E-03
C4-RCHO	1.36E-05
C5-RCHO	6.32E-06
C6-RCHO	1.94E-05
ACETONE	4.51E-03
MEK	5.31E-04
BENZALD	6.85E-05

The parameters included in the input file for the Nanjing scenario (NANJIN.INP) are listed in Table C-3. TEMPR, H_2O, HEIGHT, EMR.HC, EMR.NOX, E.CO, E.ISOP, E.APIN and E.UNKN represent time-varying hourly temperature in K, concentration of water vapor in ppm, mixing height in m, emission fraction of anthropogenic VOCs,

emission fraction of NO_x, and emission rates of carbon monoxide (CO), isoprene, terpene and other biogenic VOCs in 10^{-3}moles m^{-2}, respectively.

Table C- 3. Parameters included in NANJIN.INP

Times (s)	TEMPR	H2O	HEIGHT	EMR.HC	EMR.NOX	E.CO	E.ISOP	E.APIN	E.UNKN
480	302.1	31470	335.8	8.48E-04	1.17E-03	9.56E-03	1.34E-03	1.84E-04	9.39E-04
540	303.8	32010	526.9	1.16E-03	1.45E-03	1.28E-02	2.00E-03	2.41E-04	1.24E-03
600	304.9	31620	844.2	1.11E-03	1.45E-03	1.25E-02	2.57E-03	2.90E-04	1.49E-03
660	305.9	31140	1106	1.15E-03	1.41E-03	1.30E-02	2.99E-03	3.27E-04	1.68E-03
720	306.7	30730	1361	1.13E-03	1.37E-03	1.29E-02	3.24E-03	3.49E-04	1.79E-03
780	307.2	30380	1538	1.13E-03	1.46E-03	1.29E-02	3.25E-03	3.53E-04	1.80E-03
840	307.6	30080	1657	1.11E-03	1.47E-03	1.26E-02	3.14E-03	3.47E-04	1.76E-03
900	307.7	29880	1689	1.12E-03	1.49E-03	1.26E-02	2.77E-03	3.21E-04	1.62E-03
960	307.6	29780	1647	1.13E-03	1.46E-03	1.27E-02	2.26E-03	2.84E-04	1.42E-03
1020	307.4	30040	1450	1.21E-03	1.43E-03	1.37E-02	1.61E-03	2.36E-04	1.17E-03

The time-varying hourly emissions fractions of anthropogenic VOCs (EMR.HC) were calculated using equation (C-3):

$$\text{EMR. HC } (\text{min}^{-1}) = \frac{\sum \text{CN}_\text{i} \times \text{E}_\text{i} \text{ moles} \cdot \text{min}^{-1}}{\sum_1^{10} \sum \text{CN}_\text{i} \times \text{E}_\text{i} \text{ moles} \cdot \text{s}^{-1} \times 60\text{s} + \sum \text{CN}_\text{i} \times \text{C}_1 \text{ moles} \cdot \text{m}^{-3} \times \text{PBL m} \times 1.296 \times 10^9 \text{m}^2} \quad \text{(C-3)}$$

Hourly emissions are needed for 8:00 am to 5:00 pm local time. CN_i refers to carbon number of the i^{th} anthropogenic VOC; E_i refers to the hourly emission rate of the i^{th} anthropogenic VOC in moles s^{-1}; C_1 refers to initial concentration of the i^{th} anthropogenic VOC at 8:00 am in moles m^{-3}; PBL refers to the mixing height of that hour in m; 1.296×10^9 m^2 is the area of one grid cell (36km $\times$ 36 km).

The initial fraction of HC (INI.HC) can be determined as shown in equation (C-4):

$$\text{INI. HC} = 1 - 60 \text{ min} \times \sum_1^{10} (\text{EMR. HC}) \text{ min}^{-1} \quad \text{(C-4)}$$

The time-varying hourly emissions of NO_x fractions (EMR.NOX) were calculated using equation (C-5):

$$\text{EMR. NOX}\,(\text{min}^{-1}) = \frac{(\text{E}_{\text{NO2}} + \text{E}_{\text{NO}})\ \text{moles} \cdot \text{min}^{-1}}{\sum_1^{10}(\text{E}_{\text{NO2}} + \text{E}_{\text{NO}})\ \text{moles} \cdot \text{s}^{-1} \times 60\text{s} \cdot + (\text{C}_{\text{NO2,1}} + \text{C}_{\text{NO,1}})\ \text{moles} \cdot \text{m}^{-3} \times \text{PBL m} \times 1.296 \times 10^9 \text{m}^2} \quad \text{(C-5)}$$

Hourly emissions are needed for 8:00 am to 5:00 pm local time. E_{NO2} and E_{NO} refer to the hourly emission rate of NO_2 and NO in moles s^{-1}, respectively; $C_{NO2,1}$ and $C_{NO,1}$ refers to initial concentration of NO_2 and NO at 8:00 am in moles m^{-3}, respectively; PBL refers to the mixing height of that hour in m; 1.296×10^9 m^2 is the area of one grid cell (36km × 36 km).

The initial fraction of NOx (INI.NOX) can be determined as shown in equation (C-6):

$$\text{INI. NOX} = 1 - 60\ \text{min} \times \sum_1^{10}(\text{EMR. NOX})\ \text{min}^{-1} \quad \text{(C-6)}$$

The hourly emission rates of carbon monoxide, biogenic isoprene, terpene and other biogenic VOCs (E.CO, E.ISOP, E.APIN, E.UNKN) were calculated using equations (C-7) to (C-10), respectively:

$$\text{E. CO}(10^{-3}\text{moles} \cdot \text{m}^{-2}) = \frac{\text{E}_{\text{CO}}}{21600}(\text{moles} \cdot \text{s}^{-1}) \quad \text{(C-7)}$$

$$\text{E. ISOP}(10^{-3}\text{moles} \cdot \text{m}^{-2}) = \frac{\text{E}_{\text{ISOP}}}{21600}(\text{moles} \cdot \text{s}^{-1}) \quad \text{(C-8)}$$

$$\text{E. APIN}(10^{-3}\text{moles} \cdot \text{m}^{-2}) = \frac{\text{E}_{\text{APIN}}}{21600}(\text{moles} \cdot \text{s}^{-1}) \quad \text{(C-9)}$$

$$\text{E. UNKN}(10^{-3}\text{moles} \cdot \text{m}^{-2}) = \frac{\text{E}_{\text{UNKN}}}{21600}(\text{moles} \cdot \text{s}^{-1}) \quad \text{(C-10)}$$

Additionally, the total emission rate of anthropogenic VOCs (E.HC) and NO_x (E.NOX) need to be determined as in equation (C-11) and (C-12):

$$\text{E. HC}(10^{-3}\text{moles} \cdot \text{m}^{-2}) = 60\ \text{s} \cdot \text{min}^{-1} \times \frac{\sum \text{CN}_\text{i} \times \text{E}_{\text{i,1}}\ \text{moles} \cdot \text{s}^{-1}}{(1 - \text{INI.HC}) \times (36000\text{m})^2} \times 10^3 \text{millimole} \cdot \text{moles}^{-1} \quad \text{(C-11)}$$

$$\text{E. NOX}(10^{-3}\text{moles} \cdot \text{m}^{-2}) = 60\ \text{s} \cdot \text{min}^{-1} \times \frac{(\text{E}_{\text{NO2}} + \text{E}_{\text{NO}})\ \text{moles} \cdot \text{s}^{-1}}{(1 - \text{INI.NOX}) \times (36000\text{m})^2} \times 10^3 \text{millimole} \cdot \text{moles}^{-1} \quad \text{(C-12)}$$

The aloft ozone concentrations (in ppm) are the concentration of ozone in the layer that is right above the mixing height in the first hour of the model simulation. The aloft ozone concentration is not time dependent.

In the case of the Nanjing scenario, the total emitted HC amount is 4.055×10^{-3} moles $\cdot m^{-2}$; the total emitted NO_x amount is 0.993×10^{-3} moles $\cdot m^{-2}$; the aloft ozone concentration is 0.0482 ppm.

APPENDIX D. LATITUDES AND LONGITUDES OF THE 34 CITIES IN CHINA

The input files included in a single-cell model were prepared based on the emissions data in China. The latitudes and longitudes of the 34 cities in China are listed in Table D-1.

Table D- 1. Cities names and corresponding latitudes and longitudes in China

City	Latitude	Longitude	City	Latitude	Longitude
Beijing	39.9075	116.3972	Nanjing	32.0617	118.7778
Changchun	43.8800	125.3228	Nanning	22.8167	108.3167
Changsha	28.1987	112.9709	Shanghai	31.2222	121.4581
Chengdu	30.6667	104.0667	Shenyang	41.7922	123.4328
Chongqing	29.5628	106.5528	Shijiazhuang	38.0414	114.4786
Fuzhou	26.0614	119.3061	Taiyuan	37.8694	112.5603
Guangzhou	23.1167	113.2500	Tianjin	39.1422	117.1767
Guiyang	26.5833	106.7167	Urumqi	43.8250	87.6000
Haikou	20.0458	110.3417	Wuhan	30.5833	114.2667
Hangzhou	30.2937	120.1614	Xi'an	34.2583	108.9286
Harbin	45.7500	126.6500	Xining	36.6255	101.7574
Hefei	31.8667	117.2833	Yinchuan	38.4667	106.2667
Hohhot	40.8106	111.6522	Zhengzhou	34.7578	113.6486
Jinan	36.6683	116.9972	Hongkong	22.2783	114.1747
Kunming	25.0389	102.7183	Macau	22.1667	113.5500
Lanzhou	36.0333	103.8000	Taipei	25.0333	121.6333
Lhasa	29.6500	91.1167			
Nanchang	28.6840	115.8531			

APPENDIX E. FRACTIONS OF HOURLY EMITTED HYDROCARBON FRACTION AND MIR OF BASE ROG MIXTURE OF 34 CITIES IN CHINA

A complete list of hourly fractions of EMR.HC in the 34 cities in China and the MIR of base ROG mixture for each city is listed in Table E-1.

Table E- 1. Hourly fractions of EMR.HC and MIR of base ROG mixture

City	MIR	8:00 AM	9:00 AM	10:00 AM	11:00 AM	12:00 PM	1:00 PM	2:00 PM	3:00 PM	4:00 PM	5:00 PM
Beijing	2.56	0.09	0.10	0.09	0.10	0.10	0.10	0.09	0.09	0.10	0.14
Changchun	3.20	0.08	0.10	0.10	0.10	0.10	0.10	0.10	0.10	0.10	0.12
Changsha	3.10	0.08	0.10	0.10	0.10	0.10	0.10	0.10	0.10	0.10	0.12
Chengdu	3.07	0.09	0.10	0.09	0.10	0.10	0.10	0.09	0.09	0.10	0.13
Chongqing	3.05	0.09	0.10	0.09	0.11	0.10	0.10	0.09	0.09	0.10	0.14
Fuzhou	2.40	0.08	0.10	0.10	0.10	0.10	0.10	0.10	0.10	0.10	0.11
Guangzhou	3.01	0.08	0.10	0.10	0.10	0.10	0.10	0.10	0.10	0.10	0.11
Guiyang	3.46	0.09	0.10	0.09	0.10	0.10	0.10	0.09	0.09	0.10	0.14
Haikou	3.61	0.09	0.10	0.09	0.11	0.10	0.10	0.09	0.09	0.10	0.15
Hangzhou	2.55	0.08	0.11	0.10	0.10	0.10	0.10	0.10	0.10	0.10	0.10
Harbin	3.78	0.08	0.10	0.09	0.10	0.10	0.10	0.09	0.09	0.10	0.13
Hefei	3.73	0.10	0.10	0.08	0.10	0.10	0.10	0.09	0.09	0.10	0.15
Hohhot	2.73	0.08	0.10	0.10	0.10	0.10	0.10	0.10	0.10	0.10	0.11
Jinan	3.55	0.08	0.10	0.10	0.10	0.10	0.10	0.10	0.10	0.10	0.12
Kunming	3.01	0.08	0.10	0.10	0.10	0.10	0.10	0.10	0.10	0.10	0.11
Lanzhou	3.10	0.09	0.10	0.09	0.10	0.10	0.10	0.09	0.09	0.10	0.14
Lhasa	3.73	0.09	0.10	0.10	0.10	0.09	0.10	0.10	0.11	0.10	0.10
Nanchang	3.82	0.09	0.10	0.10	0.10	0.10	0.10	0.10	0.10	0.10	0.12
Nanjing	2.74	0.08	0.10	0.10	0.10	0.10	0.10	0.10	0.10	0.10	0.11
Nanning	3.22	0.09	0.10	0.09	0.10	0.10	0.10	0.10	0.10	0.10	0.12
Shanghai	2.27	0.07	0.10	0.10	0.10	0.10	0.10	0.10	0.10	0.10	0.11
Shenyang	2.75	0.07	0.10	0.10	0.10	0.10	0.10	0.10	0.10	0.10	0.11
Shijiazhuang	3.08	0.08	0.10	0.10	0.10	0.10	0.10	0.10	0.10	0.10	0.12
Taiyuan	2.84	0.08	0.10	0.10	0.10	0.10	0.10	0.10	0.10	0.10	0.11
Tianjin	3.64	0.08	0.10	0.10	0.10	0.10	0.10	0.10	0.10	0.10	0.11
Urumqi	2.86	0.10	0.10	0.10	0.10	0.09	0.10	0.10	0.11	0.10	0.10
Wuhan	3.45	0.08	0.10	0.10	0.10	0.10	0.10	0.10	0.10	0.10	0.12
Xi'an	2.36	0.12	0.12	0.09	0.10	0.09	0.09	0.09	0.10	0.10	0.11
Xining	2.97	0.09	0.10	0.10	0.10	0.10	0.10	0.10	0.10	0.10	0.12
Yinchuan	4.58	0.08	0.10	0.10	0.10	0.10	0.10	0.10	0.10	0.10	0.11
Zhengzhou	3.44	0.08	0.10	0.10	0.10	0.10	0.10	0.10	0.10	0.10	0.12
Hongkong	8.40	0.12	0.09	0.08	0.08	0.08	0.09	0.09	0.10	0.13	0.13
Macau	4.62	0.09	0.10	0.10	0.10	0.09	0.10	0.10	0.10	0.10	0.11
Taipei	2.05	0.25	0.24	0.04	0.08	0.05	0.06	0.07	0.08	0.06	0.08

APPENDIX F. EXPANDED REACTIONS FOR PROCESS ANALYSIS IN MODIFIED SAPRC-99 MECHANISM

Table F- 1. Expanded reactions for process analysis in modified SAPRC-99 mechanism

Reaction code	**Reaction process**	**Reaction rate (cm^3 $molecules^{-1}$ s^{-1})**
<1>	NO2 = NO + O3P	Photolysis
<1_X1>	NO2_X1 = NO_X1 + O3P	Photolysis
<19>	NO3 = NO2 + O3P	Photolysis
<19_X1>	NO3_X1 = NO2_X1 + O3P	Photolysis
<34>	HO2 + NO = HO + NO2	3.40e-12
<34_X0_1>	HO2 + NO_X1 = HO + NO2_X1	3.40e-12
<34_X1_0>	HO2_X1 + NO = HO + NO2	3.40e-12
<34_X1_1>	HO2_X1 + NO_X1 = HO + NO2_X1	3.40e-12
<MER1>	C_O2 + NO = NO2 + HCHO + HO2	2.80e-12
<MER1_X0_1>	C_O2 + NO_X1 = NO2_X1 + HCHO + HO2	2.80e-12
<MER1_X1_0>	C_O2_X1 + NO = NO2 + HCHO_X1 + HO2_X1	2.80e-12
<MER1_X1_1>	C_O2_X1 + NO_X1 = NO2_X1 + HCHO_X1 + HO2_X1	2.80e-12
<RRNO>	RO2_R + NO = NO2 + HO2	2.70e-12
<RRNO_X0_1>	RO2_R + NO_X1 = NO2_X1 + HO2	2.70e-12
<RRNO_X1_0>	RO2_R_X1 + NO = NO2 + HO2_X1	2.70e-12
<RRNO_X1_1>	RO2_R_X1 + NO_X1 = NO2_X1 + HO2_X1	2.70e-12
<R2NO>	R2O2 + NO = NO2	2.70e-12
<R2NO_X0_1>	R2O2 + NO_X1 = NO2_X1	2.70e-12
<R2NO_X1_0>	R2O2_X1 + NO = NO2	2.70e-12
<R2NO_X1_1>	R2O2_X1 + NO_X1 = NO2_X1	2.70e-12
<APNO>	CCO_O2 + NO = C_O2 + NO2	7.80e-12
<APNO_X0_1>	CCO_O2 + NO_X1 = C_O2 + NO2_X1	7.80e-12
<APNO_X1_0>	CCO_O2_X1 + NO = C_O2_X1 + NO2	7.80e-12
<APNO_X1_1>	CCO_O2_X1 + NO_X1 = C_O2_X1 + NO2_X1	7.80e-12
<PPNO>	RCO_O2 + NO = NO2 + CCHO + RO2_R	1.25e-11
<PPNO_X0_1>	RCO_O2 + NO_X1 = NO2_X1 + CCHO + RO2_R	1.25e-11
<PPNO_X1_0>	RCO_O2_X1 + NO = NO2 + CCHO_X1 + RO2_R_X1	1.25e-11

Table F-1. Continued

Reaction code	Reaction process	Reaction rate (cm^3 $molecules^{-1}$ s^{-1})
<PPNO_X1_1>	RCO_O2_X1 + NO_X1 = NO2_X1 + CCHO_X1 + RO2_R_X1	1.25e-11
<BPNO>	BZCO_O2 + NO = NO2 + BZ_O + R2O2	1.25e-11
<BPNO_X0_1>	BZCO_O2 + NO_X1 = NO2_X1 + BZ_O + R2O2	1.25e-11
<BPNO_X1_0>	BZCO_O2_X1 + NO = NO2 + BZ_O_X1 + R2O2_X1	1.25e-11
<BPNO_X1_1>	BZCO_O2_X1 + NO_X1 = NO2_X1 + BZ_O_X1 + R2O2_X1	1.25e-11
<MPNO>	MA_RCO3 + NO = NO2 + HCHO + CCO_O2	1.25e-11
<MPNO_X0_1>	MA_RCO3 + NO_X1 = NO2_X1 + HCHO + CCO_O2	1.25e-11
<MPNO_X1_0>	MA_RCO3_X1 + NO = NO2 + HCHO_X1 + CCO_O2_X1	1.25e-11
<MPNO_X1_1>	MA_RCO3_X1 + NO_X1 = NO2_X1 + HCHO_X1 + CCO_O2_X1	1.25e-11
<FAHN>	HOCOO + NO = HCOOH + NO2 + HO2	2.80e-12
<FAHN_X0_1>	HOCOO + NO_X1 = HCOOH + NO2_X1 + HO2	2.80e-12
<FAHN_X1_0>	HOCOO_X1 + NO = HCOOH_X1 + NO2 + HO2_X1	2.80e-12
<FAHN_X1_1>	HOCOO_X1 + NO_X1 = HCOOH_X1 + NO2_X1 + HO2_X1	2.80e-12

APPENDIX G. CALCULATION OF EMISSIONS OF DETAILED VOCS FOR S11D BASED ON LUMPED S99

Emissions of VOCs from different source sectors were originally provided for the lumped S99 mechanism. The emission splitting factors to map S99 emissions to detailed S11D species are listed in Table G-1.

Table G- 1. Mapping of lumped S99 emissions to detailed S11D model species

S11D Species	S99 Species	Emission Splitting Factor for S99 to S11D Mapping	S11D Species	S99 Species	Emission Splitting Factor for S99 to S11D Mapping
ACET	ACET	1.000	ISOP	ISOP	1.000
ACRO	MACR	0.440	M224C5	ALK3	0.003
ACYL	ALK2	0.421	M22C4	ALK3	0.008
BUTDE13	OLE2	0.090	M234C5	ALK4	0.005
BUTENE1	OLE1	0.116	M23C4	ALK4	0.017
C2BENZ	ARO2	0.064	M23C5	ALK5	0.052
C2BUTE	OLE2	0.338	M24C5	ALK4	0.011
C2PENT	OLE2	0.050	M2C3	ALK3	0.429
C4RCHO1	RCHO	0.099	M2C4	ALK2	0.142
C5RCHO1	RCHO	0.050	M2C5	ALK4	0.207
C6RCHO1	RCHO	0.158	M2C6	ALK5	0.109
CCHO	CCHO	1.000	M2C7	ALK5	0.027
CYCC5	ALK4	0.040	M3C5	ALK4	0.155
CYCC6	ALK5	0.200	M3C6	ALK5	0.132
CYCC7	ALK5	0.102	M3C7	ALK5	0.027
ETHANE	ALK1	1.000	MACR	MACR	0.560
ETHE	ETHE	1.000	MECYCC5	ALK4	0.062
HCHO	HCHO	1.000	MEK	MEK	1.000
HEXENE1	OLE1	0.014	METTOL	ARO2	0.043
IC3BEN	ARO1	0.016	MTBE	ALK3	0.114

S11D Species	S99 Species	Emission Splitting Factor for S99 to S11D Mapping
MVK	MVK	1.000
MXYLENE	ARO2	0.562
NC10	ALK5	0.094
NC11	ALK5	0.057
NC12	ALK5	0.084
NC3BEN	ARO1	0.009
NC4	ALK3	0.445
NC5	ALK4	0.279
NC6	ALK4	0.166
NC7	ALK4	0.058
NC8	ALK5	0.060
NC9	ALK5	0.056
OETTOL	ARO2	0.022
OXYLENE	ARO2	0.172
PENTEN1	OLE1	0.026
PETTOL	ARO2	0.028
PROPANE	ALK2	0.437
PROPENE	OLE1	0.844
RCHO	RCHO	0.694
STYRENE	ARO1	0.031
T2BUTE	OLE2	0.417
T2PENT	OLE2	0.105
TMB123	ARO2	0.026
TMB124	ARO2	0.056
TMB135	ARO2	0.026
TOLUENE	ARO1	0.740

The emission rates of each 66 individual VOC species from each emission sector and the median value of normalized incremental reactivity (NIR) of each individual VOC species are listed in Table G-2. The unit of emission rate is in kmol/day; the unit of NIR_{50} is in mol O_3/mol VOC.

Table G- 2. Emission rates of 66 VOC species from explicit emission sector in kmol/day and NIR_{50} of each individual VOC species

Species	Industrial	Transportation	Wildfire	Residential	Biogenic	Other Countries	Power	NIR_{50}
ACET	1.22E+01	1.84E+00	5.86E+00	3.09E+00	2.53E+01	1.14E+00	2.68E-04	0.1
ACRO	2.02E-02	1.84E-01	0	1.61E-01	0	5.48E-02	0	29.0
ACYL	2.75E+01	1.42E+00	1.09E+00	5.36E+00	2.27E-02	4.16E+00	3.82E-02	0.2
BUTDE13	2.19E+00	5.48E-01	1.09E-01	3.58E-01	1.21E+00	1.36E-01	1.33E-02	19.0
BUTENE1	3.19E+00	8.26E-01	4.76E-01	8.12E-01	4.35E+00	6.18E-01	2.90E-02	8.0

Table G-2. Continued

C2BENZ	2.70E+00	3.18E-01	2.77E-02	2.54E-01	1.75E-02	3.19E-01	9.27E-02	7.0
C2BUTE	8.19E+00	2.05E+00	4.08E-01	1.34E+00	4.55E+00	5.10E-01	4.99E-02	18.0
C2BUTE	8.19E+00	2.05E+00	4.08E-01	1.34E+00	4.55E+00	5.10E-01	4.99E-02	18.0
C2PENT	1.22E+00	3.06E-01	6.08E-02	2.00E-01	6.78E-01	7.60E-02	7.44E-03	1.22E+00
C4RCHO1	7.30E-04	1.84E-01	1.45E+00	6.95E-02	8.16E-02	6.60E-02	0	7.30E-04
C5RCHO1	3.66E-04	9.23E-02	7.27E-01	3.48E-02	4.09E-02	3.31E-02	0	3.66E-04
C6RCHO1	1.16E-03	2.94E-01	2.31E+00	1.11E-01	1.30E-01	1.05E-01	0	1.16E-03
CCHO	7.03E-04	4.25E+00	2.15E+01	1.54E+00	1.03E+01	1.73E+00	0	7.03E-04
CYCC5	2.00E+00	2.88E-01	9.65E-03	2.28E-01	7.83E-02	5.85E-01	1.52E-02	2.00E+00
CYCC6	1.21E+01	1.25E+00	3.33E-02	1.81E+00	1.54E-01	1.49E+00	5.95E-03	1.21E+01
CYCC7	6.14E+00	6.38E-01	1.70E-02	9.23E-01	7.83E-02	7.60E-01	3.03E-03	6.14E+00
ETHANE	4.84E+01	1.48E+00	9.03E+00	8.34E+00	7.91E-01	1.12E+01	2.08E-01	4.84E+01
ETHE	5.55E+01	1.09E+01	8.60E+00	1.51E+01	4.92E+01	6.60E+00	0	5.55E+01
HCHO	3.56E+00	6.08E+00	1.37E+01	2.41E+00	9.49E+00	3.81E+00	4.01E-02	3.56E+00
HEXENE1	3.78E-01	9.80E-02	5.65E-02	9.63E-02	5.16E-01	7.33E-02	3.44E-03	3.78E-01
IC3BEN	1.30E+00	5.49E-02	1.11E-01	7.64E-02	3.45E-02	9.77E-02	5.03E-03	1.30E+00
ISOP	1.83E-01	3.84E-02	4.15E+00	1.39E-01	2.65E+02	2.35E+00	0	1.83E-01
M224C5	1.29E-01	4.94E-03	5.40E-04	1.93E-02	3.36E-02	3.76E-02	1.86E-04	1.29E-01
M22C4	3.08E-01	1.18E-02	1.29E-03	4.60E-02	8.03E-02	8.98E-02	4.44E-04	3.08E-01
M234C5	2.29E-01	3.29E-02	1.10E-03	2.59E-02	8.93E-03	6.67E-02	1.73E-03	2.29E-01
M23C4	8.82E-01	1.27E-01	4.25E-03	1.00E-01	3.45E-02	2.57E-01	6.70E-03	8.82E-01
M23C5	3.12E+00	3.24E-01	8.62E-03	4.69E-01	3.98E-02	3.86E-01	1.54E-03	3.12E+00
M24C5	5.35E-01	7.70E-02	2.58E-03	6.08E-02	2.09E-02	1.56E-01	4.06E-03	5.35E-01
M2C3	1.62E+01	6.20E-01	6.78E-02	2.42E+00	4.22E+00	4.72E+00	2.34E-02	1.62E+01
M2C4	9.30E+00	4.79E-01	3.69E-01	1.81E+00	7.68E-03	1.41E+00	1.29E-02	9.30E+00
M2C5	1.04E+01	1.50E+00	5.02E-02	1.18E+00	4.08E-01	3.04E+00	7.92E-02	1.04E+01
M2C6	6.60E+00	6.85E-01	1.82E-02	9.91E-01	8.41E-02	8.16E-01	3.25E-03	6.60E+00
M2C7	1.66E+00	1.72E-01	4.58E-03	2.49E-01	2.11E-02	2.05E-01	8.17E-04	1.66E+00
M3C5	7.84E+00	1.13E+00	3.77E-02	8.90E-01	3.06E-01	2.29E+00	5.95E-02	7.84E+00
M3C6	7.94E+00	8.25E-01	2.19E-02	1.19E+00	1.01E-01	9.82E-01	3.91E-03	7.94E+00
M3C7	1.63E+00	1.69E-01	4.49E-03	2.44E-01	2.07E-02	2.01E-01	8.02E-04	1.63E+00
MACR	2.57E-02	2.34E-01	0	2.05E-01	0	6.97E-02	0	2.57E-02
MECYCC5	3.14E+00	4.52E-01	1.51E-02	3.56E-01	1.23E-01	9.16E-01	2.38E-02	3.14E+00
MEK	2.67E+00	4.40E-01	4.68E+00	9.66E-01	3.30E-01	7.56E-01	0	2.67E+00
METTOL	1.82E+00	2.15E-01	1.87E-02	1.71E-01	1.18E-02	2.15E-01	6.25E-02	1.82E+00
MTBE	4.32E+00	1.65E-01	1.81E-02	6.45E-01	1.13E+00	1.26E+00	6.23E-03	4.32E+00
MVK	0	0	0	0	0	1.19E-03	0	0
MXYLENE	2.35E+01	2.78E+00	2.42E-01	2.21E+00	1.53E-01	2.78E+00	8.08E-01	2.35E+01
NC10	5.66E+00	5.88E-01	1.56E-02	8.50E-01	7.21E-02	7.00E-01	2.79E-03	5.66E+00

Table G-2. Continued

NC11	3.42E+00	3.56E-01	9.45E-03	5.14E-01	4.36E-02	4.23E-01	1.69E-03	3.42E+00
NC12	5.08E+00	5.27E-01	1.40E-02	7.62E-01	6.47E-02	6.28E-01	2.50E-03	5.08E+00
NC3BEN	7.35E-01	3.10E-02	6.24E-02	4.31E-02	1.95E-02	5.52E-02	2.84E-03	7.35E-01
NC4	1.68E+01	6.44E-01	7.04E-02	2.51E+00	4.39E+00	4.90E+00	2.43E-02	1.68E+01
NC5	1.41E+01	2.03E+00	6.80E-02	1.60E+00	5.52E-01	4.12E+00	1.07E-01	1.41E+01
NC6	8.39E+00	1.21E+00	4.04E-02	9.52E-01	3.28E-01	2.45E+00	6.37E-02	8.39E+00
NC7	2.95E+00	4.24E-01	1.42E-02	3.35E-01	1.15E-01	8.60E-01	2.24E-02	2.95E+00
NC8	3.61E+00	3.75E-01	9.96E-03	5.42E-01	4.60E-02	4.46E-01	1.78E-03	3.61E+00
NC9	3.37E+00	3.50E-01	9.30E-03	5.06E-01	4.29E-02	4.16E-01	1.66E-03	3.37E+00
OETTOL	9.08E-01	1.07E-01	9.34E-03	8.54E-02	5.89E-03	1.07E-01	3.12E-02	9.08E-01
OXYLENE	7.22E+00	8.52E-01	7.43E-02	6.80E-01	4.69E-02	8.55E-01	2.48E-01	7.22E+00
PENTEN1	7.22E-01	1.87E-01	1.08E-01	1.84E-01	9.86E-01	1.40E-01	6.57E-03	7.22E-01
PETTOL	1.19E+00	1.41E-01	1.23E-02	1.12E-01	7.74E-03	1.41E-01	4.10E-02	1.19E+00
PROPANE	2.86E+01	1.47E+00	1.13E+00	5.57E+00	2.36E-02	4.32E+00	3.97E-02	2.86E+01
PROPENE	2.31E+01	5.99E+00	3.45E+00	5.89E+00	3.16E+01	4.48E+00	2.10E-01	2.31E+01
RCHO	5.12E-03	1.29E+00	1.02E+01	4.88E-01	5.72E-01	4.63E-01	0	5.12E-03
STYRENE	2.56E+00	1.08E-01	2.17E-01	1.50E-01	6.77E-02	1.92E-01	9.87E-03	2.56E+00
T2BUTE	1.01E+01	2.53E+00	5.03E-01	1.65E+00	5.60E+00	6.28E-01	6.15E-02	1.01E+01
T2PENT	2.54E+00	6.36E-01	1.26E-01	4.15E-01	1.41E+00	1.58E-01	1.55E-02	2.54E+00
TMB123	1.09E+00	1.28E-01	1.12E-02	1.02E-01	7.07E-03	1.29E-01	3.74E-02	1.09E+00
TMB124	2.36E+00	2.78E-01	2.43E-02	2.22E-01	1.53E-02	2.79E-01	8.11E-02	2.36E+00
TMB135	1.07E+00	1.26E-01	1.10E-02	1.01E-01	6.95E-03	1.27E-01	3.68E-02	1.07E+00
TOLUENE	6.17E+01	2.60E+00	5.24E+00	3.62E+00	1.64E+00	4.63E+00	2.38E-01	6.17E+01
BACL	1.99E-01	3.70E-02	0	3.04E-01	0	1.00E-02	0	1.99E-01
BALD	0	1.10E-01	7.85E-02	2.39E-02	5.04E-02	3.84E-01	0	0
CCO_OH	0	0	1.60E+01	0	3.56E+00	2.90E-01	0	0
CRES	4.44E-02	3.35E-02	0	2.34E-01	0	1.28E-02	0	4.44E-02
GLY	3.59E-03	1.35E-01	0	3.95E+00	0	6.92E-02	0	3.59E-03
HCOOH	0	0	6.45E+00	0	4.64E+00	1.55E-01	0	0
IPROD	1.02E-03	7.79E-01	0	1.57E-01	0	3.46E-01	0	1.02E-03
MEOH	4.13E+00	3.03E-03	1.55E+01	5.83E+00	3.80E+02	4.55E+00	0	4.13E+00
MGLY	2.32E-03	8.27E-02	1.70E+00	1.45E+00	0	8.66E-02	0	2.32E-03
PHEN	1.30E-01	0	4.36E+00	1.07E-01	0	6.89E-02	0	1.30E-01
PROD2	2.89E+00	1.32E-01	8.65E-01	4.52E-01	0	2.16E-01	0	2.89E+00
RCO_OH	0	0	0	0	4.05E-01	7.71E-03	0	0
SESQ	0	0	0	0	1.22E+00	5.68E-02	0	0
TRP1	4.29E-01	9.09E-02	9.06E-03	1.12E+00	2.81E+01	4.59E-01	0	4.29E-01

APPENDIX H. DESCRIPTION OF EACH SPECIES INCLUDED IN THE PROCESS ANALYSIS

Table H- 1. Description and reaction code of species in IRR

Name in the IRR outputs	Description	Reaction(s) code in the expanded SAPRC-99[a]
po3p	O · produced from NO_2 from other sources.	<1> + <19>
po3p_X1	O · produced from NO_2 from the explicit source.	<1_X1> + <19_X1>
pno2inog	Production of NO_2 due to HO_2 · reaction with NO from other sources.	<34> + <34_X0_1>
pno2inog_X1	Production of NO_2 due to HO_2 · reaction with NO from the explicit source.	<34_X1_0> + <34_X1_1>
pno2org	Production of NO_2 due to RO_2 · reaction with NO from other sources.o	<MER1> + <MER1_X0_1> + <RRNO> + <RRNO_X0_1> + <R2NO> + <R2NO_X0_1> + <APNO> + <APNO_X0_1> + <PPNO> + <PPNO_X0_1> + <BPNO> + <BPNO_X0_1> + <MPNO> + <MPNO_X0_1> + <FAHN> + <FAHN_X0_1>
pno2org_X1	Production of NO_2 due to RO_2 · reaction with NO from the explicit source.	<MER1_X1_0>+<MER1_X1_1>+ <RRNO_X1_0>+<RRNO_X1_1>+ <R2NO_X1_0>+<R2NO_X1_1>+ <APNO_X1_0>+<APNO_X1_1>+ <PPNO_X1_0>+<PPNO_X1_1>+ <BPNO_X1_0>+<BPNO_X1_1>+ <MPNO_X1_0>+<MPNO_X1_1> + <FAHN_X1_0>+<FAHN_X1_1>
prodh2o2	Production of H_2O_2 from other sources.	PROD [HO2H][b]

Table H-1. Continued

prodh2o2_X1	Production of H_2O_2 from the explicit source.	PROD [HO2H_X1]
prodhno3	Production of HNO_3 from other sources.	PROD [HNO3]
prodhno3_X1	Production of HNO_3 from the explicit source.	PROD [HNO3_X1]
Prodrooh	Production of ROOH from other sources.	PROD [ROOH]
prodrooh_X1	Production of ROOH from the explicit source.	PROD [ROOH_X1]
po3net	Net ozone production.	NET [O3][c]

a. The related chemical reactions in the expanded SAPRC-99 mechanism is listed in Table F-1.
b. PROD is the IRR command to calculate the production rate of a model species that takes all reactions that produce that species into account.
c. NET is the IRR command to calculate the net formation of certain species.

APPENDIX I. DIURNAL VARIATIONS OF HOURLY AVERAGED OZONE AND THE CONTRIBUTIONS OF EACH SECTOR BASED ON REGIME INDICATOR I2

The temporal variations of hourly averaged ozone and the diurnal contribution of each explicit emission sector based on indicator I2 in four metropolitan cities in China (Beijing, Shanghai, Chongqing and Guangzhou) in August 2013 are shown in Figure I-1. Overall, the contributions from industries and transportation sectors are higher than those based on indicator I1 but the contributions of biogenic sources are lower.

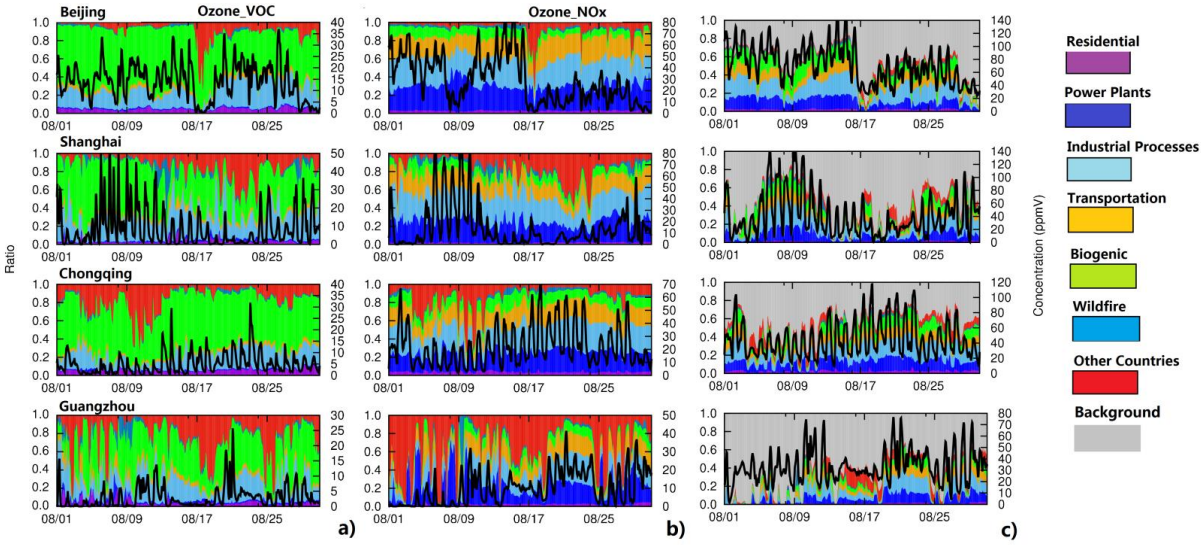

Figure I- 1. Diurnal variations of hourly averaged ozone and the contributions of each sector to a) VOC-attributed ozone formation; b) NO_x-attributed ozone formation and c) total ozone concentrations in Beijing, Shanghai, Chongqing and Guangzhou, China in August 2013 based on indicator I2. Concentrations of ozone, and ozone attributed to NO_x and VOC sources are shown as black lines against the second y axis on the right of each panel. Note that the scales for ozone concentrations are different. Ozone concentrations are in units of ppbV.

APPENDIX J. COMPARISON OF MONTHLY AVERAGED DIURNAL VARIATIONS OF HOURLY O_3 AND NO_2 CONCENTRATIONS IN AUGUST 2013 IN 60 DIFFERENT CHINESE CITIES

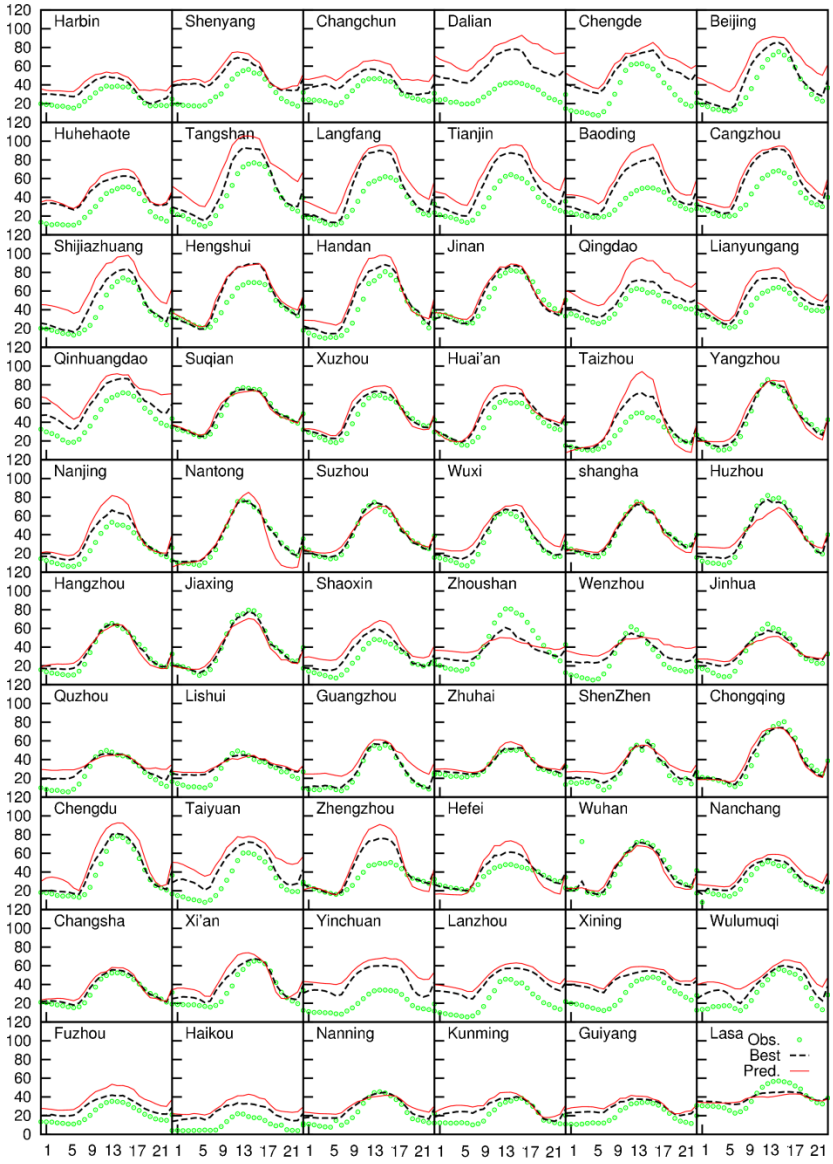

Figure J- 1. Comparison of monthly averaged diurnal variations of hourly O_3 concentrations in 60 cities in China in August 2013. Red lines are the values predicted at the grid cell where the monitors are located; Black dash lines are the values predicted within the 3×3 grid cell regions surrounding the monitoring site that are closest to the observations. Units are in ppbV.

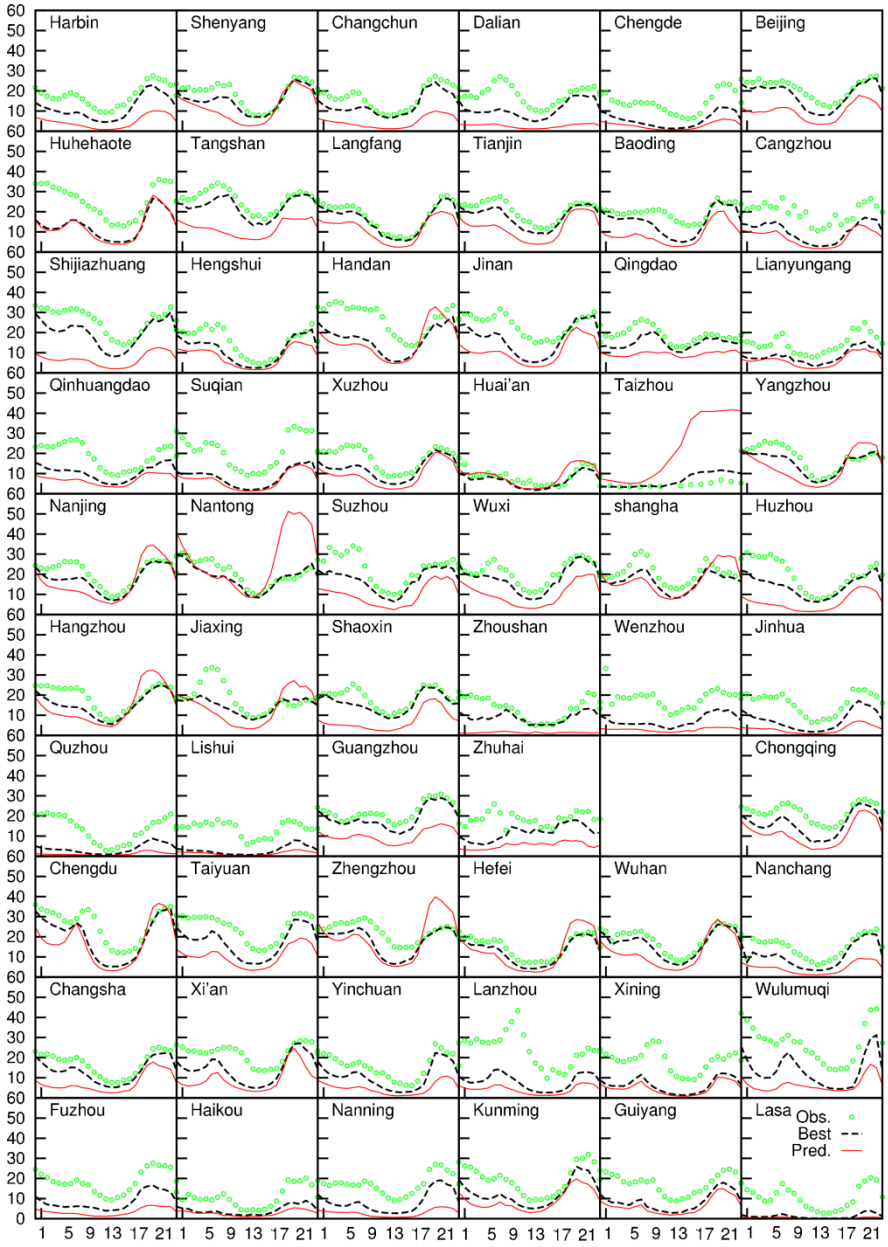

Figure J- 2. Comparison of monthly averaged diurnal variations of hourly NO_2 concentrations in 60 cities in China in August 2013. Observation data in Shenzhen is not available. Red lines are the values predicted at the grid cell where the monitors are located; Black dash lines are the values predicted within the 3×3 grid cell regions surrounding the monitoring site that are closest to the observations. Units are in ppbV.

APPENDIX K. ANALYSIS OF PREDICTED ISOPRENE INCREASE IN THE LATE AFTERNOON

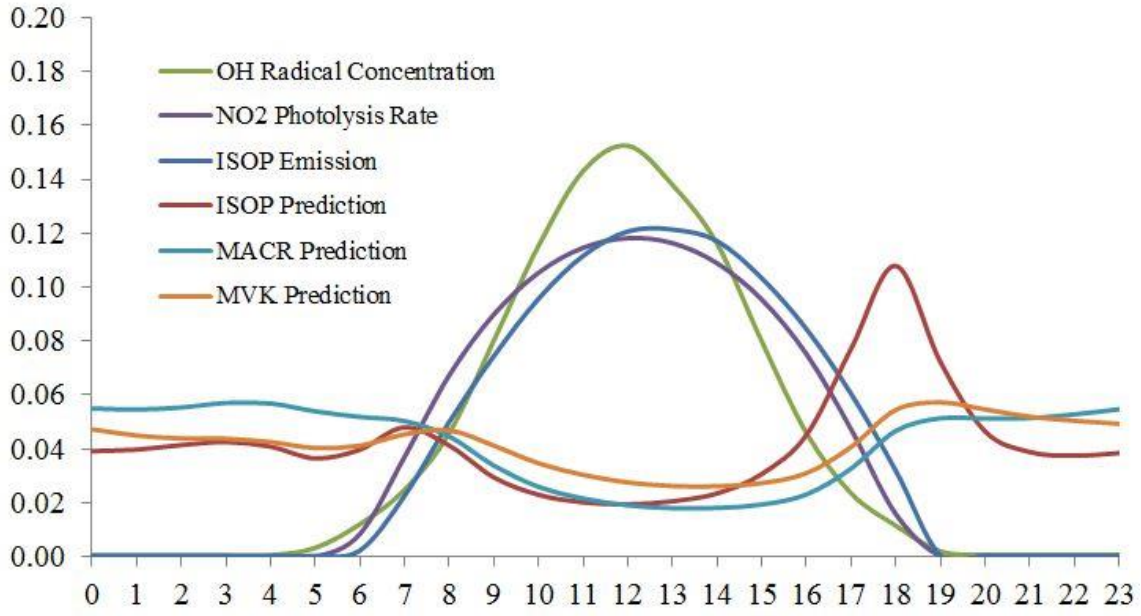

Figure K- 1. Diurnal variation in the normalized monthly averaged predicted concentration of OH radical, isoprene (ISOP), methacrolein (MACR) and methyl vinyl ketone (MVK) in Nanjing in August 2013. Photolysis rate of NO_2 is based on the online TUV model and emission rate of isoprene is based on MEGAN predictions.